ON THE TENSION BETWEEN OPTIMALITY AND ADVERSARIAL ROBUSTNESS IN POLICY OPTIMIZATION

Haoran Li *
School of Mathematical Sciences
University of Chinese Academy of Sciences
Beijing, China
lihaoran21@mails.ucas.ac.cn

Jiayu Lv *
School of Advanced Interdisciplinary Sciences
University of Chinese Academy of Sciences
Beijing, China
lvjiayu24@mails.ucas.ac.cn

Congying Han
School of Mathematical Sciences
University of Chinese Academy of Sciences
Beijing, China
hancy@ucas.ac.cn

Zicheng Zhang
JD.com
Beijing, China
zhangzicheng6@jd.com

Anqi Li †
School of Mathematical Sciences
Nankai University
Tianjin, China
anqili@nankai.edu.cn

Yan Liu
School of Statistics and Data Science
Nankai University
Tianjin, China
liuyan23@nankai.edu.cn

Tiande Guo
School of Mathematical Sciences
University of Chinese Academy of Sciences
Beijing, China
tdguo@ucas.ac.cn

Nan Jiang
Siebel School of Computing and Data Science
University of Illinois Urbana-Champaign
Urbana, IL 61801, USA
nanjiang@illinois.edu

ABSTRACT

Achieving optimality and adversarial robustness in deep reinforcement learning has long been regarded as conflicting goals. Nonetheless, recent theoretical insights presented in CAR (Li et al., 2024) suggest a potential alignment, raising the important question of how to realize this in practice. This paper first identifies a key gap between theory and practice by comparing standard policy optimization (SPO) and adversarially robust policy optimization (ARPO). Although they share theoretical consistency, *a fundamental tension between robustness and optimality arises in practical policy gradient methods*. SPO tends toward convergence to vulnerable first-order stationary policies (FOSPs) with strong natural performance, whereas ARPO typically favors more robust FOSPs at the expense of reduced returns. Furthermore, we attribute this tradeoff to the *reshaping effect of the strongest adversaries* in ARPO, which significantly complicates the global landscape by inducing *deceptive sticky FOSPs*. This improves robustness but makes navigation more challenging. To alleviate this, we develop the *BARPO*, a bilevel framework unifying SPO and ARPO by modulating adversary strength, thereby facilitating navigability while preserving global optima. Extensive empirical results demonstrate that BARPO consistently outperforms vanilla ARPO, providing a practical approach to reconcile theoretical and empirical performance. The code is available at https://github.com/RyanHaoranLi/BARPO.

*Equal contribution
†Corresponding author

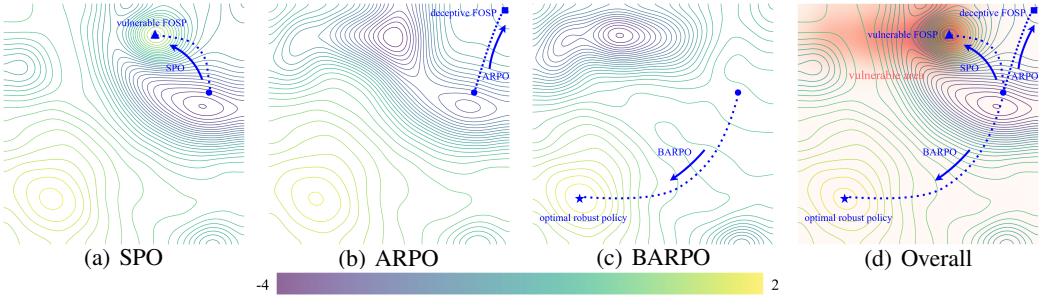

(a) SPO (b) ARPO (c) BARPO (d) Overall

Figure 1: Schematic illustration of the optimization landscapes under SPO, ARPO, and BARPO. (a) SPO ascents along fragile directions, leading to vulnerable FOSPs with high natural value. (b) ARPO becomes trapped in robust regions but is limited to low-return solutions. (c) BARPO reshapes the landscape by lifting robust but low-return regions, enabling convergence to robust FOSPs with high returns. (d) Overall comparison of the three paradigms: contour lines represent natural returns, while background color indicates robustness, with darker red denoting lower robustness.

1 INTRODUCTION

Deep reinforcement learning (DRL) has demonstrated remarkable success across a variety of complex tasks (Mnih et al., 2015; Lillicrap et al., 2016; Silver et al., 2016) and real-world applications, including robotics (Ibarz et al., 2021; Liu et al., 2022; Tang et al., 2025), autonomous driving (Kiran et al., 2021; Chen et al., 2022; 2024), and large model training (Xin et al., 2025; Kumar et al., 2025; Guo et al., 2025). Despite such substantial progress, DRL agents remain highly vulnerable to imperceptible attacks on their state observations, leading to severe performance degradation and even complete system failure (Huang et al., 2017; Behzadan & Munir, 2017a; Lin et al., 2017; Kos & Song, 2017; Pattanaik et al., 2018; Weng et al., 2019; Inkawhich et al., 2020; Ilahi et al., 2021). This vulnerability threatens the reliable deployment of DRL in safety-critical environments, highlighting the urgent need for robust agents capable of withstanding subtle perturbations and malicious attacks.

Motivated by these challenges, Zhang et al. (2020c) introduced the state-adversarial Markov decision process (SA-MDP) framework, providing a theoretical foundation for adversarial robustness in reinforcement learning. Building on this framework, they demonstrated that an optimal robust policy (ORP) may not always exist, indicating a potential conflict between the objectives of optimality and robustness. Recently, Li et al. (2024; 2025) further explored the concept of ORP in practical settings and proposed the ISA-MDP formulation, a refinement that formally establishes the existence of an ORP that coincides with the Bellman optimality policy. These theoretical results suggest that the objectives of adversarial robustness and optimality are, in principle, aligned in most practical tasks.

This insight drives the pursuit of DRL agents that not only maintain strong performance in clean environments but also exhibit resilience to adversarial attacks. This theoretical consistency is critical for deploying DRL agents in real-world applications, where strong malicious attacks are comparatively rare. However, in practice, achieving this alignment remains challenging. Despite sharing this theoretical consistency, conventional policy optimization methods struggle under adversarial settings (Zhang et al., 2021; Sun et al., 2022; 2024). It remains an open problem whether this theoretical alignment can be technically realized, leaving a critical gap between theory and practice.

In this paper, we delve into the optimization behavior and learning dynamics of two training paradigms: *standard policy optimization (SPO)* and *adversarially robust policy optimization (ARPO)*. SPO aims to maximize the standard value function, i.e., $\max_\pi V^\pi(s),\ \forall\, s$, while ARPO optimizes the worst-case adversarial value function, i.e., $\max_\pi \min_\nu V^{\pi\circ\nu}(s),\ \forall\, s$. By conducting a systematic comparison, we reveal a novel optimality-robustness tension in policy gradient methods.

In our analysis, we first prove that both SPO and ARPO converge to first-order stationary policies (FOSPs) rather than global optima. Next, by examining the learning behaviors around these FOSPs, we uncover a key discrepancy: ARPO consistently produces policies with markedly higher robustness to state perturbations, whereas SPO-derived FOSPs remain vulnerable. These findings help explain the empirical vulnerability of SPO, despite the theoretical existence of an ORP, and emphasize the importance of ARPO in building robust DRL agents. Finally, we reveal that this robustness

gain comes at a significant cost: ARPO-trained policies exhibit substantially lower natural returns compared to SPO. Altogether, these results expose a fundamental robustness-performance tradeoff in policy-gradient methods, highlighting a practical challenge for closing the theory-practice gap.

To understand this tradeoff, we analyze the optimization landscape and value geometry induced by SPO and ARPO. We attribute the tension to the *reshaping effect* induced by the strongest adversaries: although they help guide the agent toward robust FOSPs, they often impede optimization by compromising the navigability of the landscape. As illustrated in Figure 1, ARPO creates robust peaks but introduces additional valleys, distorting the global landscape to a more rugged terrain. These new valleys act as traps for the optimization path, hindering gradient-based methods from ascending towards the global or better local peaks. Instead, the optimization process stalls at these *deceptive sticky FOSPs*, which often result in lower natural returns compared to those achieved by SPO. This reshaping effect presents a core barrier to learning both optimality and robustness.

To address this challenge, we propose a bilevel optimization framework that bridges SPO and ARPO, which adjusts the adversary strength to promote traversable optimization paths while maintaining robustness. This modulation prevents the optimization landscape from becoming overly rugged, helping to avoid local traps while still encouraging robustness. Importantly, it preserves the globally optimal robust policy shared by both SPO and ARPO. To enhance convergence and efficiency, we incorporate SPO dynamics into the bilevel framework, further smoothing the optimization landscape. The resulting approach, *Bilevel ARPO (BARPO)*, consistently achieves superior natural and robust returns, offering a promising approach to bridging the gap between theoretical alignment and practical performance. To summarize, this paper makes the following cohesive contributions:

- We explain the nature of vulnerability in standard policy optimization (SPO) within the theoretically aligned framework. While an optimal robust policy exists, SPO typically converges to fragile first-order stationary policies (FOSPs), which offer strong natural performance but lack robustness.
- We uncover a new form of optimality-robustness tension arising in policy optimization. Unlike prior notions of conflicting objectives, adversarially robust policy optimization (ARPO) shares the same global optima with SPO but prefers more robust FOSPs that typically yield lower returns.
- We elucidate the underlying mechanism behind this trade-off. The strongest adversaries in ARPO reshape the optimization landscape by introducing numerous sticky FOSPs, which improve robustness but hinder effective policy improvement by making the landscape more difficult to navigate.
- We propose a unified bilevel framework that connects SPO and ARPO, and instantiate it as Bilevel ARPO (BARPO), a novel method that reshapes the landscape to reduce the prevalence of poor sticky FOSPs while retaining access to robust global optima. Empirical results demonstrate that BARPO significantly improves practical performance, narrowing the gap between theory and practice.

2 Preliminaries and Notations

MDP and SPO. A *Markov Decision Process (MDP)* is formulated as a tuple $(\mathcal{S}, \mathcal{A}, r, \mathbb{P}, \gamma, \mu_0)$, where $\mathcal{S}$ is the state space. $\mathcal{A}$ is the action space. The reward function $r : \mathcal{S} \times \mathcal{A} \to \mathbb{R}$ assigns a scalar reward to each state-action pair. The transition dynamics $\mathbb{P} : \mathcal{S} \times \mathcal{A} \to \Delta(\mathcal{S})$ define the probability distribution over next states, and $\mu_0 \in \Delta(\mathcal{S})$ denotes the initial state distribution. The discount factor $\gamma \in [0, 1)$ controls the trade-off between immediate and future rewards. A stationary policy $\pi : \mathcal{S} \to \Delta(\mathcal{A})$ maps each state to a probability space over actions. Under a given policy π, the state value function is $V^\pi(s) = \mathbb{E}_{\pi,\mathbb{P}}[\sum_{t=0}^{\infty} \gamma^t r(s_t, a_t) | s_0 = s]$, and the action-value function (or Q-function) is $Q^\pi(s, a) = \mathbb{E}_{\pi,\mathbb{P}}[\sum_{t=0}^{\infty} \gamma^t r(s_t, a_t) | s_0 = s, a_0 = a]$. A fundamental property of MDPs is the existence of a stationary and deterministic optimal policy π^*, termed *Bellman optimality policy (BOP)*, that maximizes all $V^\pi(s)$ and $Q^\pi(s, a)$ for all states and actions. In practice, particularly for large-scale state and action spaces, *standard policy optimization (SPO)* methods are widely used for their efficiency (Silver et al., 2014; Schulman et al., 2016; 2015; Lillicrap et al., 2016; Mnih et al., 2016; Schulman et al., 2017; Haarnoja et al., 2018). For the parameterized π_θ, SPO aims to solve:

$$\max_{\theta:\pi_\theta \in \Pi} V^{\pi_\theta}(s),\ \forall\, s \in \mathcal{S},\ \text{where } \Pi := \{\pi_\theta | \pi_\theta(\cdot|s) \in \Delta(\mathcal{A}),\ \forall\, s \in \mathcal{S}\}. \tag{SPO}$$

To simplify notations, we take the expectation over the distribution μ_0: $V^{\pi_\theta}(\mu_0) = \mathbb{E}_{s\sim\mu_0}[V^{\pi_\theta}(s)]$.

ISA-MDP and ARPO. An *Intrinsic State-adversarial Markov Decision Process (ISA-MDP)* is defined by the tuple $(\mathcal{S}, \mathcal{A}, r, \mathbb{P}, \gamma, \mu_0, B^*)$. This formulation extends the standard MDP by incor-

porating structured neighborhoods of allowable state perturbations. For each state $s \in \mathcal{S}$, the set-value function $B^*(s) \subseteq \mathcal{S}$ specifies admissible perturbations which cannot alter the optimal action. An adversary is represented by a mapping $\nu : \mathcal{S} \to \mathcal{S}$ that perturbs the observed state s to a nearby state $s_\nu := \nu(s) \in B^*(s)$. Under this adversary, the policy operates on the perturbed state, denoted by $(\pi \circ \nu)(a|s) := \pi(a|\nu(s))$. Under this setting, the adversarial value function is given by $V^{\pi\circ\nu}(s) = \mathbb{E}_{\pi\circ\nu,\mathbb{P}}[\sum_{t=0}^{\infty}\gamma^t r(s_t,a_t)|s_0 = s]$, and the corresponding adversarial Q-function is $Q^{\pi\circ\nu}(s,a) = \mathbb{E}_{\pi\circ\nu,\mathbb{P}}[\sum_{t=0}^{\infty}\gamma^t r(s_t,a_t)|s_0 = s, a_0 = a]$. For any policy π, there exists the strongest adversary $\nu^*(\pi)$ that minimizes the value function across all states, defined by $\nu^*(\pi) = \arg\min_\nu V^{\pi\circ\nu}(s),\ \forall s$. Within this framework, an *optimal robust policy (ORP)* π^* exists, which simultaneously maximizes performance against its strongest adversary for all states, i.e., $V^{\pi^*\circ\nu^*(\pi^*)}(s) = \max_\pi V^{\pi\circ\nu^*(\pi)}(s)$ for all $s \in \mathcal{S}$ and π^* aligns with Bellman optimality policy.

We refer to the robust optimization problem in ISA-MDP as *Adversarial Robust Policy Optimization (ARPO)*. Despite its centrality to robust decision-making, ARPO has not been thoroughly explored. In this work, we adopt the direct parameterized adversary, resulting in the following formulation:

$$\max_{\theta:\pi_\theta\in\Pi}\min_{\vartheta:\nu_\vartheta\in\Psi} V^{\pi_\theta\circ\nu_\vartheta}(s),\ \forall\, s\in\mathcal{S},\ \text{where}\ \Psi := \{\nu_\vartheta|\nu_\vartheta(s) = s + \vartheta_s \in B^*(s),\ \forall\, s\}\,. \quad \text{(ARPO)}$$

Similar to SPO, we consider the expected objective: $V^{\pi_\theta\circ\nu_\vartheta}(\mu_0) = \mathbb{E}_{s\sim\mu_0}[V^{\pi_\theta\circ\nu_\vartheta}(s)]$. In particular, SPO corresponds to solving the outer maximization while fixing the inner solution to $\vartheta \equiv 0$.

FOSP refers to a stationary point in the optimization sense, where the policy gradient vanishes. Formally, we define π_θ (or θ) as a *first-order stationary policy (FOSP)* for SPO if it satisfies:

$$\nabla_\theta V^{\pi_\theta}(\mu_0) = 0, \quad \nabla^2_{\theta\theta} V^{\pi_\theta}(\mu_0) \preceq 0. \quad \text{(FOSP in SPO)}$$

Similarly, π_θ (or θ) is a FOSP for ARPO if it satisfies the following conditions:

$$\nabla_\theta V^{\pi_\theta\circ\nu^*(\pi_\theta)}(\mu_0) = 0, \quad \nabla^2_{\theta\theta} V^{\pi_\theta\circ\nu^*(\pi_\theta)}(\mu_0) \preceq 0. \quad \text{(FOSP in ARPO)}$$

We further define $(\pi_\theta, \nu^*(\pi_\theta))$ (or $(\theta, \vartheta^*(\theta))$) as a first-order stationary policy-adversary for ARPO.

Terminology Clarification. To avoid ambiguity, we define the following terms used throughout the paper: 1) *Natural returns* (or *performance*): the estimate of standard value function $V^\pi(\mu_0)$. 2) *Robust returns* (against ν): the approximation of adversarial value function $V^{\pi\circ\nu}(\mu_0)$. 3) *Robustness* (against ν): an estimation of the relative degradation in performance $\frac{V^{\pi\circ\nu}(\mu_0) - V^\pi(\mu_0)}{V^\pi(\mu_0)} \leq 0$.

3 Optimality-Robustness Tension in Policy Optimization

This section identifies the inherent tradeoff between optimality and robustness in policy gradient methods. Although SPO and ARPO share the consistent globally optimal robust policy, their convergence behaviors diverge significantly. In practice, SPO often tends to vulnerable policies with high natural performance, while ARPO prefers more robust policies, typically at the cost of reduced returns. Notably, we explore the value geometry and optimization landscape, attributing this divergence to the adversarial reshaping of ARPO. The strongest adversary distorts the global terrain by introducing numerous local minima, which trap the navigation in robust but suboptimal policies.

3.1 Robust Convergence Behavior of ARPO

We begin with a rigorous convergence analysis of ARPO, showing that it generally converges to a first-order stationary policy (FOSP) rather than the global optimum. To better understand this, we examine the nature of FOSPs in both ARPO and SPO by analyzing empirical behaviors and local learning dynamics. Our findings reveal that ARPO promotes stronger robustness near convergence, even without reaching the globally optimal policy. In contrast, SPO achieves high natural returns but lacks robustness against perturbations. Furthermore, this analysis uncovers a connection between robustness and generalization, suggesting that sufficient robustness may improve generalization.

3.1.1 Convergence to First-Order Stationary Policies

To enable a formal gradient-based analysis of ARPO, we first derive the policy gradient expression for the adversary. This formulation facilitates sample-based estimation and numerical computation within the inner optimization. The complete derivation and proof are provided in Appendix C.1.

Table 1: Natural and robust performance of SPO and ARPO for continuous control tasks in MuJoCo.

Environment	Method	Natural Return	Return under Attack							Worst-case Robustness
			Random	Critic	MAD	RS	SA-RL	PA-AD	Worst	
Hopper	SPO	**3081** $\pm$ 638	**2923** $\pm$ 767	2035 $\pm$ 1035	1763 $\pm$ 619	756 $\pm$ 36	79 $\pm$ 2	823 $\pm$ 182	79 $\pm$ 2	-0.974
($\epsilon = 0.075$)	ARPO	2101 $\pm$ 588 $\downarrow$ 32%	2058 $\pm$ 559	**3156** $\pm$ 528	**2225** $\pm$ 641	**1001** $\pm$ 30	**1032** $\pm$ 47	**1799** $\pm$ 547	**1001** $\pm$ 30	**-0.524** $\uparrow$ 46%
Walker2d	SPO	**4662** $\pm$ 22	**4628** $\pm$ 21	**4584** $\pm$ 15	**4507** $\pm$ 675	1062 $\pm$ 150	719 $\pm$ 1079	336 $\pm$ 252	336 $\pm$ 252	-0.928
($\epsilon = 0.05$)	ARPO	2095 $\pm$ 983 $\downarrow$ 56%	1815 $\pm$ 930	2360 $\pm$ 1021	1944 $\pm$ 976	**1360** $\pm$ 835	**1270** $\pm$ 502	**1460** $\pm$ 739	**1270** $\pm$ 502	**-0.394** $\uparrow$ 58%
Halfcheetah	SPO	**5048** $\pm$ 526	**4463** $\pm$ 650	**3281** $\pm$ 1101	918 $\pm$ 541	1049 $\pm$ 50	-213 $\pm$ 103	-69 $\pm$ 22	-213 $\pm$ 103	-1.042
($\epsilon = 0.15$)	ARPO	1412 $\pm$ 99 $\downarrow$ 72%	1363 $\pm$ 285	1359 $\pm$ 59	**1402** $\pm$ 64	**1230** $\pm$ 75	**1079** $\pm$ 48	**1216** $\pm$ 458	**1079** $\pm$ 48	**-0.236** $\uparrow$ 77%
Ant	SPO	**5381** $\pm$ 1308	**5329** $\pm$ 976	**4696** $\pm$ 1015	1768 $\pm$ 929	1097 $\pm$ 633	-1398 $\pm$ 318	-3107 $\pm$ 1071	-3107 $\pm$ 1071	-1.577
($\epsilon = 0.15$)	ARPO	1709 $\pm$ 564 $\downarrow$ 68%	2026 $\pm$ 38	1976 $\pm$ 131	**1839** $\pm$ 350	**1661** $\pm$ 593	**1648** $\pm$ 666	**1675** $\pm$ 573	**1648** $\pm$ 666	**-0.034** $\uparrow$ 98%

Theorem 3.1 (Policy Gradient for Adversary)**.** *Given a policy π_θ, for all state $s \in \mathcal{S}$, consider the direct parameterization representation for adversary $\nu_\vartheta : \mathcal{S} \to \mathcal{S}$, $s \mapsto s + \vartheta_s \in B(s)$. Then, for any state $s_i \in \mathcal{S}$, we have the state-wise policy gradient for the adversary as follows:*

$$\nabla_{\vartheta_{s_i}} V^{\pi_\theta \circ \nu_\vartheta}(s) = \frac{1}{1-\gamma} \mathbb{E}_{(s',a') \sim d^{\pi_\theta \circ \nu_\vartheta}} \left[Q^{\pi_\theta \circ \nu_\vartheta}(s', a') \nabla_{\vartheta_{s'}} \log \pi_\theta(a' | s' + \vartheta_{s'}) \cdot \mathbb{I}(s' = s_i) \right],$$

where $d^{\pi \circ \nu}$ is the state-action visitation distribution under $\pi \circ \nu$, and $\mathbb{I}(\cdot)$ is the indicator function.

Based on this analytical expression, we further characterize the convergence behavior of ARPO. The detailed analysis and proofs are provided in Appendix C.2. Justifications and potential relaxations of assumptions, and the connection with core contributions are further discussed in Appendix H.1.

Theorem 3.2 (Convergence of ARPO)**.** *Denote $\Delta := \max_\theta \min_\vartheta V^{\pi_\theta \circ \nu_\vartheta}(\mu_0) - \min_\vartheta V^{\pi_{\theta_0} \circ \nu_\vartheta}(\mu_0)$. Assume that the sampled policy gradient is Lipschitz continuous and bounded by $M_{\hat{v}}$, the sampled estimation of the value function is locally μ-strongly convex, the state-action visitation distribution is Lipschitz continuous, and the variance of the stochastic gradient is bounded by σ^2. Set the step size as $\eta_k = \sqrt{\Delta / (\sigma^2 L K)}$. Then, the ARPO with δ-approximate adversary and $K \geq \frac{\Delta L}{\sigma^2}$ satisfies:*

$$\frac{1}{K} \sum_{k=0}^{K-1} \mathbb{E} \left[\left\| \nabla_\theta V^{\pi_{\theta_k} \circ \nu^*(\pi_{\theta_k})}(\mu_0) \right\|_2^2 \right] \leq 4\sigma \sqrt{\frac{\Delta L}{K}} + \frac{2 L_{\theta\vartheta}^2 \delta}{\mu},$$

where $L_{\theta\vartheta}$ and $L = \frac{L_{\theta\vartheta} L_{\vartheta\theta}}{\mu} + L_{\theta\theta} + M_{\hat{v}} \left(\frac{L_{d\vartheta} L_{\vartheta\theta}}{\mu} + L_{d\theta} \right)$ are the Lipschitz constants.

Theorem 3.2 shows that, instead of converging to the globally optimal robust policy, ARPO approximates an FOSP of the value function under the strongest adversary. The convergence rate is $O(K^{-1/2})$, and the approximation error depends on the strength of the adversary. Similarly, SPO achieves convergence to the FOSP of the standard value function at the same rate (Agarwal et al., 2019; 2021). These underscore the gap between theoretical optimum and practical convergence.

3.1.2 Learning Behaviors Near First-Order Stationary Policies

Based on the above convergence results, we further explore the characteristics of SPO and ARPO around their FOSPs, highlighting the critical difference between robustness and natural performance.

Empirical Behaviors Near FOSPs. We empirically examine the properties of FOSPs obtained by ARPO across both simple and complex environments. Specifically, we analyze a toy ISA-MDP with two states and two actions using directly parameterized policies, alongside continuous control tasks in MuJoCo employing neural network policies. In both settings, we observe that *FOSPs discovered by ARPO tend to exhibit robustness but generally achieve substantially reduced returns than those achieved by SPO*. The detailed analysis and complete proofs are provided in Appendix D.

Proposition 3.1. *There exists an ISA-MDP such that the following statement holds. Let π_S be a FOSP under SPO, and let π_A be a FOSP under ARPO. Then, π_A is a robust policy with $V^{\pi_A}(\mu_0) - V^-(\mu_0) < \frac{1}{2}(V^{\pi_S}(\mu_0) - V^-(\mu_0))$, where $V^-(\mu_0) = \min_\pi V^\pi(\mu_0)$ denotes the worst-case value.*

Furthermore, as shown in Table 1, in complex high-dimensional tasks, SPO achieves strong natural performance but suffers substantial degradation under adversarial attacks. In contrast, ARPO exhibits substantially greater robustness, particularly in more challenging environments such as

HalfCheetah and Ant. However, its natural performance remains consistently and noticeably lower, often reaching less than half the returns achieved by SPO. These empirical results underscore the practical disparity between the FOSPs obtained by SPO and ARPO, revealing an inherent tradeoff between robustness and optimality in policy gradient methods.

Learning Dynamics Near FOSPs. To better understand the practical performance of SPO and ARPO, we analyze their learning dynamics around their FOSPs. This sheds light on how these paradigms behave near convergence and reveals critical insights into how robustness impacts generalization. Specifically, we characterize the Hessian structures at the FOSPs for both SPO and ARPO, which reflect the local curvature of the value landscape and provide a measure of policy flatness.

Theorem 3.3 (Flatness Bound of FOSPs)**.** *Let (θ^*, ϑ^*) be a first-order stationary policy-adversary in ARPO, satisfying the second-order optimality condition. Denote $\lambda_{\min}(\cdot)$ and $\lambda_{\max}(\cdot)$ as the smallest and largest eigenvalues, and let d be the state space dimension. Suppose (θ^*, ϑ^*) is locally stable, the initialization (θ_0, ϑ_0) satisfies $V^{\pi_{\theta_0} \circ \nu_{\vartheta_0}}(\mu_0) < V^{\pi_{\theta^*} \circ \nu_{\vartheta^*}}(\mu_0)$, the policy gradient noise is coercive with coefficient κ. Then, for single-loop ARPO with step size $\eta \geq 2/\lambda_{\min}(-\nabla^2_{\theta\theta} V^{\pi_{\theta^*} \circ \nu_{\vartheta^*}}(\mu_0))$, attack budget $\epsilon \leq 2/\lambda_{\max}(\nabla^2_{\vartheta\vartheta} V^{\pi_{\theta^*} \circ \nu_{\vartheta^*}}(\mu_0))$, and batch size $B \geq d\epsilon^2 \kappa_\vartheta \lambda_{\max}(\nabla^2_{\vartheta\vartheta} V^{\pi_{\theta^*} \circ \nu_{\vartheta^*}}(\mu_0))^2$, the following inequality between Hessians holds:*

$$\left(\|\nabla^2_{\theta\theta} V^{\pi_{\theta^*} \circ \nu_{\vartheta^*}}(\mu_0)\|_F^2 + \frac{B}{\kappa_\theta \eta^2} \right) \left(1 - \frac{\epsilon^2 \kappa_\vartheta}{B} \|\nabla^2_{\vartheta\vartheta} V^{\pi_{\theta^*} \circ \nu_{\vartheta^*}}(\mu_0)\|_F^2 \right) \leq \frac{B}{\kappa_\theta \eta^2}. \tag{1}$$

Similarly, for a locally stable FOSP θ^* in SPO, if the initialization θ_0 satisfies $V^{\pi_{\theta_0}}(\mu_0) < V^{\pi_{\theta^*}}(\mu_0)$, and the policy gradient noise is coercive with κ_θ, then $\|\nabla^2_{\theta\theta} V^{\pi_{\theta^*}}(\mu_0)\|_F^2 \leq \frac{B}{\kappa_\theta \eta^2}$.

The detailed derivations are in Appendix C.3. From inequality (1), we observe that for FOSP in ARPO, if the adversary-side curvature is bounded as $\|\nabla^2_{\vartheta\vartheta} V^{\pi_{\theta^*} \circ \nu_{\vartheta^*}}(\mu_0)\|_F^2 \leq B/(2\kappa_\vartheta \epsilon^2)$, then the policy-side curvature in ARPO matches that of SPO, i.e., $\|\nabla^2_{\theta\theta} V^{\pi_{\theta^*} \circ \nu_{\vartheta^*}}(\mu_0)\|_F^2 \leq B/(\kappa_\theta \eta^2)$. This implies that if ARPO achieves sufficiently strong robustness, i.e., flat adversarial curvature, it can preserve generalization comparable to SPO. Moreover, greater robustness may further enhance generalization. However, if robustness is insufficient, generalization may be significantly degraded.

3.2 Reshaping Effect of Strongest Adversaries Hindering Policy Improvement

In this subsection, we investigate how the strongest adversary in ARPO reshapes the optimization landscape and value space geometry, shedding light on a key factor behind the optimality-robustness tension. We show that although the strongest adversary promotes convergence to robust FOSPs, it also severely distorts the global landscape, thereby impeding effective policy improvement.

Adversarial Reshaping Promotes Robust FOSPs. As illustrated in Figure 2, we compare ARPO with SPO. It follows directly from the definition that the robust objective $V^{\pi_\theta \circ \nu^*(\pi_\theta)}(\mu_0)$ is always less than or equal to the standard objective $V^{\pi_\theta}(\mu_0)$. In blue regions where π_θ exhibits strong robustness, the gap $V^{\pi_\theta}(\mu_0) - V^{\pi_\theta \circ \nu^*(\pi_\theta)}(\mu_0)$ remains small, leading to only a slight shift in the location of θ within the landscape relative to that under SPO. In contrast, in red regions where π_θ is more vulnerable, the gap becomes substantial, resulting in a sharp decline in the objective value at the corresponding location. This adversarial reshaping significantly increases the ruggedness of the optimization landscape, thereby steering the learning process toward robust policies as FOSPs.

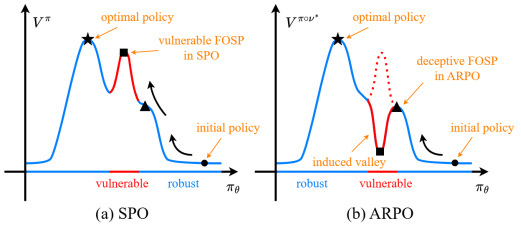

Figure 2: Intuitive examples of reshaping.

Distorted Landscape Impairs Policy Navigation. However, the robust policy space typically exhibits vulnerable connectivity. Adversarial reshaping introduces deep valleys that fragment the terrain, isolate different FOSPs, and obstruct gradient-based traversal. The proof is in Appendix D.

Proposition 3.2 (Vulnerable Connectivity Leading to Separated FOSPs)**.** *There exists an ISA-MDP where the robust policy space Π_{Robust} contains a cut point; that is, there exists a policy π such that $\Pi_{Robust} \setminus \{\pi\}$ is disconnected. Therefore, ARPO tends to yield more isolated FOSPs than SPO.*

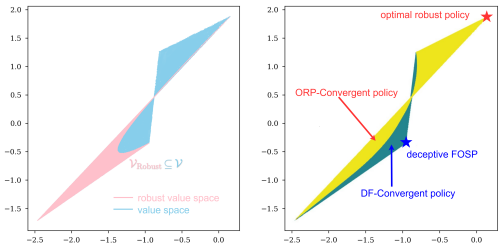

Figure 3: Adversarially robust value geometry.

As illustrated in Figure 4(b), the valleys introduced by the adversary create barriers that obstruct ARPO from reaching better FOSPs or the globally optimal robust policy. This fragmentation increases the difficulty of learning and often traps the agent in suboptimal FOSPs. As further shown in Figure 3, even in a simple ISA-MDP, approximately one-third of initial policies converge to a deceptive FOSP with low value, highlighting the stickiness of these deceptive solutions and how the reshaped terrain can mislead the learning dynamics. These results reveal a core optimization challenge in adversarially robust DRL: adversarial reshaping not only fosters robustness but also introduces deceptive FOSPs that impede consistent policy improvement.

4 Bridging Optimality and Robustness via a Bilevel Framework

The above analysis highlights the strong influence of worst-case adversaries on the optimization landscape. In this section, we seek to mitigate the distorting effects of such adversarial reshaping while preserving strong robustness. To this end, we propose a bilevel optimization framework that interpolates between standard and adversarially robust policy optimization by modulating the strength of the adversary. Furthermore, we derive a surrogate for the strongest adversary to construct a practical algorithm that smooths the distorted landscape while maintaining robust performance.

4.1 Unifying Standard and Adversarially Robust Policy Optimization

To bridge standard and adversarially robust policy training, we introduce the following bilevel optimization framework that relaxes the inner optimization to allow non-strongest adversaries. This relaxation enables a better balance between adversarial robustness and landscape smoothness:

$$\max_{\theta} V^{\pi_\theta \circ \nu^\diamond(\theta)}(\mu_0), \quad \text{s.t. } \nu^\diamond(\theta) = \arg\max_{\vartheta} G(\pi_\theta, \nu_\vartheta). \qquad \text{(General Bilevel ARPO)}$$

Here, the inner objective $G(\pi, \nu)$ defines the adversary behavior, extending robustness beyond worst-case scenarios. This formulation generalizes both SPO and ARPO. Specifically, when $\nu^\diamond(s;\theta) \equiv s$, this framework reduces to SPO; and when $G(\pi,\nu) = -V^{\pi\circ\nu}(\mu_0)$, it recovers ARPO. Importantly, within the ISA-MDP setting, this unified framework preserves the same optimal robust policy as both SPO and ARPO, preserving the theoretical alignment of optimality and robustness.

4.2 Bilevel Adversarially Robust Policy Optimization with KL-Surrogate

To make the proposed bilevel framework applicable in practice, we need to specify a suitable inner objective G that both promotes policy learning and maintains strong robustness. To this end, we consider adversaries practically derived via policy gradient methods, and identify the KL divergence between the original and perturbed policies as an effective surrogate for the strongest adversary.

Theorem 4.1 (Surrogate Adversary)**.** *For any policy π_θ, state $s \in \mathcal{S}$, and $K > 0$, let the adversary ϑ be computed via K-step gradient descent on the adversarial value function, i.e., $\vartheta_{s,k} = \vartheta_{s,k-1} - \eta_{s,k-1}\nabla_{\vartheta_s} V^{\pi_\theta \circ \nu_\vartheta}(s)|_{\vartheta_s=\vartheta_{s,k-1}}, 1 \le k \le K$. Assume that step sizes $\eta_{s,k} \le 1/(\lambda_s + \delta)$ for some $\delta > 0$, and $G(s;\pi,\nu) := \mathcal{D}_{\mathrm{KL}}(\pi(\cdot|s)\|(\pi \circ \nu)(\cdot|s)) \ll 1$. Then, we have the lower bound of robustness:*

$$V^{\pi_\theta}(s) - V^{\pi_\theta \circ \nu_\vartheta}(s) \ge \frac{2\delta}{\lambda_{\max}(F_{s,\theta})K} G(s;\pi_\theta,\nu_\vartheta) + O\left(G(s;\pi_\theta,\nu_\vartheta)^{\frac{3}{2}}\right),$$

where $F_{s,\theta}$ is the Fisher information matrix of $\log(\pi_\theta \circ \nu_\vartheta)(a|s)$ with respect to $\vartheta_s = 0$, defined as $F_{s,\theta} := F(\theta, s) = \mathbb{E}_{a\sim\pi_\theta(\cdot|s)}\left[(\nabla_{\vartheta_s}\log\pi_\theta(a|s+\vartheta_s)|_{\vartheta_s=0})(\nabla_{\vartheta_s}\log\pi_\theta(a|s+\vartheta_s)|_{\vartheta_s=0})^T\right]$, $\lambda_s = \max_{s+\vartheta_s\in B(s)} \lambda_{\max}(\nabla^2_{\vartheta\vartheta} V^{\pi_\theta\circ\nu_\vartheta}(s)|_{\vartheta=\vartheta_s})$ and $\lambda_{\max}(\cdot)$ is the largest eigenvalue of matrix.

The detailed proof is provided in Appendix E. Theorem 4.1 indicates that, for gradient-based strong adversaries, the KL divergence serves as a valid first-order surrogate for minimizing the adversarial

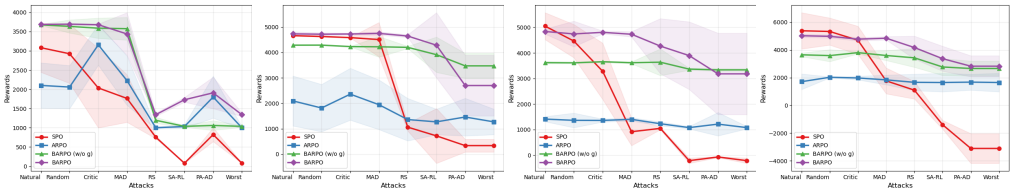

(a) Hopper (b) Walker2d (c) Halfcheetah (d) Ant

Figure 5: Natural and robust performance of SPO, ARPO, BARPO without guidance, and BARPO for four continuous control tasks in MuJoCo. BARPO (w/o g) consistently outperforms ARPO.

value. This surrogate is both appropriate and reliable from an optimization perspective. Motivated by this insight, we propose the following instantiation of our framework, termed *Bilevel ARPO*:

$$\max_{\theta} V^{\pi_\theta \circ \nu^\diamond(\theta)}(\mu_0), \quad \text{s.t. } \nu^\diamond(s;\theta) = \arg\max_{\vartheta} \mathcal{D}_{\mathrm{KL}}(\pi_\theta(\cdot|s) \| (\pi_\theta \circ \nu_\vartheta)(\cdot|s)),\ \forall\, s \in \mathcal{S}. \tag{BARPO}$$

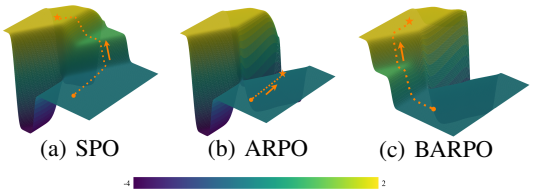

(a) SPO (b) ARPO (c) BARPO

Figure 4: Illustrative Optimization Landscapes

As illustrated in Figures 1 and 4, BARPO effectively reshapes the landscape by elevating low-value but robust regions, thereby creating smoother paths toward better FOSPs and even global optima. This restructuring facilitates learning navigability while promoting updates along robust trajectories, ensuring simultaneous improvements of optimality and robustness. In contrast, SPO tends to follow vulnerable directions, frequently ascending fragile peaks. Meanwhile, ARPO strictly follows the most robust path but often gets stuck in valleys from overly strong adversaries, hindering escape from poor FOSPs. We further delve into the theoretical understanding of BARPO in Appendices H.3 and H.4.

5 Experiments

In this section, we conduct comprehensive comparison experiments and ablation studies to empirically substantiate our theoretical insights and evaluate the practical effectiveness of BARPO.

5.1 Implementation Details

Environments and Baselines. Following baselines (Zhang et al., 2020c; Oikarinen et al., 2021; Liang et al., 2022), we perform experiments on four challenging MuJoCo benchmarks (Todorov et al., 2012) with continuous action spaces: Hopper, Walker2d, HalfCheetah, and Ant. We compare BARPO against several state-of-the-art robust training methods. SA-PPO (Zhang et al., 2020c) incorporates a KL-based regularization and solves the inner maximization problem using PGD (Madry et al., 2018) and CROWN-IBP (Zhang et al., 2020b), respectively. RADIAL-PPO (Oikarinen et al., 2021) incorporates adversarial regularization guided by robustness verification bounds derived from IBP (Gowal et al., 2019). WocaR-PPO (Liang et al., 2022) estimates worst-case values and also employs KL-based regularization. We use the official implementations of these baselines to train 17 agents per method under identical settings. Regularization coefficients are tuned appropriately for each method. To mitigate the effects of high variance in reinforcement learning training, we report the median performance across 17 runs to ensure reproducibility. More details are in Appendix F.

Evaluations. We evaluate the robustness of agents on MuJoCo tasks using six adversarial attack methods: (1) Random Attack: adds uniform random noise to state observations; (2) Critic Attack (Pattanaik et al., 2018): perturbs states based on the action-value function; (3) MAD Attack (Zhang et al., 2020c): maximizes the discrepancy between policies in clean and perturbed states; (4) RS Attack (Zhang et al., 2020c): first learns a robust action-value function, then conducts critic-based attacks guided by it; (5) SA-RL (Zhang et al., 2021): employs a learned adversary

Table 2: Average returns ($\pm$ std) over 50 episodes for baselines and BAR-PPO on MuJoCo tasks. Results include natural return, returns under six attacks, the worst return and robustness under these attacks. Bold and underlined values indicate the top and second performances, respectively.

Environment	Method	Natural Return	Return under Attack							Worst-case Robustness
			Random	Critic	MAD	RS	SA-RL	PA-AD	Worst	
Hopper ($\epsilon = 0.075$)	PPO	3081 $\pm$ 638	2923 $\pm$ 767	2035 $\pm$ 1035	1763 $\pm$ 619	756 $\pm$ 36	79 $\pm$ 2	823 $\pm$ 182	79 $\pm$ 2	-0.974
	SA	3518 $\pm$ 272	2835 $\pm$ 866	3662 $\pm$ 6	3045 $\pm$ 797	**1407** $\pm$ 36	1476 $\pm$ 255	1286 $\pm$ 282	1286 $\pm$ 282	**-0.634**
	RADIAL	3254 $\pm$ 714	3170 $\pm$ 754	**3706** $\pm$ 11	2558 $\pm$ 888	1307 $\pm$ 420	993 $\pm$ 717	1696 $\pm$ 574	993 $\pm$ 717	-0.718
	WocaR	3629 $\pm$ 35	3637 $\pm$ 29	3657 $\pm$ 30	3150 $\pm$ 737	1171 $\pm$ 1013	1452 $\pm$ 66	**2124** $\pm$ 872	1171 $\pm$ 1013	-0.677
	BAR	**3684** $\pm$ 20	**3692** $\pm$ 24	3678 $\pm$ 19	**3437** $\pm$ 555	1340 $\pm$ 42	**1728** $\pm$ 62	1908 $\pm$ 410	**1340** $\pm$ 42	-0.636
Walker2d ($\epsilon = 0.05$)	PPO	4662 $\pm$ 22	4628 $\pm$ 21	4584 $\pm$ 15	4507 $\pm$ 675	1062 $\pm$ 150	719 $\pm$ 1079	336 $\pm$ 252	336 $\pm$ 252	-0.928
	SA	**4875** $\pm$ 278	**4907** $\pm$ 187	**5029** $\pm$ 74	**4833** $\pm$ 132	2775 $\pm$ 1308	3356 $\pm$ 1433	997 $\pm$ 1152	997 $\pm$ 1152	-0.795
	RADIAL	2531 $\pm$ 1089	2170 $\pm$ 1102	2063 $\pm$ 1068	2316 $\pm$ 1171	1239 $\pm$ 800	426 $\pm$ 22	1353 $\pm$ 921	426 $\pm$ 22	-0.832
	WocaR	4226 $\pm$ 938	4347 $\pm$ 892	4342 $\pm$ 875	4373 $\pm$ 850	3358 $\pm$ 1242	2385 $\pm$ 840	1064 $\pm$ 999	1064 $\pm$ 999	-0.752
	BAR	4732 $\pm$ 86	4718 $\pm$ 59	4727 $\pm$ 36	4750 $\pm$ 65	**4646** $\pm$ 53	**4285** $\pm$ 1282	**2699** $\pm$ 1192	**2699** $\pm$ 1192	**-0.436**
Halfcheetah ($\epsilon = 0.15$)	PPO	**5048** $\pm$ 526	4463 $\pm$ 650	3281 $\pm$ 1101	918 $\pm$ 541	1049 $\pm$ 50	-213 $\pm$ 103	-69 $\pm$ 22	-213 $\pm$ 103	-1.042
	SA	4780 $\pm$ 1456	**4983** $\pm$ 1122	**5035** $\pm$ 1245	3759 $\pm$ 1963	2727 $\pm$ 1707	1443 $\pm$ 1082	1551 $\pm$ 1139	1443 $\pm$ 1082	-0.698
	RADIAL	4739 $\pm$ 80	4642 $\pm$ 75	4546 $\pm$ 329	2961 $\pm$ 1478	1327 $\pm$ 1112	1522 $\pm$ 1059	1968 $\pm$ 1284	1327 $\pm$ 1112	-0.720
	WocaR	4723 $\pm$ 462	4798 $\pm$ 69	4846 $\pm$ 349	4543 $\pm$ 566	3302 $\pm$ 1718	2270 $\pm$ 1318	2498 $\pm$ 1224	2270 $\pm$ 1318	-0.519
	BAR	4837 $\pm$ 99	4741 $\pm$ 501	4803 $\pm$ 54	**4729** $\pm$ 105	**4265** $\pm$ 1077	**3894** $\pm$ 1322	**3181** $\pm$ 1593	**3181** $\pm$ 1593	**-0.342**
Ant ($\epsilon = 0.15$)	PPO	**5381** $\pm$ 1308	**5329** $\pm$ 976	4696 $\pm$ 1015	1768 $\pm$ 929	1097 $\pm$ 633	-1398 $\pm$ 318	-3107 $\pm$ 1071	-3107 $\pm$ 1071	-1.577
	SA	5367 $\pm$ 94	5217 $\pm$ 410	**5012** $\pm$ 113	**5114** $\pm$ 294	**4396** $\pm$ 1225	**4227** $\pm$ 177	2355 $\pm$ 1620	2355 $\pm$ 1620	-0.539
	RADIAL	4358 $\pm$ 98	4309 $\pm$ 206	3628 $\pm$ 267	4205 $\pm$ 127	3742 $\pm$ 696	2364 $\pm$ 47	3261 $\pm$ 134	2364 $\pm$ 47	-0.462
	WocaR	4069 $\pm$ 598	3911 $\pm$ 659	3978 $\pm$ 190	3689 $\pm$ 841	3176 $\pm$ 908	1868 $\pm$ 99	1830 $\pm$ 102	1830 $\pm$ 102	-0.550
	BAR	5024 $\pm$ 117	4979 $\pm$ 114	4777 $\pm$ 122	4843 $\pm$ 120	4171 $\pm$ 826	3367 $\pm$ 902	**2825** $\pm$ 757	**2825** $\pm$ 757	**-0.438**

against the victim to perturb the state; (6) PA-AD (Sun et al., 2022): trains an adversarial agent to identify a vulnerable perturbation direction, followed by an FGSM attack along that direction.

BAR-PPO. We implement both ARPO and BARPO on top of the PPO algorithm (Schulman et al., 2017), a widely adopted policy-gradient method that serves as a standard baseline in adversarially robust DRL research. To improve convergence and efficiency, we integrate SPO dynamics into the bilevel framework using a regularization weight κ, resulting in a practical instantiation of BARPO, referred to as BAR-PPO. For solving the inner optimization problem, we employ SGLD (Gelfand & Mitter, 1991) to obtain the adversarial perturbation policy $\nu^{\diamond}$. In the outer optimization, we treat the inner solution as fixed and omit second-order terms to facilitate efficient updates of the primary policy. A complete description and further implementation details can be found in Appendix F. In the following, *BARPO* refers to the combination of SPO-based guidance with the bilevel framework, *BARPO without guidance* uses only the bilevel framework, *ARPO* uses only the maximin framework, and *ARPO with guidance* improves the maximin training through combining the SPO guidance.

5.2 Comparison Results

BARPO Consistently Improves over ARPO. Figure 5 compares the natural and robust performance of four methods: SPO, ARPO, BARPO without SPO guidance, and BARPO with SPO guidance. Detailed evaluation results are provided in Appendix G.1. Notably, BARPO without SPO guidance consistently outperforms ARPO across all environments, improving both natural and robust returns. Even in environments like Walker2d and Halfcheetah, it achieves substantial gains in robustness. Specifically, BARPO without SPO guidance improves the natural return by approximately 75%, 104%, 156%, and 113% on Hopper, Walker2d, Halfcheetah, and Ant, respectively, while boosting robust return by about 4%, 173%, 209%, and 61% in the worst-case setting. Remarkably, in the Hopper and Walker2d tasks, BARPO without SPO guidance achieves natural returns on par with state-of-the-art methods. As further illustrated in Figure 6, BARPO improves the training dynamics by guiding policy learning toward regions in the landscape that yield higher returns.

BAR-PPO Exhibits Superior Natural and Robust Performance. As shown in Table 2, BAR-PPO demonstrates strong overall performance across all four MuJoCo environments, achieving both high natural returns and robust resilience to adversarial perturbations. In particular, BAR-PPO outperforms vanilla PPO in terms of natural returns on Hopper and Walker2d, and achieves comparable performance on Halfcheetah and Ant. In terms of worst-case robust returns, BAR-PPO significantly surpasses all baselines, with improvements of 4%, 154%, 40%, and 20% over the second best, respectively. Notably, BAR-PPO achieves the highest robustness across Walker2d, Halfcheetah, and Ant, and is on par with the strongest robustness on Hopper, with a negligible gap of only 0.3%.

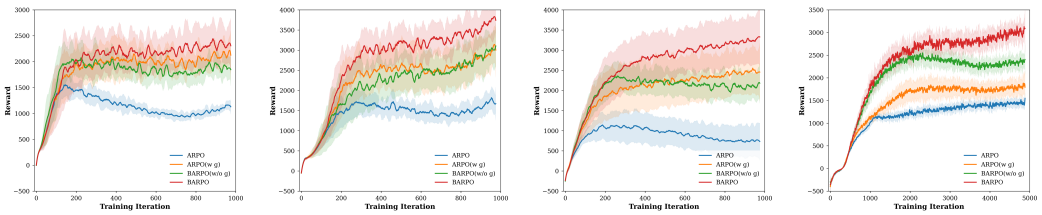

(a) Hopper (b) Walker2d (c) Halfcheetah (d) Ant

Figure 6: Natural training curves of ARPO and BARPO with and without SPO-guidance.

Table 3: Comparisons between BARPO and ARPO with SPO-based guidance.

Environment	Method	Natural Return	Return under Attack							Worst-case Robustness
			Random	Critic	MAD	RS	SA-RL	PA-AD	Worst	
Hopper	ARPO (w g)	**3699** ± 11	3652 ± 222	**3693** ± 8	3132 ± 692	1130 ± 30	1278 ± 359	1756 ± 415	1130 ± 30	-0.694
($\epsilon = 0.075$)	BARPO	3684 ± 20 ↓0.4%	**3692** ± 24	3678 ± 19	**3437** ± 555	**1340** ± 42	**1728** ± 62	**1908** ± 410	**1340** ± 42 ↑19%	**-0.636** ↑8.4%
Walker2d	ARPO (w g)	4206 ± 30	4231 ± 40	4283 ± 38	4226 ± 68	3139 ± 1442	3565 ± 988	2496 ± 1871	2496 ± 1871	**-0.406**
($\epsilon = 0.05$)	BARPO	**4732** ± 86 ↑11%	**4718** ± 59	**4727** ± 36	**4750** ± 65	**4646** ± 53	**4285** ± 1282	**2699** ± 1192	**2699** ± 1192 ↑8.1%	-0.436 ↓7.4%
Halfcheetah	ARPO (w g)	**4997** ± 71	**4934** ± 57	**5040** ± 50	2570 ± 1588	3605 ± 48	1356 ± 1165	1086 ± 758	1086 ± 758	-0.783
($\epsilon = 0.15$)	BARPO	4837 ± 99 ↓3.2%	4741 ± 501	4803 ± 54	**4729** ± 105	**4265** ± 1077	**3894** ± 1322	**3181** ± 1593	**3181** ± 1593 ↑193%	**-0.342** ↑56%
Ant	ARPO (w g)	**5390** ± 120	**5227** ± 186	4768 ± 92	4059 ± 921	2670 ± 1365	1185 ± 253	1757 ± 811	1185 ± 253	-0.773
($\epsilon = 0.15$)	BARPO	5024 ± 117 ↓6.8%	4979 ± 114	**4777** ± 122	**4843** ± 120	**4171** ± 826	**3367** ± 902	**2825** ± 757	**2825** ± 757 ↑138%	**-0.438** ↑43%

5.3 Ablation Studies

Effect of SPO-Guidance. As shown in Figures 5 and 6, incorporating SPO-based guidance further enhances the natural performance of BARPO, particularly in more complex environments such as Halfcheetah and Ant. In certain cases, the enhancement in natural returns is accompanied by corresponding improvements in robust returns, as observed in the Hopper and Ant tasks. However, this incorporation often involves a trade-off, where improvements in natural performance may lead to a reduction in the worst-case robustness, as presented in the Walker2d and Halfcheetah environments.

Comparisons between BARPO and ARPO with SPO-Guidance. To further validate the effectiveness of BARPO, we compare it with ARPO enhanced by SPO-based guidance. As presented in Table 3, on the Hopper, Halfcheetah, and Ant tasks, BARPO exhibits a slight reduction in natural returns compared to ARPO with guidance, approximately 0.4%, 3.2%, and 6.8%, respectively. However, BARPO achieves significantly higher robust returns and markedly stronger robustness, with improvements of 19%, 193%, 138% in robust returns, and 8.4%, 56%, and 43% in robustness metrics. On the Walker2d task, BARPO attains gains in both natural and robust returns, with a minor compromise in robustness. These findings indicate that although integrating SPO guidance into ARPO can enhance performance to some extent, this direct combination does not effectively mitigate the reshaping effect induced by the strongest adversary. Consequently, numerous sticky FOSPs with low returns persist, posing challenges for optimization. In contrast, BARPO substantially reshapes the landscape, enabling the discovery of improved navigation that yields higher returns.

We also conduct additional ablations in Appendices G.6 and G.7 to identify the effects of bilevel structure, SPO guidance, and KL surrogate. These further validate the effectiveness of BARPO.

6 Conclusion

In this paper, we explore whether the theoretical alignment between optimality and robustness can be realized in practical policy optimization, and propose BARPO, a novel bilevel framework that unifies standard and adversarially robust policy optimization. Through extensive analysis, we reveal a fundamental tradeoff between optimality and robustness in existing policy gradient methods, exposing a critical gap between theory and practice. Notably, our work demystifies the underlying cause of this tension from the perspective of optimization landscapes and value space geometry. Specifically, the strongest adversaries in ARPO significantly reshape the learning landscapes by introducing numerous sticky and deceptive local optima. While this promotes robustness, it also hinders effective policy improvement by making the landscape more rugged and difficult to navigate. BARPO refines the landscapes by modulating the adversary strength, thereby creating pathways toward superior policies and reducing the prevalence of poor sticky local optima. Surprisingly, this bilevel framework empirically showcases the potential for approaching the globally optimal robust policy, suggesting a promising step toward bridging theoretical guarantees and practical performance.

ETHICS STATEMENT

All authors of this paper have carefully reviewed and adhered to the ICLR Code of Ethics.

REPRODUCIBILITY STATEMENT

All benchmarks, as well as the experimental setup, are based on or derived from open-sourced work. We have given relevant references in the paper, and the details of our algorithm and experiments are provided in Section 5 and Appendices F and G.

We have provided detailed analysis and complete proofs for each theorem and proposition in the Appendices C, D, E, and H.

ACKNOWLEDGMENTS

Congying Han, Haoran Li, Jiayu Lv, and Tiande Guo acknowledge funding support from the National Key R&D Program of China (2021YFA1000403) and the National Natural Science Foundation of China (Nos. 12431012, U23B2012).

REFERENCES

Alekh Agarwal, Sahand Negahban, and Martin J Wainwright. Fast global convergence of gradient methods for high-dimensional statistical recovery. *The Annals of Statistics*, 40(5):2452, 2012.

Alekh Agarwal, Nan Jiang, Sham M Kakade, and Wen Sun. Reinforcement learning: Theory and algorithms. *CS Dept., UW Seattle, Seattle, WA, USA, Tech. Rep*, 32:96, 2019.

Alekh Agarwal, Sham M Kakade, Jason D Lee, and Gaurav Mahajan. On the theory of policy gradient methods: Optimality, approximation, and distribution shift. *Journal of Machine Learning Research*, 22(98):1–76, 2021.

Zeyuan Allen-Zhu, Yuanzhi Li, and Zhao Song. A convergence theory for deep learning via over-parameterization. In *International Conference on Machine Learning*, pp. 242–252. PMLR, 2019.

Heinz H Bauschke, Jérôme Bolte, and Marc Teboulle. A descent lemma beyond lipschitz gradient continuity: first-order methods revisited and applications. *Mathematics of Operations Research*, 42(2):330–348, 2017.

Heinz H Bauschke, Minh N Dao, and Scott B Lindstrom. Regularizing with bregman–moreau envelopes. *SIAM Journal on Optimization*, 28(4):3208–3228, 2018.

Vahid Behzadan and Arslan Munir. Vulnerability of deep reinforcement learning to policy induction attacks. In *Machine Learning and Data Mining in Pattern Recognition: 13th International Conference, MLDM 2017, New York, NY, USA, July 15-20, 2017, Proceedings 13*, pp. 262–275. Springer, 2017a.

Vahid Behzadan and Arslan Munir. Whatever does not kill deep reinforcement learning, makes it stronger. *arXiv preprint arXiv:1712.09344*, 2017b.

Roman Belaire, Arunesh Sinha, and Pradeep Varakantham. On minimizing adversarial counterfactual error in adversarial reinforcement learning. In *The Thirteenth International Conference on Learning Representations*, 2025.

Shubham Bharti, Xuezhou Zhang, Adish Singla, and Jerry Zhu. Provable defense against backdoor policies in reinforcement learning. *Advances in Neural Information Processing Systems*, 35: 14704–14714, 2022.

Jérôme Bolte, Shoham Sabach, and Marc Teboulle. Proximal alternating linearized minimization for nonconvex and nonsmooth problems. *Mathematical Programming*, 146(1):459–494, 2014.

Jérôme Bolte, Shoham Sabach, Marc Teboulle, and Yakov Vaisbourd. First order methods beyond convexity and lipschitz gradient continuity with applications to quadratic inverse problems. *SIAM Journal on Optimization*, 28(3):2131–2151, 2018.

Alexander Bukharin, Yan Li, Yue Yu, Qingru Zhang, Zhehui Chen, Simiao Zuo, Chao Zhang, Songan Zhang, and Tuo Zhao. Robust multi-agent reinforcement learning via adversarial regularization: Theoretical foundation and stable algorithms. *Advances in Neural Information Processing Systems*, 36, 2024.

Li Chen, Penghao Wu, Kashyap Chitta, Bernhard Jaeger, Andreas Geiger, and Hongyang Li. End-to-end autonomous driving: Challenges and frontiers. *IEEE Transactions on Pattern Analysis and Machine Intelligence*, 2024.

Long Chen, Yuchen Li, Chao Huang, Bai Li, Yang Xing, Daxin Tian, Li Li, Zhongxu Hu, Xiaoxiang Na, Zixuan Li, et al. Milestones in autonomous driving and intelligent vehicles: Survey of surveys. *IEEE Transactions on Intelligent Vehicles*, 8(2):1046–1056, 2022.

Robert Dadashi, Adrien Ali Taiga, Nicolas Le Roux, Dale Schuurmans, and Marc G Bellemare. The value function polytope in reinforcement learning. In *International Conference on Machine Learning*, pp. 1486–1495. PMLR, 2019.

Kuangyu Ding, Jingyang Li, and Kim-Chuan Toh. Nonconvex stochastic bregman proximal gradient method with application to deep learning. *Journal of Machine Learning Research*, 26(39):1–44, 2025.

Juncheng Dong, Hao-Lun Hsu, Qitong Gao, Vahid Tarokh, and Miroslav Pajic. Variational adversarial training towards policies with improved robustness. In *Proceedings of the 28th International Conference on Artificial Intelligence and Statistics (AISTATS)*, 2025.

Dmitriy Drusvyatskiy and Adrian S Lewis. Error bounds, quadratic growth, and linear convergence of proximal methods. *Mathematics of operations research*, 43(3):919–948, 2018.

Simon Du, Jason Lee, Haochuan Li, Liwei Wang, and Xiyu Zhai. Gradient descent finds global minima of deep neural networks. In *International Conference on Machine Learning*, pp. 1675–1685. PMLR, 2019.

Yu Feng and Yuhai Tu. The inverse variance–flatness relation in stochastic gradient descent is critical for finding flat minima. *Proceedings of the National Academy of Sciences*, 118(9):e2015617118, 2021.

Marc Fischer, Matthew Mirman, Steven Stalder, and Martin Vechev. Online robustness training for deep reinforcement learning. *arXiv preprint arXiv:1911.00887*, 2019.

Tim Franzmeyer, Stephen Marcus McAleer, Joao F Henriques, Jakob Nicolaus Foerster, Philip Torr, Adel Bibi, and Christian Schroeder de Witt. Illusory attacks: Information-theoretic detectability matters in adversarial attacks. In *The Twelfth International Conference on Learning Representations*, 2024.

Saul B Gelfand and Sanjoy K Mitter. Recursive stochastic algorithms for global optimization in r^d. *SIAM Journal on Control and Optimization*, 29(5):999–1018, 1991.

Adam Gleave, Michael Dennis, Cody Wild, Neel Kant, Sergey Levine, and Stuart Russell. Adversarial policies: Attacking deep reinforcement learning. In *International Conference on Learning Representations*, 2020. URL https://openreview.net/forum?id=HJgEMpVFwB.

Ian J Goodfellow, Jonathon Shlens, and Christian Szegedy. Explaining and harnessing adversarial examples. In *International Conference on Learning Representations*, 2015.

Sven Gowal, Krishnamurthy Dj Dvijotham, Robert Stanforth, Rudy Bunel, Chongli Qin, Jonathan Uesato, Relja Arandjelovic, Timothy Mann, and Pushmeet Kohli. Scalable verified training for provably robust image classification. In *Proceedings of the IEEE/CVF International Conference on Computer Vision*, pp. 4842–4851, 2019.

Zhaoyuan Gu, Zhenzhong Jia, and Howie Choset. Adversary a3c for robust reinforcement learning. *arXiv preprint arXiv:1912.00330*, 2019.

Daya Guo, Dejian Yang, Haowei Zhang, Junxiao Song, Ruoyu Zhang, Runxin Xu, Qihao Zhu, Shirong Ma, Peiyi Wang, Xiao Bi, et al. Deepseek-r1 incentivizes reasoning in llms through reinforcement learning. *Nature*, 645:633–638, 2025. doi: 10.1038/s41586-025-09422-z.

Junfeng Guo, Ang Li, Lixu Wang, and Cong Liu. Policycleanse: Backdoor detection and mitigation for competitive reinforcement learning. In *Proceedings of the IEEE/CVF International Conference on Computer Vision*, pp. 4699–4708, 2023.

Tuomas Haarnoja, Aurick Zhou, Pieter Abbeel, and Sergey Levine. Soft actor-critic: Off-policy maximum entropy deep reinforcement learning with a stochastic actor. In *International Conference on Machine Learning*, pp. 1861–1870. PMLR, 2018.

Sihong He, Songyang Han, Sanbao Su, Shuo Han, Shaofeng Zou, and Fei Miao. Robust multi-agent reinforcement learning with state uncertainty. *Transactions on Machine Learning Research*, 2023. ISSN 2835-8856. URL https://openreview.net/forum?id=CqTkapZ6H9.

Sandy Huang, Nicolas Papernot, Ian Goodfellow, Yan Duan, and Pieter Abbeel. Adversarial attacks on neural network policies. In *5th International Conference on Learning Representations (ICLR) Workshop Proceedings*, 2017.

Julian Ibarz, Jie Tan, Chelsea Finn, Mrinal Kalakrishnan, Peter Pastor, and Sergey Levine. How to train your robot with deep reinforcement learning: lessons we have learned. *The International Journal of Robotics Research*, 40(4-5):698–721, 2021.

Inaam Ilahi, Muhammad Usama, Junaid Qadir, Muhammad Umar Janjua, Ala Al-Fuqaha, Dinh Thai Hoang, and Dusit Niyato. Challenges and countermeasures for adversarial attacks on deep reinforcement learning. *IEEE Transactions on Artificial Intelligence*, 3(2):90–109, 2021.

Matthew Inkawhich, Yiran Chen, and Hai Li. Snooping attacks on deep reinforcement learning. In *Proceedings of the 19th International Conference on Autonomous Agents and MultiAgent Systems*, AAMAS '20, pp. 557–565, Richland, SC, 2020. International Foundation for Autonomous Agents and Multiagent Systems. ISBN 9781450375184.

Garud N Iyengar. Robust dynamic programming. *Mathematics of Operations Research*, 30(2): 257–280, 2005.

Parameswaran Kamalaruban, Yu-Ting Huang, Ya-Ping Hsieh, Paul Rolland, Cheng Shi, and Volkan Cevher. Robust reinforcement learning via adversarial training with langevin dynamics. *Advances in Neural Information Processing Systems*, 33:8127–8138, 2020.

Hamed Karimi, Julie Nutini, and Mark Schmidt. Linear convergence of gradient and proximal-gradient methods under the polyak-łojasiewicz condition. In *Joint European conference on machine learning and knowledge discovery in databases*, pp. 795–811. Springer, 2016.

Panagiota Kiourti, Kacper Wardega, Susmit Jha, and Wenchao Li. Trojdrl: evaluation of backdoor attacks on deep reinforcement learning. In *2020 57th ACM/IEEE Design Automation Conference (DAC)*, pp. 1–6. IEEE, 2020.

B Ravi Kiran, Ibrahim Sobh, Victor Talpaert, Patrick Mannion, Ahmad A Al Sallab, Senthil Yogamani, and Patrick Pérez. Deep reinforcement learning for autonomous driving: A survey. *IEEE Transactions on Intelligent Transportation Systems*, 23(6):4909–4926, 2021.

Ezgi Korkmaz. Adversarial robust deep reinforcement learning requires redefining robustness. In *Proceedings of the AAAI Conference on Artificial Intelligence*, volume 37, pp. 8369–8377, 2023.

Jernej Kos and Dawn Song. Delving into adversarial attacks on deep policies. In *International Conference on Learning Representations Workshop*, 2017. URL https://openreview.net/forum?id=BJcib5mFe.

Aounon Kumar, Alexander Levine, and Soheil Feizi. Policy smoothing for provably robust reinforcement learning. In *International Conference on Learning Representations*, 2022. URL https://openreview.net/forum?id=mwdfai8NBrJ.

Aviral Kumar, Vincent Zhuang, Rishabh Agarwal, Yi Su, John D Co-Reyes, Avi Singh, Kate Baumli, Shariq Iqbal, Colton Bishop, Rebecca Roelofs, Lei M Zhang, Kay McKinney, Disha Shrivastava, Cosmin Paduraru, George Tucker, Doina Precup, Feryal Behbahani, and Aleksandra Faust. Training language models to self-correct via reinforcement learning. In *The Thirteenth International Conference on Learning Representations*, 2025. URL https://openreview.net/forum?id=CjwERcAU7w.

Jeongyeol Kwon, Dohyun Kwon, Stephen Wright, and Robert D Nowak. A fully first-order method for stochastic bilevel optimization. In *International Conference on Machine Learning*, pp. 18083–18113. PMLR, 2023.

Jaeho Lee and Maxim Raginsky. Minimax statistical learning with wasserstein distances. *Advances in Neural Information Processing Systems*, 31, 2018.

Haochuan Li, Jian Qian, Yi Tian, Alexander Rakhlin, and Ali Jadbabaie. Convex and non-convex optimization under generalized smoothness. *Advances in Neural Information Processing Systems*, 36:40238–40271, 2023.

Haoran Li, Zicheng Zhang, Wang Luo, Congying Han, Yudong Hu, Tiande Guo, and Shichen Liao. Towards optimal adversarial robust q-learning with Bellman infinity-error. In *Proceedings of the 41st International Conference on Machine Learning*, volume 235 of *Proceedings of Machine Learning Research*, pp. 29324–29372. PMLR, 21–27 Jul 2024. URL https://proceedings.mlr.press/v235/li24cl.html.

Haoran Li, Zicheng Zhang, Wang Luo, Congying Han, Jiayu Lv, Tiande Guo, and Yudong Hu. Towards optimal adversarial robust reinforcement learning with infinity measurement error. *arXiv preprint arXiv:2502.16734*, 2025.

Yongyuan Liang, Yanchao Sun, Ruijie Zheng, and Furong Huang. Efficient adversarial training without attacking: Worst-case-aware robust reinforcement learning. *Advances in Neural Information Processing Systems*, 35:22547–22561, 2022.

Yongyuan Liang, Yanchao Sun, Ruijie Zheng, Xiangyu Liu, Benjamin Eysenbach, Tuomas Sandholm, Furong Huang, and Stephen Marcus McAleer. Game-theoretic robust reinforcement learning handles temporally-coupled perturbations. In *The Twelfth International Conference on Learning Representations*, 2024. URL https://openreview.net/forum?id=wZWTHU7AsQ.

Timothy P. Lillicrap, Jonathan J. Hunt, Alexander Pritzel, Nicolas Heess, Tom Erez, Yuval Tassa, David Silver, and Daan Wierstra. Continuous control with deep reinforcement learning. In *International Conference on Learning Representations*, 2016. URL https://openreview.net/forum?id=kJP8gA8BxRY.

Yen-Chen Lin, Zhang-Wei Hong, Yuan-Hong Liao, Meng-Li Shih, Ming-Yu Liu, and Min Sun. Tactics of adversarial attack on deep reinforcement learning agents. In *International Joint Conference on Artificial Intelligence*, pp. 3756–3762, 2017. URL https://doi.org/10.24963/ijcai.2017/525.

Xiangyu Liu, Souradip Chakraborty, Yanchao Sun, and Furong Huang. Rethinking adversarial policies: A generalized attack formulation and provable defense in RL. In *The Twelfth International Conference on Learning Representations*, 2024a. URL https://openreview.net/forum?id=pDCublKPmG.

Xiangyu Liu, Chenghao Deng, Yanchao Sun, Yongyuan Liang, and Furong Huang. Beyond worst-case attacks: Robust RL with adaptive defense via non-dominated policies. In *The Twelfth International Conference on Learning Representations*, 2024b. URL https://openreview.net/forum?id=DFTHW0MyiW.

Zhihao Liu, Quan Liu, Wenjun Xu, Lihui Wang, and Zude Zhou. Robot learning towards smart robotic manufacturing: A review. *Robotics and Computer-Integrated Manufacturing*, 77:102360, 2022.

Chris Lu, Timon Willi, Alistair Letcher, and Jakob Nicolaus Foerster. Adversarial cheap talk. In *International Conference on Machine Learning*, pp. 22917–22941. PMLR, 2023.

Zhaosong Lu and Sanyou Mei. First-order penalty methods for bilevel optimization. *SIAM Journal on Optimization*, 34(2):1937–1969, 2024.

Aleksander Madry, Aleksandar Makelov, Ludwig Schmidt, Dimitris Tsipras, and Adrian Vladu. Towards deep learning models resistant to adversarial attacks. In *International Conference on Learning Representations*, 2018. URL https://openreview.net/forum?id=rJzIBfZAb.

Volodymyr Mnih, Koray Kavukcuoglu, David Silver, Andrei A Rusu, Joel Veness, Marc G Bellemare, Alex Graves, Martin Riedmiller, Andreas K Fidjeland, Georg Ostrovski, et al. Human-level control through deep reinforcement learning. *Nature*, 518(7540):529–533, 2015.

Volodymyr Mnih, Adria Puigdomenech Badia, Mehdi Mirza, Alex Graves, Timothy Lillicrap, Tim Harley, David Silver, and Koray Kavukcuoglu. Asynchronous methods for deep reinforcement learning. In *International Conference on Machine Learning*, pp. 1928–1937. PMLR, 2016.

Takashi Mori, Liu Ziyin, Kangqiao Liu, and Masahito Ueda. Power-law escape rate of sgd. In *International Conference on Machine Learning*, pp. 15959–15975. PMLR, 2022.

Ion Necoara, Yu Nesterov, and Francois Glineur. Linear convergence of first order methods for non-strongly convex optimization. *Mathematical programming*, 175(1):69–107, 2019.

Buqing Nie, Jingtian Ji, Yangqing Fu, and Yue Gao. Improve robustness of reinforcement learning against observation perturbations via l_∞ lipschitz policy networks. In *Proceedings of the AAAI Conference on Artificial Intelligence*, volume 38, pp. 14457–14465, 2024.

Arnab Nilim and Laurent Ghaoui. Robustness in markov decision problems with uncertain transition matrices. *Advances in neural information processing systems*, 16, 2003.

Tuomas Oikarinen, Wang Zhang, Alexandre Megretski, Luca Daniel, and Tsui-Wei Weng. Robust deep reinforcement learning through adversarial loss. *Advances in Neural Information Processing Systems*, 34:26156–26167, 2021.

Anay Pattanaik, Zhenyi Tang, Shuijing Liu, Gautham Bommannan, and Girish Chowdhary. Robust deep reinforcement learning with adversarial attacks. In *International Conference on Autonomous Agents and Multiagent Systems*, pp. 2040–2042, 2018. URL http://dl.acm.org/citation.cfm?id=3238064.

Lerrel Pinto, James Davidson, Rahul Sukthankar, and Abhinav Gupta. Robust adversarial reinforcement learning. In *International conference on machine learning*, pp. 2817–2826. PMLR, 2017.

Matteo Pirotta, Marcello Restelli, and Luca Bascetta. Policy gradient in lipschitz markov decision processes. *Machine Learning*, 100:255–283, 2015.

John Schulman, Sergey Levine, Pieter Abbeel, Michael Jordan, and Philipp Moritz. Trust region policy optimization. In *International Conference on Machine Learning*, pp. 1889–1897. PMLR, 2015.

John Schulman, Philipp Moritz, Sergey Levine, Michael Jordan, and Pieter Abbeel. High-dimensional continuous control using generalized advantage estimation. In *International Conference on Learning Representations*, 2016.

John Schulman, Filip Wolski, Prafulla Dhariwal, Alec Radford, and Oleg Klimov. Proximal policy optimization algorithms. *arXiv preprint arXiv:1707.06347*, 2017.

Qianli Shen, Yan Li, Haoming Jiang, Zhaoran Wang, and Tuo Zhao. Deep reinforcement learning with robust and smooth policy. In *International Conference on Machine Learning*, pp. 8707–8718. PMLR, 2020.

David Silver, Guy Lever, Nicolas Heess, Thomas Degris, Daan Wierstra, and Martin Riedmiller. Deterministic policy gradient algorithms. In *International Conference on Machine Learning*, pp. 387–395. PMLR, 2014.

David Silver, Aja Huang, Chris J Maddison, Arthur Guez, Laurent Sifre, George Van Den Driessche, Julian Schrittwieser, Ioannis Antonoglou, Veda Panneershelvam, Marc Lanctot, et al. Mastering the game of go with deep neural networks and tree search. *Nature*, 529(7587):484–489, 2016.

Aman Sinha, Hongseok Namkoong, and John Duchi. Certifiable distributional robustness with principled adversarial training. In *International Conference on Learning Representations*, 2018. URL https://openreview.net/forum?id=Hk6kPgZA-.

Chung-En Sun, Sicun Gao, and Tsui-Wei Weng. Breaking the barrier: Enhanced utility and robustness in smoothed DRL agents. In *Proceedings of the 41st International Conference on Machine Learning*, volume 235 of *Proceedings of Machine Learning Research*, pp. 46957–46987. PMLR, 21–27 Jul 2024. URL https://proceedings.mlr.press/v235/sun24b.html.

Yanchao Sun, Ruijie Zheng, Yongyuan Liang, and Furong Huang. Who is the strongest enemy? towards optimal and efficient evasion attacks in deep RL. In *International Conference on Learning Representations*, 2022. URL https://openreview.net/forum?id=JM2kFbJvvI.

Richard S Sutton. Learning to predict by the methods of temporal differences. *Machine Learning*, 3:9–44, 1988.

Chen Tang, Ben Abbatematteo, Jiaheng Hu, Rohan Chandra, Roberto Martín-Martín, and Peter Stone. Deep reinforcement learning for robotics: A survey of real-world successes. In *Proceedings of the AAAI Conference on Artificial Intelligence*, volume 39, pp. 28694–28698, 2025.

Emanuel Todorov, Tom Erez, and Yuval Tassa. Mujoco: A physics engine for model-based control. In *2012 IEEE/RSJ International Conference on Intelligent Robots and Systems*, pp. 5026–5033. IEEE, 2012.

Lun Wang, Zaynah Javed, Xian Wu, Wenbo Guo, Xinyu Xing, and Dawn Song. Backdoorl: Backdoor attack against competitive reinforcement learning. In *International Joint Conference on Artificial Intelligence*, pp. 3699–3705, 2021. URL https://doi.org/10.24963/ijcai.2021/509.

Mingze Wang and Lei Wu. A theoretical analysis of noise geometry in stochastic gradient descent. *arXiv preprint arXiv:2310.00692*, 2023.

Yisen Wang, Xingjun Ma, James Bailey, Jinfeng Yi, Bowen Zhou, and Quanquan Gu. On the convergence and robustness of adversarial training. In Kamalika Chaudhuri and Ruslan Salakhutdinov (eds.), *Proceedings of the 36th International Conference on Machine Learning*, volume 97 of *Proceedings of Machine Learning Research*, pp. 6586–6595. PMLR, 09–15 Jun 2019. URL https://proceedings.mlr.press/v97/wang19i.html.

Tsui-Wei Weng, Krishnamurthy Dj Dvijotham, Jonathan Uesato, Kai Xiao, Sven Gowal, Robert Stanforth, and Pushmeet Kohli. Toward evaluating robustness of deep reinforcement learning with continuous control. In *International Conference on Learning Representations*, 2019.

Wolfram Wiesemann, Daniel Kuhn, and Berç Rustem. Robust markov decision processes. *Mathematics of Operations Research*, 38(1):153–183, 2013.

Stephan Wojtowytsch. Stochastic gradient descent with noise of machine learning type part ii: Continuous time analysis. *Journal of Nonlinear Science*, 34(1):16, 2024.

Fan Wu, Linyi Li, Zijian Huang, Yevgeniy Vorobeychik, Ding Zhao, and Bo Li. CROP: Certifying robust policies for reinforcement learning through functional smoothing. In *International Conference on Learning Representations*, 2022a. URL https://openreview.net/forum?id=HOjLHrlZhmx.

Jingfeng Wu, Wenqing Hu, Haoyi Xiong, Jun Huan, Vladimir Braverman, and Zhanxing Zhu. On the noisy gradient descent that generalizes as sgd. In *International Conference on Machine Learning*, pp. 10367–10376. PMLR, 2020.

Lei Wu, Mingze Wang, and Weijie Su. The alignment property of sgd noise and how it helps select flat minima: A stability analysis. *Advances in Neural Information Processing Systems*, 35:4680–4693, 2022b.

Huajian Xin, Z.Z. Ren, Junxiao Song, Zhihong Shao, Wanjia Zhao, Haocheng Wang, Bo Liu, Liyue Zhang, Xuan Lu, Qiushi Du, Wenjun Gao, Haowei Zhang, Qihao Zhu, Dejian Yang, Zhibin Gou, Z.F. Wu, Fuli Luo, and Chong Ruan. Deepseek-prover-v1.5: Harnessing proof assistant feedback for reinforcement learning and monte-carlo tree search. In *The Thirteenth International Conference on Learning Representations*, 2025. URL https://openreview.net/forum?id=I4YAIwrsXa.

Bohang Zhang, Jikai Jin, Cong Fang, and Liwei Wang. Improved analysis of clipping algorithms for non-convex optimization. *Advances in Neural Information Processing Systems*, 33:15511–15521, 2020a.

Bohang Zhang, Du Jiang, Di He, and Liwei Wang. Rethinking lipschitz neural networks and certified robustness: A boolean function perspective. *Advances in Neural Information Processing Systems*, 35:19398–19413, 2022.

Huan Zhang, Hongge Chen, Chaowei Xiao, Sven Gowal, Robert Stanforth, Bo Li, Duane Boning, and Cho-Jui Hsieh. Towards stable and efficient training of verifiably robust neural networks. In *International Conference on Learning Representations*, 2020b. URL https://openreview.net/forum?id=Skxuk1rFwB.

Huan Zhang, Hongge Chen, Chaowei Xiao, Bo Li, Mingyan Liu, Duane Boning, and Cho-Jui Hsieh. Robust deep reinforcement learning against adversarial perturbations on state observations. *Advances in Neural Information Processing Systems*, 33:21024–21037, 2020c.

Huan Zhang, Hongge Chen, Duane S Boning, and Cho-Jui Hsieh. Robust reinforcement learning on state observations with learned optimal adversary. In *International Conference on Learning Representations*, 2021. URL https://openreview.net/forum?id=sCZbhBvqQaU.

Jingzhao Zhang, Tianxing He, Suvrit Sra, and Ali Jadbabaie. Why gradient clipping accelerates training: A theoretical justification for adaptivity. In *International Conference on Learning Representations*, 2020d. URL https://openreview.net/forum?id=BJgnXpVYwS.

Zhanpeng Zhou, Mingze Wang, Yuchen Mao, Bingrui Li, and Junchi Yan. Sharpness-aware minimization efficiently selects flatter minima late in training. In *The Thirteenth International Conference on Learning Representations*, 2025. URL https://openreview.net/forum?id=aD2uwhLbnA.

Zhanxing Zhu, Jingfeng Wu, Bing Yu, Lei Wu, and Jinwen Ma. The anisotropic noise in stochastic gradient descent: Its behavior of escaping from sharp minima and regularization effects. In Kamalika Chaudhuri and Ruslan Salakhutdinov (eds.), *Proceedings of the 36th International Conference on Machine Learning*, volume 97 of *Proceedings of Machine Learning Research*, pp. 7654–7663. PMLR, 09–15 Jun 2019. URL https://proceedings.mlr.press/v97/zhu19e.html.

Difan Zou, Yuan Cao, Dongruo Zhou, and Quanquan Gu. Gradient descent optimizes over-parameterized deep relu networks. *Machine learning*, 109:467–492, 2020.

A Outline of Appendix

• **Appendix B:** We review related work on adversarial attacks and defenses for reinforcement learning against perturbations on state observation.

• **Appendix C:** Detailed theoretical analysis of ARPO, including proofs for the adversary's policy gradient (Theorem 3.1) in Appendix C.1, convergence (Theorem 3.2) in Appendix C.2, and learning dynamics in Appendix C.3.

• **Appendix D:** An intuitive analysis of a toy ISA-MDP, corresponding to Propositions 3.1 and 3.2.

• **Appendix E:** The analysis and proof for the KL-based surrogate adversary (Theorem 4.1).

• **Appendix F:** Additional implementation details, including pseudocode for ARPO (Appendix F.1) and BARPO (Appendix F.2), hyperparameter settings (Appendix F.3), and compute resources (Appendix F.4).

• **Appendix G:** Additional experimental results, including detailed comparisons (Appendix G.1), statistical significance analysis (Appendix G.2), extended experiments on Humanoid (Appendix G.3), and ablation studies on the regularization coefficient κ (Appendix G.4) and our proposed components (Appendices G.6 and G.7).

• **Appendix H:** Further discussions clarifying our contributions and convergence proof (Appendix H.1), the novelty of the bilevel framework (Appendix H.2), and a deeper theoretical examination of BARPO (Appendices H.3 and H.4).

• **Appendices I and J:** A discussion of limitations, future work, and a clarification on the use of large language models.

B Related Work

B.1 Attacks on State Observations of DRL Agents

Adversarial Attacks on State Observations of DRL Agents. The susceptibility of DRL agents to adversarial attacks was initially exposed by Huang et al. (2017), who demonstrated that DRL policies could be significantly disrupted using the Fast Gradient Sign Method (FGSM) (Goodfellow et al., 2015) in Atari environments. This seminal discovery laid the foundation for a wave of subsequent studies on adversarial strategies and policy robustness in DRL. Building on this, Lin et al. (2017) and Kos & Song (2017) proposed limited-step perturbation techniques aimed at misleading DRL policies, revealing that even small, strategically applied modifications could impair agent behavior. In a further advancement, Pattanaik et al. (2018) exploited the critic function alongside gradient descent to craft adversarial inputs that degrade policy performance more systematically. Behzadan & Munir (2017a) extended the threat model by introducing black-box attacks on DQN, confirming that adversarial examples could successfully transfer across different network architectures, thereby emphasizing their real-world applicability. Meanwhile, Inkawhich et al. (2020) demonstrated that even adversaries with access restricted to action and reward signals, without internal model information, could still inflict considerable harm. In the domain of continuous control, Weng et al. (2019) devised a two-step adversarial framework leveraging learned dynamics models to generate more effective attacks. Furthermore, Zhang et al. (2021) and Sun et al. (2022) advanced the field by training adversarial agents using reinforcement learning, giving rise to adaptive attack strategies known as SA-RL and PA-AD. Korkmaz (2023) investigated adversarial directions in the Arcade Learning Environment and discovered that even state-of-the-art robust agents (Zhang et al., 2020c; Oikarinen et al., 2021) remain susceptible to perturbations aligned with policy-independent sensitivity axes. Most recently, Liang et al. (2024) proposed a temporally-coupled attack strategy that exploits temporal correlations to further compromise the performance of robust policies.

Other Attacks on DRL Agents. Research by Kiourti et al. (2020); Wang et al. (2021); Bharti et al. (2022); Guo et al. (2023) delved deeper into backdoor attacks within reinforcement learning, revealing profound vulnerabilities that pose significant threats to policy integrity. In a novel contribution, Lu et al. (2023) proposed an adversarial cheap talk framework, where an attacker is trained via meta-learning to manipulate agent behavior through indirect communication. Franzmeyer et al. (2024) introduced a dual ascent-based approach to train an end-to-end illusory attack capable of deceiving DRL agents effectively. In the context of multi-agent environments, Gleave et al. (2020)

examined how adversarial policies can manipulate or destabilize cooperative or competitive dynamics among agents.

Collectively, these studies reveal the broad and persistent vulnerability of DRL agents to adversarial manipulation across diverse threat models and environments. From observation perturbations and black-box attacks to communication-based deception and multi-agent exploitation, adversaries have consistently demonstrated the ability to significantly degrade policy performance, highlighting the urgent need for continued advancements in defense mechanisms.

B.2 Developing Robust DRL Agents Against Perturbations on State Observation

Early Attempts to Develop Robust Agents. Early efforts by Kos & Song (2017); Behzadan & Munir (2017b) explored incorporating adversarial states into the replay buffer during training on Atari environments, although these approaches yielded only limited robustness improvements. To address this, Fischer et al. (2019) proposed a decoupled architecture for DQN, separating it into a Q-network and a policy network, and robustly trained the policy component using generated adversarial states under provable robustness guarantees.

Smoothing Techniques. Shen et al. (2020) demonstrated that applying smoothness regularization can simultaneously improve both the natural performance and robustness of TRPO (Schulman et al., 2015) and DDPG (Silver et al., 2014) algorithms. Building on this idea, Wu et al. (2022a) and Kumar et al. (2022) employed Randomized Smoothing (RS) techniques to achieve certifiable robustness guarantees. More recently, Sun et al. (2024) proposed an innovative smoothing approach designed to mitigate the common issue of robustness overestimation, thereby enhancing both natural and robust returns in tandem. Importantly, these smoothing methods are complementary to our work and can be seamlessly integrated into our proposed algorithms.

Robust Multi-Agent DRL. In the context of multi-agent systems, He et al. (2023) investigated state adversaries within Markov Games and developed robust multi-agent Q-learning and actor-critic algorithms to achieve robust equilibrium solutions. Building on robustness regularization techniques (Shen et al., 2020; Zhang et al., 2020c), Bukharin et al. (2024) extended these methods to multi-agent environments by considering sub-optimal Lipschitz continuous policies in smooth settings. Liu et al. (2024a) proposed an adversarial training framework employing two timescales to ensure effective convergence towards robust policies. Another research direction involves alternating training between agents and learned adversaries (Zhang et al., 2021; Sun et al., 2022), which Liang et al. (2024) further formalized within a game-theoretic framework.

Beyond the Worst-Case Robustness. Furthermore, Liu et al. (2024b) introduced an adaptive defense mechanism during testing, leveraging a set of non-dominated policies. The latest work by Belaire et al. (2025) considers the partial observability setting and balances the value optimization with robustness based on beliefs.

Adversarially Robust Training for DRL Agents. In this paper, we mainly focus on the adversarially robust training paradigm. Zhang et al. (2020c) formally modeled state-adversarial reinforcement learning as a state-adversarial Markov Decision Process and highlighted the potential absence of an Optimal Robust Policy. To tackle this, they introduced a TV-distance-based regularization technique to balance robustness with nominal performance. Building on this, Oikarinen et al. (2021) employed certified robustness bounds to construct the adversarial loss, which they integrated with standard training objectives. Liang et al. (2022) enhanced training efficiency by estimating worst-case value functions and combining them with classical Temporal Difference (TD) target (Sutton, 1988) or Generalized Advantage Estimation (GAE) (Schulman et al., 2016). Nie et al. (2024) proposed a DRL framework for discrete action spaces based on SortNet (Zhang et al., 2022), which ensures global Lipschitz continuity and eliminates the need for training additional adversarial agents. More recently, Li et al. (2024; 2025) developed the universal ISA-MDP framework, within which they formally proved the existence of the ORP and demonstrated its consistency with Bellman optimality policies. Moreover, they established that an infinity-measurement error is a necessary condition for adversarial robustness. However, their theoretical analysis is limited to worst-case settings for RE-

INFORCE and PPO. In contrast, our analysis builds upon practical policy gradient methods, making it broadly applicable to real-world policy optimization.

These studies underscore the crucial importance of developing robust DRL policies and highlight the ongoing challenges in enhancing adversarial robustness in DRL agents.

B.3 Robust RL Agents Against Perturbations on Transition Dynamics

Research on robustness against transition uncertainty (Pinto et al., 2017; Gu et al., 2019; Kamalaruban et al., 2020; Dong et al., 2025) is primarily formulated as Robust Markov Decision Processes (RMDPs) (Nilim & Ghaoui, 2003; Iyengar, 2005; Wiesemann et al., 2013). This paradigm differs fundamentally from SA-MDP. In SA-MDP, the adversary corrupts the policy input, forcing the agent to act on distorted observations. Consequently, robustness depends on the policy's stability with respect to state variations. In contrast, RMDPs involve perturbations to the environment's dynamics. The agent observes the true state, but the transition leads to a worst-case outcome. Since the decision precedes the perturbation, state-space smoothness does not guarantee robustness against dynamic shifts.

C Adversarially Robust Policy Optimization

In this section, we present a detailed theoretical analysis of ARPO. In the subsection C.1, we show the analysis of policy gradient for the adversary. In the subsection C.2, we show the convergence analysis of ARPO. And in the subsection C.3, we explore the learning dynamics in the neighborhood of FOSPs in both ARPO and SPO.

C.1 Policy Gradient for Adversary

Theorem C.1 (Policy Gradient for Adversary)**.** *Given a policy π_θ, for all state $s \in \mathcal{S}$, we have*

$$\begin{aligned}\nabla_\vartheta V^{\pi_\theta \circ \nu_\vartheta}(s) &= \mathbb{E}_{\tau\sim\pi_\theta\circ\nu_\vartheta,\mathbb{P}}\left[R(\tau)\sum_{t=0}^{\infty}\nabla_\vartheta \log \pi_\theta(a_t|\nu_\vartheta(s_t))\right]\\ &= \mathbb{E}_{\tau\sim\pi_\theta\circ\nu_\vartheta,\mathbb{P}}\left[\sum_{t=0}^{\infty}\gamma^t Q^{\pi_\theta\circ\nu_\vartheta}(s_t,a_t)\nabla_\vartheta \log \pi_\theta(a_t|\nu_\vartheta(s_t))\right]\\ &= \frac{1}{1-\gamma}\mathbb{E}_{(s',a')\sim d^{\pi_\theta\circ\nu_\vartheta}}\left[Q^{\pi_\theta\circ\nu_\vartheta}(s',a')\nabla_\vartheta \log \pi_\theta(a'|\nu_\vartheta(s'))\right].\end{aligned}$$

Specifically, consider the direct parameterization representation for adversary $\nu_\vartheta : \mathcal{S} \to \mathcal{S},\ s \mapsto s + \vartheta_s \in B(s)$. Then, for any state $s_i \in \mathcal{S}$, we have the state-wise policy gradient for the adversary

$$\begin{aligned}&\nabla_{\vartheta_{s_i}} V^{\pi_\theta\circ\nu_\vartheta}(s)\\ &= \mathbb{E}_{\tau\sim\pi_\theta\circ\nu_\vartheta,\mathbb{P}}\left[R(\tau)\sum_{t=0}^{\infty}\nabla_{\vartheta_{s_t}} \log \pi_\theta(a_t|s_t+\vartheta_{s_t})\cdot\mathbb{I}(s_t=s_i)\right],\\ &= \mathbb{E}_{\tau\sim\pi_\theta\circ\nu_\vartheta,\mathbb{P}}\left[\sum_{t=0}^{\infty}\gamma^t Q^{\pi_\theta\circ\nu_\vartheta}(s_t,a_t)\nabla_{\vartheta_{s_t}} \log \pi_\theta(a_t|s_t+\vartheta_{s_t})\cdot\mathbb{I}(s_t=s_i)\right]\\ &= \frac{1}{1-\gamma}\mathbb{E}_{(s',a')\sim d^{\pi_\theta\circ\nu_\vartheta}}\left[Q^{\pi_\theta\circ\nu_\vartheta}(s',a')\nabla_{\vartheta_{s'}} \log \pi_\theta(a'|s'+\vartheta_{s'})\cdot\mathbb{I}(s'=s_i)\right],\end{aligned} \tag{2}$$

where $d^{\pi\circ\nu}$ is the state-action visitation distribution under $\pi\circ\nu$ and $\mathbb{I}(\cdot)$ is the indicator function.

Remark C.1. *Equation (2) indicates that for computing the strongest adversary, we can decompose it into calculating the strongest adversary in every state after sampling.*

Proof. The definition of $V^{\pi_\theta\circ\nu_\vartheta}(s)$

$$V^{\pi_\theta\circ\nu_\vartheta}(s) = \mathbb{E}_{\tau\sim\pi_\theta\circ\nu_\vartheta,\mathbb{P}}\left[\sum_{t=0}^{\infty}\gamma^t r(s_t,a_t)|s_0=s\right] = \mathbb{E}_{\tau\sim\pi_\theta\circ\nu_\vartheta,\mathbb{P}}\left[R(\tau)|s_0=s\right].$$

The probability of attaining trajectory $\tau = \{s_0, a_0, s_1, a_1, \dots\}$ under π_θ and ν_ϑ with initial state distribution μ_0 is

$$\begin{aligned} P_{\theta,\vartheta}(\tau) &= \mu_0(s_0)\pi_\theta(a_0|\nu_\vartheta(s_0)) \prod_{i=1}^{\infty} \mathbb{P}(s_i|s_{i-1}, a_{i-1})\pi_\theta(a_i|\nu_\vartheta(s_i)) \\ &= \mu_0(s_0)(\pi_\theta \circ \nu_\vartheta)(a_0|s_0) \prod_{i=1}^{\infty} \mathbb{P}(s_i|s_{i-1}, a_{i-1})(\pi_\theta \circ \nu_\vartheta)(a_i|s_i). \end{aligned}$$

For any state s, compute the gradient of the adversarial value function with respect to ν.

$$\begin{aligned} &\nabla_\vartheta V^{\pi_\theta \circ \nu_\vartheta}(s) \\ &= \nabla_\vartheta \int_\tau R(\tau) P_{\theta,\vartheta}(\tau|s_0 = s) \\ &= \int_\tau R(\tau) \nabla_\vartheta P_{\theta,\vartheta}(\tau|s_0 = s) \\ &= \int_\tau R(\tau) P_{\theta,\vartheta}(\tau|s_0 = s) \nabla_\vartheta \log P_{\theta,\vartheta}(\tau|s_0 = s) \\ &= \int_\tau R(\tau) P_{\theta,\vartheta}(\tau) \sum_{t=0}^{\infty} \nabla_\vartheta \log(\pi_\theta \circ \nu_\vartheta)(a_t|s_t) \\ &= \mathbb{E}_{\tau \sim \pi_\theta \circ \nu_\vartheta, \mathbb{P}} \left[R(\tau) \sum_{t=0}^{\infty} \nabla_\vartheta \log(\pi_\theta \circ \nu_\vartheta)(a_t|s_t) \right] \\ &= \mathbb{E}_{\tau \sim \pi_\theta \circ \nu_\vartheta, \mathbb{P}} \left[R(\tau) \sum_{t=0}^{\infty} \nabla_\vartheta \log \pi_\theta(a_t|\nu_\vartheta(s_t)) \right]. \end{aligned}$$

Let $\tau_{:t} = \{s_0, a_0, s_1, a_1, \dots, s_t, a_t\}$. Furthermore, we have that

$$\begin{aligned} &\nabla_\vartheta V^{\pi_\theta \circ \nu_\vartheta}(s) \\ &= \mathbb{E}_{\tau \sim \pi_\theta \circ \nu_\vartheta, \mathbb{P}} \left[\sum_{i=0}^{\infty} \gamma^i r(s_i, a_i) \sum_{t=0}^{\infty} \nabla_\vartheta \log \pi_\theta(a_t|\nu_\vartheta(s_t)) \right] \\ &= \mathbb{E}_{\tau \sim \pi_\theta \circ \nu_\vartheta, \mathbb{P}} \left[\sum_{t=0}^{\infty} \sum_{i=0}^{\infty} \gamma^i r(s_i, a_i) \nabla_\vartheta \log \pi_\theta(a_t|\nu_\vartheta(s_t)) \right] \\ &= \mathbb{E}_{\tau \sim \pi_\theta \circ \nu_\vartheta, \mathbb{P}} \left[\sum_{t=0}^{\infty} \mathbb{E}_{\tau_{t:}} \left[\sum_{i=0}^{\infty} \gamma^i r(s_i, a_i) \nabla_\vartheta \log \pi_\theta(a_t|\nu_\vartheta(s_t)) \mid \tau_{:t-1} \right] \right] \\ &= \mathbb{E}_{\tau \sim \pi_\theta \circ \nu_\vartheta, \mathbb{P}} \left[\sum_{t=0}^{\infty} \mathbb{E}_{\tau_{t:}} \left[\left(\sum_{i<t} \gamma^i r(s_i, a_i) + \sum_{i \geq t} \gamma^i r(s_i, a_i) \right) \nabla_\vartheta \log \pi_\theta(a_t|\nu_\vartheta(s_t)) \mid \tau_{:t-1} \right] \right] \\ &= \mathbb{E}_{\tau \sim \pi_\theta \circ \nu_\vartheta, \mathbb{P}} \left[\sum_{t=0}^{\infty} \mathbb{E}_{\tau_{t:}} \left[\sum_{i=t}^{\infty} \gamma^i r(s_i, a_i) \nabla_\vartheta \log \pi_\theta(a_t|\nu_\vartheta(s_t)) \mid \tau_{:t-1} \right] \right] \\ &= \mathbb{E}_{\tau \sim \pi_\theta \circ \nu_\vartheta, \mathbb{P}} \left[\sum_{t=0}^{\infty} \sum_{i=t}^{\infty} \gamma^i r(s_i, a_i) \nabla_\vartheta \log \pi_\theta(a_t|\nu_\vartheta(s_t)) \right] \\ &= \mathbb{E}_{\tau \sim \pi_\theta \circ \nu_\vartheta, \mathbb{P}} \left[\sum_{t=0}^{\infty} \mathbb{E}_{\tau_{t+1:}} \left[\sum_{i=t}^{\infty} \gamma^i r(s_i, a_i) \nabla_\vartheta \log \pi_\theta(a_t|\nu_\vartheta(s_t)) \mid \tau_{:t} \right] \right] \\ &= \mathbb{E}_{\tau \sim \pi_\theta \circ \nu_\vartheta, \mathbb{P}} \left[\sum_{t=0}^{\infty} \mathbb{E}_{\tau_{t+1:}} \left[\sum_{i=t}^{\infty} \gamma^i r(s_i, a_i) \mid s_t, a_t \right] \nabla_\vartheta \log \pi_\theta(a_t|\nu_\vartheta(s_t)) \right] \\ &= \mathbb{E}_{\tau \sim \pi_\theta \circ \nu_\vartheta, \mathbb{P}} \left[\sum_{t=0}^{\infty} \gamma^t Q^{\pi_\theta \circ \nu_\vartheta}(s_t, a_t) \nabla_\vartheta \log \pi_\theta(a_t|\nu_\vartheta(s_t)) \right]. \end{aligned}$$

Algorithm 1 Adversarially Robust Policy Optimization with δ-Approximation Adversary

Input: training steps K in outer loop, outer loop step size η_k, inner loop PGD step K_P, inner loop PGD step size η_P, inner loop approximation accuracy δ, batch size B
Output: adversarially robust policy π_θ

Initialize θ and ϑ
for $k = 1$ **to** K **do**
  Initialize indicator vector $I = 1_{|\mathcal{S}|}$, PGD step number $j = 0$
  while $\|I\|_1 > 0$ & $j < K_P$ **do**
    Sample trajectories $\tau \sim \pi_\theta \circ \nu_\vartheta, \mathbb{P}$ until the batch is full.
    Compute the unbiased estimation of the action-value function $Q^{\pi_\theta \circ \nu_\vartheta}(s_t, a_t)$: $\widehat{Q^{\pi_\theta \circ \nu_\vartheta}}(s_t, a_t) := \sum_{t' \geq t} \gamma^{t'-t} r(s_{t'}, a_{t'})$, for all (s_t, a_t) in the batch
    for s in the batch **do**
      $\nu_\vartheta(s) \longleftarrow \nu_\vartheta(s) - \eta_P \cdot \operatorname{sign}\left(\widehat{Q^{\pi_\theta \circ \nu_\vartheta}}(s, a) \cdot \nabla_\vartheta \log \pi_\theta(a|\nu_\vartheta(s))\right) \cdot I(s)$
      $\nu_\vartheta(s) \longleftarrow \operatorname{clip}(\nu_\vartheta(s), s - \epsilon, s + \epsilon)$
      $I(s) = \mathbb{I}\left(\max_{s_\nu \in B(s)} \left\langle \nu_\vartheta(s) - s_\nu, \frac{1}{1-\gamma} \widehat{Q^{\pi_\theta \circ \nu_\vartheta}}(s, a) \cdot \nabla_\vartheta \log \pi_\theta\left(a|\nu_\vartheta(s)\right) \right\rangle > \delta\right)$
      $j \longleftarrow j + 1$
    end for
  end while
  Compute the unbiased estimation of the gradient of the value function $\nabla_\theta V^{\pi_\theta \circ \nu_\vartheta}(\mu_0)$: $\widehat{\nabla_\theta V^{\pi_\theta \circ \nu_\vartheta}}(\mu_0) := \frac{1}{(1-\gamma)|B|} \sum_{(s,a) \in B} \widehat{Q^{\pi_\theta \circ \nu_\vartheta}}(s, a) \cdot \nabla_\theta \log \pi_\theta\left(a|\nu_\vartheta(s)\right)$
  $\theta \longleftarrow \theta + \eta_k \widehat{\nabla_\theta V^{\pi_\theta \circ \nu_\vartheta}}(\mu_0)$
end for

Furthermore, through the definition of the state-action visitation distribution following the policy $\pi_\theta \circ \nu_\vartheta$ starting from s: $d_s^{\pi_\theta \circ \nu_\vartheta}(s', a') = \mathbb{E}_{s_t \sim \mathbb{P}(\cdot|s_{t-1}, a_{t-1}), a_t \sim \pi_\theta \circ \nu_\vartheta(\cdot|s_t)}\left[(1-\gamma) \sum_{t=0}^{\infty} \gamma^t \mathbb{I}(s_t = s', a_t = a')|s_0 = s\right]$, we have that

$$\nabla_\vartheta V^{\pi_\theta \circ \nu_\vartheta}(s) = \frac{1}{1-\gamma} \mathbb{E}_{(s', a') \sim d^{\pi_\theta \circ \nu_\vartheta}}\left[Q^{\pi_\theta \circ \nu_\vartheta}(s', a') \nabla_\vartheta \log \pi_\theta(a'|\nu_\vartheta(s'))\right].$$

Specifically, for the representation for adversary $\nu_\vartheta : \mathcal{S} \to \mathcal{S},\ s \mapsto s + \vartheta_s \in B(s)$, we have

$$\begin{aligned}
&\nabla_{\vartheta_{s_i}} V^{\pi_\theta \circ \nu_\vartheta}(s) \\
&= \mathbb{E}_{\tau \sim \pi_\theta \circ \nu_\vartheta, \mathbb{P}}\left[R(\tau) \sum_{t=0}^{\infty} \nabla_{\vartheta_{s_i}} \log \pi_\theta(a_t|\nu_\vartheta(s_t))\right] \\
&= \mathbb{E}_{\tau \sim \pi_\theta \circ \nu_\vartheta, \mathbb{P}}\left[R(\tau) \sum_{t=0}^{\infty} \nabla_{\vartheta_{s_i}} \log \pi_\theta(a_t|s_t + \vartheta_{s_t})\right] \\
&= \mathbb{E}_{\tau \sim \pi_\theta \circ \nu_\vartheta, \mathbb{P}}\left[R(\tau) \sum_{t=0}^{\infty} \nabla_{\vartheta_{s_t}} \log \pi_\theta(a_t|s_t + \vartheta_{s_t}) \cdot \mathbb{I}(s_t = s_i)\right].
\end{aligned}$$

Similarly, we have

$$\begin{aligned}
\nabla_{\vartheta_{s_i}} V^{\pi_\theta \circ \nu_\vartheta}(s) &= \mathbb{E}_{\tau \sim \pi_\theta \circ \nu_\vartheta, \mathbb{P}}\left[\sum_{t=0}^{\infty} \gamma^t Q^{\pi_\theta \circ \nu_\vartheta}(s_t, a_t) \nabla_{\vartheta_{s_t}} \log \pi_\theta(a_t|s_t + \vartheta_{s_t}) \cdot \mathbb{I}(s_t = s_i)\right] \\
&= \frac{1}{1-\gamma} \mathbb{E}_{(s', a') \sim d^{\pi_\theta \circ \nu_\vartheta}}\left[Q^{\pi_\theta \circ \nu_\vartheta}(s', a') \nabla_{\vartheta_{s'}} \log \pi_\theta(a'|s' + \vartheta_{s'}) \cdot \mathbb{I}(s' = s_i)\right].
\end{aligned}$$

This completes the proof. □

C.2 Convergence of Adversarially Robust Policy Optimization

We analyze the convergence properties of ARPO with δ-Approximation Adversary (Algorithm 1) in this subsection.

C.2.1 NOTATIONS

For a sampling trajectory $\tau = (s_0, a_0, r_0, \dots) \sim \pi_\theta \circ \nu_\vartheta, \mathbb{P}$, denote the unbiased estimation of the action-value function $Q^{\pi_\theta \circ \nu_\vartheta}$ as

$$\widehat{Q^{\pi_\theta \circ \nu_\vartheta}}(s_t, a_t) := \sum_{t' \geq t} \gamma^{t'-t} r(s_{t'}, a_{t'}), \forall (s_t, a_t) \in \tau.$$

For simplicity of writing and reading of the latter, denote the sampled estimate as:

$$\hat{v}(s, a; \theta, \vartheta) := \frac{1}{1-\gamma} \operatorname{sg}\left(\widehat{Q^{\pi_\theta \circ \nu_\vartheta}}(s, a)\right) \cdot \log \pi_\theta \left(a | \nu_\vartheta(s)\right), \tag{3}$$

whereas $\operatorname{sg}(\cdot)$ is the stop-gradient operator, meaning that $\widehat{Q^{\pi_\theta \circ \nu_\vartheta}}(s, a)$ is seen as a function according to (s, a) and is detached from the gradient operation for (θ, ϑ) in the following context. This implies that

$$\nabla_\theta \hat{v}(s, a; \theta, \vartheta) = \frac{1}{1-\gamma} \widehat{Q^{\pi_\theta \circ \nu_\vartheta}}(s, a) \cdot \nabla_\theta \log \pi_\theta \left(a | \nu_\vartheta(s)\right)$$
$$\nabla_\vartheta \hat{v}(s, a; \theta, \vartheta) = \frac{1}{1-\gamma} \widehat{Q^{\pi_\theta \circ \nu_\vartheta}}(s, a) \cdot \nabla_\vartheta \log \pi_\theta \left(a | \nu_\vartheta(s)\right).$$

Furthermore, denote the unbiased estimation of the gradient of the value function $\nabla_\theta V^{\pi_\theta \circ \nu_\vartheta}(\mu_0)$ as

$$\widehat{\nabla_\theta V^{\pi_\theta \circ \nu_\vartheta}}(\mu_0) := \frac{1}{|\tau|} \sum_{(s,a) \in \tau} \nabla_\theta \hat{v}(s, a; \theta, \vartheta),$$

and denote the unbiased estimation of the gradient of the value function $\nabla_\vartheta V^{\pi_\theta \circ \nu_\vartheta}(\mu_0)$ as

$$\widehat{\nabla_\vartheta V^{\pi_\theta \circ \nu_\vartheta}}(\mu_0) := \frac{1}{|\tau|} \sum_{(s,a) \in \tau} \nabla_\vartheta \hat{v}(s, a; \theta, \vartheta).$$

C.2.2 PREPARATIONS

We quantify the solution of inner optimization, that is, the adversary, by extending the First-Order Stationary Condition (FOSC) proposed by Wang et al. (2019).

Definition C.1 (δ-Approximation Adversary)**.** *For a given policy π_θ and the sampled estimation $\widehat{Q^{\pi_\theta \circ \nu_\vartheta}}(s, a)$, if $\nu_\vartheta(s)$ satisfies the following condition:*

$$\max_{s_\nu \in B(s)} \left\langle \nu_\vartheta(s) - s_\nu, \frac{1}{1-\gamma} \widehat{Q^{\pi_\theta \circ \nu_\vartheta}}(s, a) \cdot \nabla_\vartheta \log \pi_\theta \left(a | \nu_\vartheta(s)\right) \right\rangle \leq \delta,$$

then, we called that the $\nu_\vartheta(s)$ is δ-approximation adversary for the strongest adversary $\nu^*(s; \pi_\theta)$.

Before our main convergence analysis, we provide a few assumptions utilized in our analysis.

Assumption C.1 (Lipschitz of Sampled Policy Gradient)**.** *The function $\hat{v}(s, a; \theta, \vartheta)$ satisfies the gradient Lipschitz conditions as follows:*

$$\sup_{s,a,\vartheta} \|\nabla_\theta \hat{v}(s, a; \theta, \vartheta) - \nabla_\theta \hat{v}(s, a; \theta', \vartheta)\|_2 \leq L_{\theta\theta} \|\theta - \theta'\|_2,$$
$$\sup_{s,a,\vartheta} \|\nabla_\vartheta \hat{v}(s, a; \theta, \vartheta) - \nabla_\vartheta \hat{v}(s, a; \theta', \vartheta)\|_2 \leq L_{\vartheta\theta} \|\theta - \theta'\|_2,$$
$$\sup_{a,\theta} \|\nabla_\theta \hat{v}(s, a; \theta, \vartheta) - \nabla_\theta \hat{v}(s, a; \theta, \vartheta')\|_2 \leq L_{\theta\vartheta} \|\vartheta(s) - \vartheta'(s)\|_2, \ \forall s,$$

where $L_{\theta\theta},\ L_{\theta\vartheta},\ L_{\vartheta\theta}$ are positive constants.

Assumption C.1 has been made in previous research on adversarial robustness (Sinha et al., 2018; Wang et al., 2019). A line of studies on deep neural networks helps to justify this assumption (Allen-Zhu et al., 2019; Du et al., 2019; Zou et al., 2020).

Assumption C.2 (Bounded Sampled Policy Gradient)**.** *The gradient of the function $\hat{v}(s,a;\theta,\vartheta)$ with respect to θ is uniformly bounded, i.e., $\exists\, M_{\hat{v}} > 0$, such that*

$$\sup_{s,a,\theta,\vartheta} \|\nabla_\theta \hat{v}(s,a;\theta,\vartheta)\| \leq M_{\hat{v}}.$$

Assumption C.2 can be verified by bounded rewards and the lower-bounded probability of the sampled action, which are mild conditions in practical algorithms.

Assumption C.3 (Locally Strongly Convex Adversary)**.** *For any state s and action a, the function $\hat{v}(s,a;\theta,\vartheta)$ is locally μ-strongly convex in $B_\epsilon(s) = \{\nu_\vartheta(s) := s + \vartheta_s \mid \|\vartheta_s\|_\infty \leq \epsilon\}$, i.e., for any ϑ_1, ϑ_2, we have that*

$$\hat{v}(s,a;\theta,\vartheta_1) \geq \hat{v}(s,a;\theta,\vartheta_2) + \langle \nabla_\vartheta \hat{v}(s,a;\theta,\vartheta_2), \vartheta_1(s) - \vartheta_2(s)\rangle + \frac{\mu}{2}\|\vartheta_1(s) - \vartheta_2(s)\|_2^2.$$

Assumption C.3 has been studied in Sinha et al. (2018); Lee & Raginsky (2018), which can be verified by the relation between robust optimization and distributional robust optimization.

Assumption C.4 (Lipschitz Conditions of State-Action Visitation Distribution)**.** *The state-action visitation distribution under policy $\pi_\theta \circ \nu_\vartheta$ $d_{\theta,\vartheta}(s,a) := d_{\mu_0}^{\pi_\theta \circ \nu_\vartheta}(s,a) = \mathbb{E}_{s_0\sim\mu_0(\cdot), s_t\sim\mathbb{P}(\cdot|s_{t-1},a_{t-1}), a_t\sim\pi_\theta\circ\nu_\vartheta(\cdot|s_t)}\left[(1-\gamma)\sum_{t=0}^\infty \gamma^t \mathbb{I}(s_t = s, a_t = a)\right]$ satisfies the Lipschitz conditions under the total variation distance as follows:*

$$\sup_\vartheta \|d_{\theta,\vartheta} - d_{\theta',\vartheta}\|_{\mathrm{TV}} \leq L_{d\theta}\|\theta - \theta'\|_2,$$
$$\sup_\theta \|d_{\theta,\vartheta} - d_{\theta,\vartheta'}\|_{\mathrm{TV}} \leq L_{d\vartheta}\|\vartheta - \vartheta'\|_2.$$

Assumption C.4 has been derived by Pirotta et al. (2015) based on Lipschitz environments and policy. Certain natural environments show smooth reward functions and transition dynamics, especially in continuous control tasks where the transition dynamics come from some physical laws (Bukharin et al., 2024; Li et al., 2025), such as MuJoCo environments, where we conduct numerical experiments. These environments are thus Lipschitz. The policy parameterized by neural networks can be seen as Lipschitz based on neural network analysis (Allen-Zhu et al., 2019; Du et al., 2019; Zou et al., 2020).

Assumption C.5 (Bounded Variance)**.** *The variance of the stochastic gradient is bounded as follows:*

$$\mathbb{E}\left[\left\|\nabla_\theta \widehat{V^{\pi_\theta\circ\nu^*}(\pi_\theta)}(\mu_0) - \nabla_\theta V^{\pi_\theta\circ\nu^*(\pi_\theta)}(\mu_0)\right\|\right] \leq \sigma^2.$$

Assumption C.5 is a common assumption in the analysis of stochastic optimization.

The proof framework of Theorem C.2 is drawn on Wang et al. (2019); Pirotta et al. (2015). We begin by proving the following four technical lemmas.

Lemma C.1 (Lipschitz of Strongest Adversary)**.** *Suppose assumptions C.1 and C.3 hold. Then we have that the strongest adversary $\vartheta^*(s;\theta_1)$ is $\frac{L_{\vartheta\theta}}{\mu}$-smooth, i.e., given a state s, for any θ_1 and θ_2, we have that*

$$\|\vartheta^*(s;\theta_1) - \vartheta^*(s;\theta_2)\|_2 \leq \frac{L_{\vartheta\theta}}{\mu}\|\theta_1 - \theta_2\|_2.$$

Proof. For any state s and action a, under assumption C.3, we have that

$$\begin{aligned}
&\hat{v}(s,a;\theta_2,\vartheta^*(\theta_1)) \\
&\geq \hat{v}(s,a;\theta_2,\vartheta^*(\theta_2)) + \langle \nabla_\vartheta \hat{v}(s,a;\theta_2,\vartheta^*(\theta_2)), \vartheta^*(s;\theta_1) - \vartheta^*(s;\theta_2)\rangle \\
&\quad + \frac{\mu}{2}\|\vartheta^*(s;\theta_1) - \vartheta^*(s;\theta_2)\|_2^2 \\
&\geq \hat{v}(s,a;\theta_2,\vartheta^*(\theta_2)) + \frac{\mu}{2}\|\vartheta^*(s;\theta_1) - \vartheta^*(s;\theta_2)\|_2^2,
\end{aligned}$$

where the last inequality comes from $\langle \nabla_\vartheta \hat{v}(s,a;\theta_2,\vartheta^*(\theta_2)), \vartheta^*(s;\theta_1) - \vartheta^*(s;\theta_2)\rangle \geq 0$. Similarly, we have

$$\begin{aligned}
&\hat{v}(s,a;\theta_2,\vartheta^*(\theta_2)) \\
&\geq \hat{v}(s,a;\theta_2,\vartheta^*(\theta_1)) + \langle \nabla_\vartheta \hat{v}(s,a;\theta_2,\vartheta^*(\theta_1)), \vartheta^*(s;\theta_2) - \vartheta^*(s;\theta_1)\rangle \\
&\quad + \frac{\mu}{2}\|\vartheta^*(s;\theta_1) - \vartheta^*(s;\theta_2)\|_2^2.
\end{aligned}$$

Combining the above two inequalities, we have

$$\begin{aligned}
&\mu\|\vartheta^*(s;\theta_1)-\vartheta^*(s;\theta_2)\|_2^2\\
\le&\langle\nabla_\vartheta\hat{v}(s,a;\theta_2,\vartheta^*(\theta_1)),\vartheta^*(s;\theta_1)-\vartheta^*(s;\theta_2)\rangle\\
\le&\langle\nabla_\vartheta\hat{v}(s,a;\theta_2,\vartheta^*(\theta_1))-\nabla_\vartheta\hat{v}(s,a;\theta_1,\vartheta^*(\theta_1)),\vartheta^*(s;\theta_1)-\vartheta^*(s;\theta_2)\rangle\\
\le&\|\nabla_\vartheta\hat{v}(s,a;\theta_2,\vartheta^*(\theta_1))-\nabla_\vartheta\hat{v}(s,a;\theta_1,\vartheta^*(\theta_1))\|_2\cdot\|\vartheta^*(s;\theta_1)-\vartheta^*(s;\theta_2)\|_2\\
\le&L_{\vartheta\theta}\|\theta_2-\theta_1\|_2\cdot\|\vartheta^*(s;\theta_1)-\vartheta^*(s;\theta_2)\|_2.
\end{aligned}$$

The second inequality comes from $\langle-\nabla_\vartheta\hat{v}(s,a;\theta_1,\vartheta^*(\theta_1)),\vartheta^*(s;\theta_1)-\vartheta^*(s;\theta_2)\rangle\ge 0$. The third inequality comes from the Cauchy-Schwarz inequality, and the last inequality comes from Assumption C.1. Therefore, we have that

$$\|\vartheta^*(s;\theta_1)-\vartheta^*(s;\theta_2)\|_2\le\frac{L_{\vartheta\theta}}{\mu}\|\theta_2-\theta_1\|_2.$$

This proof is concluded. □

Lemma C.2 (Lipschitz of Sampled Policy Gradient against Strongest Adversary)**.** *Suppose assumptions C.1 and C.3 hold. Then we have that the sampling estimation $\hat{v}(s,a;\theta,\vartheta^*(\theta))$ is $L_{\hat{v}}$-smooth, i.e., for any θ_1 and θ_2, we have that*

$$\|\nabla_\theta\hat{v}(s,a;\theta_1,\vartheta^*(\theta_1))-\nabla_\theta\hat{v}(s,a;\theta_2,\vartheta^*(\theta_2))\|_2\le L_{\hat{v}}\|\theta_1-\theta_2\|_2,$$

where $L_{\hat{v}}=\frac{L_{\theta\vartheta}L_{\vartheta\theta}}{\mu}+L_{\theta\theta}$.

Proof. For any θ_1 and θ_2, we have that

$$\begin{aligned}
&\|\nabla_\theta\hat{v}(s,a;\theta_1,\vartheta^*(\theta_1))-\nabla_\theta\hat{v}(s,a;\theta_2,\vartheta^*(\theta_2))\|_2\\
\le&\|\nabla_\theta\hat{v}(s,a;\theta_1,\vartheta^*(\theta_1))-\nabla_\theta\hat{v}(s,a;\theta_1,\vartheta^*(\theta_2))\|_2\\
&+\|\nabla_\theta\hat{v}(s,a;\theta_1,\vartheta^*(\theta_2))-\nabla_\theta\hat{v}(s,a;\theta_2,\vartheta^*(\theta_2))\|_2\\
\le&L_{\theta\vartheta}\|\vartheta^*(s;\theta_1)-\vartheta^*(s;\theta_2)\|_2+L_{\theta\theta}\|\theta_1-\theta_2\|_2\\
\le&\left(\frac{L_{\theta\vartheta}L_{\vartheta\theta}}{\mu}+L_{\theta\theta}\right)\|\theta_1-\theta_2\|_2.
\end{aligned}$$

The first inequality comes from the triangle inequality, the second inequality comes from Assumption C.1, and the last inequality comes from Lemma C.1. Therefore, the proof is concluded. □

Lemma C.3 (Smoothness of Adversarial Value Function against Strongest Adversary)**.** *Suppose assumptions C.1, C.2, C.3, and C.4 hold. Then we have that $V^{\pi_\theta\circ\nu^*(\pi_\theta)}(\mu_0)$ is L-smooth, i.e., for any θ_1 and θ_2, we have that*

$$\begin{aligned}
&\left|V^{\pi_{\theta_1}\circ\nu^*(\pi_{\theta_1})}(\mu_0)-V^{\pi_{\theta_2}\circ\nu^*(\pi_{\theta_2})}(\mu_0)-\langle\nabla_\theta V^{\pi_{\theta_2}\circ\nu^*(\pi_{\theta_2})}(\mu_0),\theta_1-\theta_2\rangle\right|\le\frac{L}{2}\|\theta_1-\theta_2\|_2^2,\\
&\|\nabla_\theta V^{\pi_{\theta_1}\circ\nu^*(\pi_{\theta_1})}(\mu_0)-\nabla_\theta V^{\pi_{\theta_2}\circ\nu^*(\pi_{\theta_2})}(\mu_0)\|_2\le L\|\theta_1-\theta_2\|_2,
\end{aligned}$$

where $L=\frac{L_{\theta\vartheta}L_{\vartheta\theta}}{\mu}+L_{\theta\theta}+M_{\hat{v}}\left(\frac{L_{d\vartheta}L_{\vartheta\theta}}{\mu}+L_{d\theta}\right)$.

Proof. For any θ_1 and θ_2, we have

$$\begin{aligned}
&\|\nabla_\theta V^{\pi_{\theta_1}\circ\nu^*(\pi_{\theta_1})}(\mu_0)-\nabla_\theta V^{\pi_{\theta_2}\circ\nu^*(\pi_{\theta_2})}(\mu_0)\|_2\\
=&\left\|\mathbb{E}_{(s,a)\sim d_{\theta_1,\vartheta^*(\theta_1)}}\left[\nabla_\theta\hat{v}(s,a;\theta_1,\vartheta^*(\theta_1))\right]-\mathbb{E}_{(s,a)\sim d_{\theta_2,\vartheta^*(\theta_2)}}\left[\nabla_\theta\hat{v}(s,a;\theta_2,\vartheta^*(\theta_2))\right]\right\|_2\\
\le&\left\|\mathbb{E}_{(s,a)\sim d_{\theta_1,\vartheta^*(\theta_1)}}\left[\nabla_\theta\hat{v}(s,a;\theta_1,\vartheta^*(\theta_1))-\nabla_\theta\hat{v}(s,a;\theta_2,\vartheta^*(\theta_2))\right]\right\|_2\\
&+\left\|\mathbb{E}_{(s,a)\sim\left(d_{\theta_1,\vartheta^*(\theta_1)}-d_{\theta_2,\vartheta^*(\theta_2)}\right)}\left[\nabla_\theta\hat{v}(s,a;\theta_2,\vartheta^*(\theta_2))\right]\right\|_2.
\end{aligned}$$

This inequality comes from the triangle inequality. For the first item, we have

$$\begin{aligned}
&\left\|\mathbb{E}_{(s,a)\sim d_{\theta_1,\vartheta^*(\theta_1)}}\left[\nabla_\theta \hat{v}(s,a;\theta_1,\vartheta^*(\theta_1)) - \nabla_\theta \hat{v}(s,a;\theta_2,\vartheta^*(\theta_2))\right]\right\|_2 \\
\leq\ &\mathbb{E}_{(s,a)\sim d_{\theta_1,\vartheta^*(\theta_1)}}\left[\|\nabla_\theta \hat{v}(s,a;\theta_1,\vartheta^*(\theta_1)) - \nabla_\theta \hat{v}(s,a;\theta_2,\vartheta^*(\theta_2))\|_2\right] \\
\leq\ &\left(\frac{L_{\theta\vartheta}L_{\vartheta\theta}}{\mu} + L_{\theta\theta}\right)\|\theta_1-\theta_2\|_2,
\end{aligned}$$

where the last inequality comes from Lemma C.2. For the second item, we have that

$$\begin{aligned}
&\left\|\mathbb{E}_{(s,a)\sim\left(d_{\theta_1,\vartheta^*(\theta_1)} - d_{\theta_2,\vartheta^*(\theta_2)}\right)}\left[\nabla_\theta \hat{v}(s,a;\theta_2,\vartheta^*(\theta_2))\right]\right\|_2 \\
\leq\ &\left\|\mathbb{E}_{(s,a)\sim\left(d_{\theta_1,\vartheta^*(\theta_1)} - d_{\theta_1,\vartheta^*(\theta_2)}\right)}\left[\nabla_\theta \hat{v}(s,a;\theta_2,\vartheta^*(\theta_2))\right]\right\|_2 \\
&+\left\|\mathbb{E}_{(s,a)\sim\left(d_{\theta_1,\vartheta^*(\theta_2)} - d_{\theta_2,\vartheta^*(\theta_2)}\right)}\left[\nabla_\theta \hat{v}(s,a;\theta_2,\vartheta^*(\theta_2))\right]\right\|_2 \\
\leq\ &\|d_{\theta_1,\vartheta^*(\theta_1)} - d_{\theta_1,\vartheta^*(\theta_2)}\|_{\mathrm{TV}} \cdot \sup_{s,a}\|\nabla_\theta \hat{v}(s,a;\theta_2,\vartheta^*(\theta_2))\| \\
&+\|d_{\theta_1,\vartheta^*(\theta_2)} - d_{\theta_2,\vartheta^*(\theta_2)}\|_{\mathrm{TV}} \cdot \sup_{s,a}\|\nabla_\theta \hat{v}(s,a;\theta_2,\vartheta^*(\theta_2))\| \\
\leq\ &L_{d\vartheta}M_{\hat{v}}\|\vartheta^*(\theta_1) - \vartheta^*(\theta_2)\|_2 + L_{d\theta}M_{\hat{v}}\|\theta_1-\theta_2\|_2 \\
\leq\ &L_{d\vartheta}M_{\hat{v}}\frac{L_{\vartheta\theta}}{\mu}\|\theta_1-\theta_2\|_2 + L_{d\theta}M_{\hat{v}}\|\theta_1-\theta_2\|_2 \\
=\ &M_{\hat{v}}\left(\frac{L_{d\vartheta}L_{\vartheta\theta}}{\mu} + L_{d\theta}\right)\|\theta_1-\theta_2\|_2.
\end{aligned}$$

The penultimate equation comes from assumptions C.2 and C.4. The last inequality comes from Lemma C.1. Thus, we have that

$$\begin{aligned}
&\|\nabla_\theta V^{\pi_{\theta_1}\circ\nu^*(\pi_{\theta_1})}(\mu_0) - \nabla_\theta V^{\pi_{\theta_2}\circ\nu^*(\pi_{\theta_2})}(\mu_0)\|_2 \\
\leq\ &\left(\frac{L_{\theta\vartheta}L_{\vartheta\theta}}{\mu} + L_{\theta\theta} + M_{\hat{v}}\left(\frac{L_{d\vartheta}L_{\vartheta\theta}}{\mu} + L_{d\theta}\right)\right)\|\theta_1-\theta_2\|_2.
\end{aligned}$$

Therefore, the proof of this lemma is concluded. □

Lemma C.4 (Bounded Error of Approximate Stochastic Gradient)**.** *Suppose assumptions C.1 and C.3 hold. Then we can control the error of the approximate stochastic gradient in the ARPO with δ-approximation adversary in definition C.1 (Algorithm 1). Specifically, we have that*

$$\left\|\nabla_\theta\widehat{V^{\pi_\theta\circ\nu_\vartheta}}(\mu_0) - \nabla_\theta\widehat{V^{\pi_\theta\circ\nu^*}(\pi_\theta)}(\mu_0)\right\|_2 \leq L_{\theta\vartheta}\sqrt{\frac{\delta}{\mu}}.$$

Proof. We have that

$$\begin{aligned}
&\left\|\nabla_\theta\widehat{V^{\pi_\theta\circ\nu_\vartheta}}(\mu_0) - \nabla_\theta\widehat{V^{\pi_\theta\circ\nu^*}(\pi_\theta)}(\mu_0)\right\|_2 \\
=\ &\left\|\frac{1}{|\tau|}\sum_{(s,a)\in\tau}\left(\nabla_\theta \hat{v}(s,a;\theta,\vartheta) - \nabla_\theta \hat{v}(s,a;\theta,\vartheta^*(\theta))\right)\right\|_2 \\
\leq\ &\frac{1}{|\tau|}\sum_{(s,a)\in\tau}\|\nabla_\theta \hat{v}(s,a;\theta,\vartheta) - \nabla_\theta \hat{v}(s,a;\theta,\vartheta^*(\theta))\|_2 \\
\leq\ &\frac{1}{|\tau|}\sum_{(s,a)\in\tau}L_{\theta\vartheta}\left\|\vartheta(s) - \vartheta^*(s;\theta)\right\|_2.
\end{aligned}$$

The first inequality comes from the triangle inequality, and the last inequality comes from Assumption C.1. Under Assumption C.3, we have that

$$\hat{v}(s,a;\theta,\vartheta) \geq \hat{v}(s,a;\theta,\vartheta^*(\theta)) + \langle\nabla_\vartheta \hat{v}(s,a;\theta,\vartheta^*(\theta)), \vartheta(s) - \vartheta^*(s;\theta)\rangle + \frac{\mu}{2}\|\vartheta(s) - \vartheta^*(s;\theta)\|_2^2,$$

$$\hat{v}(s,a;\theta,\vartheta^*(\theta)) \geq \hat{v}(s,a;\theta,\vartheta) + \langle\nabla_\vartheta \hat{v}(s,a;\theta,\vartheta), \vartheta^*(s;\theta) - \vartheta(s)\rangle + \frac{\mu}{2}\|\vartheta(s) - \vartheta^*(s;\theta)\|_2^2.$$

Combining the above two inequalities, we have that

$$\begin{aligned}
&\mu\|\vartheta(s) - \vartheta^*(s;\theta)\|_2^2 \\
&\leq \langle \nabla_\vartheta \hat{v}(s,a;\theta,\vartheta) - \nabla_\vartheta \hat{v}(s,a;\theta,\vartheta^*(\theta)), \vartheta(s) - \vartheta^*(s;\theta)\rangle \\
&\leq \delta - \langle \nabla_\vartheta \hat{v}(s,a;\theta,\vartheta^*(\theta)), \vartheta(s) - \vartheta^*(s;\theta)\rangle \\
&\leq \delta.
\end{aligned}$$

The second inequality comes from that ν_ϑ is a δ-approximate maximizer of $\hat{v}(s,a;\theta,\vartheta)$, i.e.,

$$\langle \nabla_\vartheta \hat{v}(s,a;\theta,\vartheta), \vartheta(s) - \vartheta^*(s;\theta)\rangle \leq \delta.$$

The last inequality comes from the optimality of ϑ^*, i.e.,

$$\langle \nabla_\vartheta \hat{v}(s,a;\theta,\vartheta^*(\theta)), \vartheta(s) - \vartheta^*(s;\theta)\rangle \geq 0.$$

Therefore, we have that

$$\left\| \nabla_\theta \widehat{V^{\pi_\theta \circ \nu_\vartheta}}(\mu_0) - \nabla_\theta \widehat{V^{\pi_\theta \circ \nu^*}}(\pi_\theta)(\mu_0) \right\|_2 \leq L_{\theta\vartheta}\sqrt{\frac{\delta}{\mu}}.$$

This completes the proof of this lemma. □

C.2.3 Main Convergence Results

Based on these assumptions, we derive the main convergence property of ARPO.

Theorem C.2 (Convergence of ARPO). *Denote* $\Delta := \max_\theta \min_\vartheta V^{\pi_\theta \circ \nu_\vartheta}(\mu_0) - \min_\vartheta V^{\pi_{\theta_0} \circ \nu_\vartheta}(\mu_0)$. *Under assumptions C.1, C.2, C.3, C.4, and C.5, set the step size* $\eta_k = \sqrt{\frac{\Delta}{\sigma^2 LK}}$. *Then, for the ARPO with* δ*-approximation adversary in Definition C.1 (Algorithm 1) and* $K \geq \frac{\Delta L}{\sigma^2}$, *we have*

$$\frac{1}{K}\sum_{k=0}^{K-1} \mathbb{E}\left[\left\| \nabla_\theta V^{\pi_{\theta_k} \circ \nu^*(\pi_{\theta_k})}(\mu_0) \right\|_2^2 \right] \leq 4\sigma\sqrt{\frac{\Delta L}{K}} + \frac{2L_{\theta\vartheta}^2 \delta}{\mu},$$

where $L = \frac{L_{\theta\vartheta} L_{\vartheta\theta}}{\mu} + L_{\theta\theta} + M_{\hat{v}}\left(\frac{L_{d\vartheta} L_{\vartheta\theta}}{\mu} + L_{d\theta}\right)$.

Proof of Theorem C.2. For convenience, we denote the objective function $V(\theta) := V^{\pi_\theta \circ \nu^*(\pi_\theta)}(\mu_0)$, the accuracy stochastic gradient $G(\theta) := \nabla_\theta \widehat{V^{\pi_\theta \circ \nu^*(\pi_\theta)}}(\mu_0)$, and the approximation stochastic gradient $\hat{G}(\theta) := \nabla_\theta \widehat{V^{\pi_\theta \circ \nu_\vartheta}}(\mu_0)$. According to the gradient Lipschitz of $V^{\pi_\theta \circ \nu^*(\pi_\theta)}$ shown in Lemma C.3, we have that

$$\begin{aligned}
&V(\theta_{k+1}) \\
&\geq V(\theta_k) + \langle \nabla_\theta V(\theta_k), \theta_{k+1} - \theta_k\rangle - \frac{L}{2}\|\theta_{k+1} - \theta_k\|_2^2 \\
&= V(\theta_k) + \eta_k \langle \nabla_\theta V(\theta_k), \hat{G}(\theta_k)\rangle - \frac{L\eta_k^2}{2}\|\hat{G}(\theta_k)\|_2^2 \\
&= V(\theta_k) + \eta_k \|\nabla_\theta V(\theta_k)\|_2^2 - \frac{L\eta_k^2}{2}\|\hat{G}(\theta_k)\|_2^2 + \eta_k \langle \nabla_\theta V(\theta_k), \hat{G}(\theta_k) - \nabla_\theta V(\theta_k)\rangle \\
&= V(\theta_k) + \eta_k \left(1 - \frac{L\eta_k}{2}\right)\|\nabla_\theta V(\theta_k)\|_2^2 \\
&\quad + \eta_k (1 - L\eta_k)\langle \nabla_\theta V(\theta_k), \hat{G}(\theta_k) - \nabla_\theta V(\theta_k)\rangle - \frac{L\eta_k^2}{2}\|\hat{G}(\theta_k) - \nabla_\theta V(\theta_k)\|_2^2 \\
&= V(\theta_k) + \eta_k \left(1 - \frac{L\eta_k}{2}\right)\|\nabla_\theta V(\theta_k)\|_2^2 + \eta_k (1 - L\eta_k)\langle \nabla_\theta V(\theta_k), \hat{G}(\theta_k) - G(\theta_k)\rangle \\
&\quad + \eta_k (1 - L\eta_k)\langle \nabla_\theta V(\theta_k), G(\theta_k) - \nabla_\theta V(\theta_k)\rangle \\
&\quad - \frac{L\eta_k^2}{2}\|\hat{G}(\theta_k) - G(\theta_k) + G(\theta_k) - \nabla_\theta V(\theta_k)\|_2^2.
\end{aligned}$$

By Young's inequality, we have

$$\left|\langle \nabla_\theta V(\theta_k), \hat{G}(\theta_k) - G(\theta_k)\rangle\right| \leq \frac{1}{2}\left(\|\nabla_\theta V(\theta_k)\|_2^2 + \|\hat{G}(\theta_k) - G(\theta_k)\|_2^2\right),$$
$$\|\hat{G}(\theta_k) - G(\theta_k) + G(\theta_k) - \nabla_\theta V(\theta_k)\|_2^2 \leq 2\left(\|\hat{G}(\theta_k) - G(\theta_k)\|_2^2 + \|G(\theta_k) - \nabla_\theta V(\theta_k)\|_2^2\right).$$

Therefore, we have that

$$\begin{aligned}
&V(\theta_{k+1}) \\
\geq\ & V(\theta_k) + \eta_k\left(1 - \frac{L\eta_k}{2}\right)\|\nabla_\theta V(\theta_k)\|_2^2 \\
&- \frac{\eta_k}{2}(1 - L\eta_k)\left(\|\nabla_\theta V(\theta_k)\|_2^2 + \|\hat{G}(\theta_k) - G(\theta_k)\|_2^2\right) \\
&+ \eta_k(1 - L\eta_k)\langle \nabla_\theta V(\theta_k), G(\theta_k) - \nabla_\theta V(\theta_k)\rangle \\
&- L\eta_k^2\left(\|\hat{G}(\theta_k) - G(\theta_k)\|_2^2 + \|G(\theta_k) - \nabla_\theta V(\theta_k)\|_2^2\right). \\
=\ & V(\theta_k) + \frac{\eta_k}{2}\|\nabla_\theta V(\theta_k)\|_2^2 - \frac{\eta_k}{2}(1 + L\eta_k)\|\hat{G}(\theta_k) - G(\theta_k)\|_2^2 \\
&+ \eta_k(1 - L\eta_k)\langle \nabla_\theta V(\theta_k), G(\theta_k) - \nabla_\theta V(\theta_k)\rangle - L\eta_k^2\|G(\theta_k) - \nabla_\theta V(\theta_k)\|_2^2.
\end{aligned}$$

Taking the conditional expectation on both sides of the above inequality, we have that

$$\begin{aligned}
&\mathbb{E}\left[V(\theta_k) - V(\theta_{k+1}) \mid \theta_k\right] \\
\leq\ & -\frac{\eta_k}{2}\mathbb{E}\left[\|\nabla_\theta V(\theta_k)\|_2^2 \mid \theta_k\right] + \frac{\eta_k}{2}(1 + L\eta_k)\,\mathbb{E}\left[\|\hat{G}(\theta_k) - G(\theta_k)\|_2^2 \mid \theta_k\right] \\
&+ \eta_k(1 - L\eta_k)\,\mathbb{E}\left[\langle \nabla_\theta V(\theta_k), \nabla_\theta V(\theta_k) - G(\theta_k)\rangle \mid \theta_k\right] \\
&+ L\eta_k^2\mathbb{E}\left[\|G(\theta_k) - \nabla_\theta V(\theta_k)\|_2^2 \mid \theta_k\right] \\
=\ & -\frac{\eta_k}{2}\mathbb{E}\left[\|\nabla_\theta V(\theta_k)\|_2^2 \mid \theta_k\right] + \frac{\eta_k}{2}(1 + L\eta_k)\,\mathbb{E}\left[\|\hat{G}(\theta_k) - G(\theta_k)\|_2^2 \mid \theta_k\right] \\
&+ L\eta_k^2\mathbb{E}\left[\|G(\theta_k) - \nabla_\theta V(\theta_k)\|_2^2 \mid \theta_k\right] \\
\leq\ & -\frac{\eta_k}{2}\mathbb{E}\left[\|\nabla_\theta V(\theta_k)\|_2^2 \mid \theta_k\right] + \frac{\eta_k}{2}(1 + L\eta_k)\frac{L_{\theta\vartheta}^2\delta}{\mu} \\
&+ L\eta_k^2\mathbb{E}\left[\|G(\theta_k) - \nabla_\theta V(\theta_k)\|_2^2 \mid \theta_k\right] \\
\leq\ & -\frac{\eta_k}{2}\mathbb{E}\left[\|\nabla_\theta V(\theta_k)\|_2^2 \mid \theta_k\right] + \frac{\eta_k}{2}(1 + L\eta_k)\frac{L_{\theta\vartheta}^2\delta}{\mu} + L\eta_k^2\sigma^2.
\end{aligned}$$

The first equation comes from the unbiased estimation $G(\theta)$, i.e., $\mathbb{E}[G(\theta)] = \nabla_\theta V(\theta)$. The second inequality comes from Lemma C.4, and the last inequality comes from Assumption C.5. Taking the telescope sum of the above inequality, we have that

$$\sum_{k=0}^{K-1}\frac{\eta_k}{2}\mathbb{E}\left[\|\nabla_\theta V(\theta_k)\|_2^2\right] \leq \mathbb{E}\left[V(\theta_K) - V(\theta_0)\right] + \sum_{k=0}^{K-1}\frac{\eta_k}{2}(1 + L\eta_k)\frac{L_{\theta\vartheta}^2\delta}{\mu} + \sum_{k=0}^{K-1}L\eta_k^2\sigma^2.$$

Because $\eta_k = \sqrt{\frac{\Delta}{\sigma^2 LK}}$ and $K \geq \frac{\Delta L}{\sigma^2}$, we have that $L\eta_k \leq 1$. Furthermore, we have that

$$\frac{1}{K}\sum_{k=0}^{K-1}\mathbb{E}\left[\|\nabla_\theta V(\theta_k)\|_2^2\right] \leq 4\sigma\sqrt{\frac{\Delta L}{K}} + \frac{2L_{\theta\vartheta}^2\delta}{\mu}.$$

Therefore, the proof of this theorem is concluded. □

C.3 Learning Dynamics Near First-Order Stationary Policies

We explore the properties of FOSPs in ARPO and SPO by analyzing the learning dynamics in their neighborhoods. Our framework of analysis is drawn on the linear stability analysis of stochastic gradient descent (Wu et al., 2022b) and sharpness-aware minimization (Zhou et al., 2025).

C.3.1 LEARNING DYNAMICS NEAR FOSPS IN ARPO

We first consider the learning dynamics near FOSPs in ARPO. Let (θ^*, ϑ^*) be a first-order stationary policy-adversary of $V^{\pi_\theta \circ \nu_\vartheta}(\mu_0)$. To simplify analysis, we consider (θ^*, ϑ^*) satisfies the following second-order optimality conditions:

$$\nabla_\theta V^{\pi_{\theta^*} \circ \nu_{\vartheta^*}}(\mu_0) = 0,\ \nabla_\vartheta V^{\pi_{\theta^*} \circ \nu_{\vartheta^*}}(\mu_0) = 0,\ \nabla^2_{\theta\theta} V^{\pi_{\theta^*} \circ \nu_{\vartheta^*}}(\mu_0) \prec 0,\ \nabla^2_{\vartheta\vartheta} V^{\pi_{\theta^*} \circ \nu_{\vartheta^*}}(\mu_0) \succ 0. \tag{4}$$

Note that it makes no sense on the gradient when the objective adds a constant. Therefore, to explore the local properties around (θ^*, ϑ^*), denote $\mathcal{L}(\theta, \vartheta) := V^{\pi_{\theta^*} \circ \nu_{\vartheta^*}}(\mu_0) - V^{\pi_\theta \circ \nu_\vartheta}(\mu_0)$. In the neighborhoods of (θ^*, ϑ^*), we considering the local quadratic approximation of $\mathcal{L}(\theta, \vartheta)$ as:

$$\mathcal{L}(\theta, \vartheta) = \underbrace{\frac{1}{2}(\theta - \theta^*)^\top H_\theta(\theta^*, \vartheta^*)(\theta - \theta^*)}_{\mathcal{L}_\theta(\theta, \vartheta)} + \underbrace{\frac{1}{2}(\vartheta - \vartheta^*)^\top H_\vartheta(\theta^*, \vartheta^*)(\vartheta - \vartheta^*)}_{\mathcal{L}_\vartheta(\theta, \vartheta)}, \tag{5}$$

where $H_\theta(\theta^*, \vartheta^*) := \nabla^2_{\theta\theta}\mathcal{L}(\theta^*, \vartheta^*)$ and $H_\vartheta(\theta^*, \vartheta^*) := \nabla^2_{\vartheta\vartheta}\mathcal{L}(\theta^*, \vartheta^*)$ are the Hessians with respect to θ and ϑ, respectively. Then, we have the following optimality conditions from (4).

$$\nabla_\theta \mathcal{L}(\theta^*, \vartheta^*) = 0,\ \nabla_\vartheta \mathcal{L}(\theta^*, \vartheta^*) = 0,\ \nabla^2_{\theta\theta}\mathcal{L}(\theta^*, \vartheta^*) \succ 0,\ \nabla^2_{\vartheta\vartheta}\mathcal{L}(\theta^*, \vartheta^*) \prec 0. \tag{6}$$

Let ξ denote the stochastic variable of sampling and let the sampled estimation $f(s; \theta, \vartheta) := -\hat{v}(s, a; \theta, \vartheta)$ as defined in (3). Denote the sampled policy gradient estimation as

$$\nabla_\theta \hat{\mathcal{L}}_\xi(\theta, \vartheta) = \frac{1}{B}\sum_{i \in \xi} \nabla_\theta f(s_i; \theta, \vartheta),\ \nabla_\vartheta \hat{\mathcal{L}}_\xi(\theta, \vartheta) = \frac{1}{B}\sum_{i \in \xi} \nabla_\vartheta f(s_i; \theta, \vartheta).$$

Consider the following single-loop adversarially robust policy optimization iteration:

$$\begin{aligned} \vartheta_{k+1} &= \vartheta_k + \epsilon \nabla_\vartheta \hat{\mathcal{L}}_\xi(\theta_k, \vartheta_k), \\ \theta_{k+1} &= \theta_k - \eta \nabla_\theta \hat{\mathcal{L}}_\xi(\theta_k, \vartheta_{k+1}). \end{aligned} \tag{Single-Loop ARPO Iterator}$$

Policy Gradient Noise. Denote the 1-batch gradient noise as $\xi_{\theta,i}(\theta, \vartheta) = \nabla_\theta f(s_i; \theta, \vartheta) - \nabla_\theta \mathcal{L}(\theta, \vartheta)$ and $\xi_{\vartheta,i}(\theta, \vartheta) = \nabla_\vartheta f(s_i; \theta, \vartheta) - \nabla_\vartheta \mathcal{L}(\theta, \vartheta)$. Let $\Sigma_\theta(\theta, \vartheta) := \mathbb{E}\left[\xi_{\theta,i}(\theta, \vartheta)\xi_{\theta,i}(\theta, \vartheta)^\top\right]$ and $\Sigma_\vartheta(\theta, \vartheta) := \mathbb{E}\left[\xi_{\vartheta,i}(\theta, \vartheta)\xi_{\vartheta,i}(\theta, \vartheta)^\top\right]$ as the 1-batch gradient noise covariance. Then, we have that

$$\Sigma_\theta(\theta, \vartheta) = \mathbb{E}\left[\nabla_\theta f(s_i; \theta, \vartheta)\nabla_\theta f(s_i; \theta, \vartheta)^\top\right] - \nabla_\theta \mathcal{L}(\theta, \vartheta)\nabla_\theta \mathcal{L}(\theta, \vartheta)^\top, \tag{7}$$

$$\Sigma_\vartheta(\theta, \vartheta) = \mathbb{E}\left[\nabla_\vartheta f(s_i; \theta, \vartheta)\nabla_\theta f(s_i; \theta, \vartheta)^\top\right] - \nabla_\vartheta \mathcal{L}(\theta, \vartheta)\nabla_\vartheta \mathcal{L}(\theta, \vartheta)^\top. \tag{8}$$

Furthermore, denote the sampled full-batch gradient noise as $\xi^B_\theta(\theta, \vartheta) := \nabla_\theta \hat{\mathcal{L}}_\xi(\theta, \vartheta) - \nabla_\theta \mathcal{L}(\theta, \vartheta) = \frac{1}{B}\sum_{i \in \xi} \xi_{\theta,i}(\theta, \vartheta)$ and $\xi^B_\vartheta(\theta, \vartheta) := \nabla_\vartheta \hat{\mathcal{L}}_\xi(\theta, \vartheta) - \nabla_\vartheta \mathcal{L}(\theta, \vartheta) = \frac{1}{B}\sum_{i \in \xi} \xi_{\vartheta,i}(\theta, \vartheta)$. Then, for the full-batch gradient noise, we have that

$$\mathbb{E}\left[\xi^B_\theta(\theta, \vartheta)\xi^B_\theta(\theta, \vartheta)^\top\right] = \frac{1}{B}\mathbb{E}\left[\xi_{\theta,i}(\theta, \vartheta)\xi_{\theta,i}(\theta, \vartheta)^\top\right] = \frac{1}{B}\Sigma_\theta(\theta, \vartheta), \tag{9}$$

$$\mathbb{E}\left[\xi^B_\vartheta(\theta, \vartheta)\xi^B_\vartheta(\theta, \vartheta)^\top\right] = \frac{1}{B}\mathbb{E}\left[\xi_{\vartheta,i}(\theta, \vartheta)\xi_{\vartheta,i}(\theta, \vartheta)^\top\right] = \frac{1}{B}\Sigma_\vartheta(\theta, \vartheta). \tag{10}$$

Based on these notations, we make a coercive assumption about gradient noise based on Hessians. Similar insights have been theoretically and empirically validated in a variety of studies about stochastic gradient descent in supervised learning settings (Zhu et al., 2019; Feng & Tu, 2021; Wu et al., 2020; 2022b; Mori et al., 2022; Wang & Wu, 2023; Wojtowytsch, 2024; Zhou et al., 2025).

Assumption C.6 (Coercive Policy Gradient Noise)**.** *There exists $\kappa > 0$, such that for all θ and ϑ, the following coercive conditions hold:*

$$\mathrm{Tr}\left(\frac{\Sigma_\theta(\theta, \vartheta)}{|\mathcal{L}(\theta, \vartheta)|}H_\theta(\theta, \vartheta)\right) \geq 2\kappa_\theta \|H_\theta(\theta, \vartheta)\|_F^2,\ \mathrm{Tr}\left(\frac{\Sigma_\vartheta(\theta, \vartheta)}{|\mathcal{L}(\theta, \vartheta)|}H_\vartheta(\theta, \vartheta)\right) \geq -2\kappa_\vartheta \|H_\vartheta(\theta, \vartheta)\|_F^2.$$

Local Stability of ARPO. Similar to the linear stability of stochastic gradient descent (Wu et al., 2022b) and sharpness-aware minimization (Zhou et al., 2025), we define the local stability of ARPO. Note that in the practical optimization process, only local stable optima can be selected.

Definition C.2 (Local Stability)**.** *The first-order stationary policy-adversary (θ^*, ϑ^*) is said to be locally stable if there exists a constant $C > 0$ such that for the Single-Loop ARPO Iterator, the local quadratic model (5) $\mathcal{L}(\theta, \vartheta)$ satisfies $\mathbb{E}[\mathcal{L}(\theta_k, \vartheta_k)] \leq C\mathbb{E}[\mathcal{L}(\theta_0, \vartheta_0)],\ \forall k \geq 0$.*

Based on these, we characterize the Hessian properties of FOSPs in ARPO.

Theorem C.3 (Flatness Bound of FOSPs in ARPO)**.** *Let (θ^*, ϑ^*) be a first-order stationary policy-adversary in ARPO and satisfy the second-order optimality condition (6). Denote $\lambda_{\min}(\cdot)$ and $\lambda_{\max}(\cdot)$ as the minimum and maximum eigenvalues, and let d be the state space dimension. If (θ^*, ϑ^*) is locally stable, $\mathcal{L}(\theta_0, \vartheta_0) > 0$, $\eta \geq 2/\lambda_{\min}(H_\theta(\theta^*, \vartheta^*))$, $\epsilon \leq 2/\lambda_{\max}(-H_\vartheta(\theta^*, \vartheta^*))$, $B \geq d\epsilon^2\kappa_\vartheta\lambda_{\max}(-H_\vartheta(\theta^*, \vartheta^*))^2$, and Assumption C.6 holds, then for single-loop ARPO, we have that*

$$\left(\|H_\theta(\theta^*, \vartheta^*)\|_F^2 + \frac{B}{\kappa_\theta\eta^2}\right)\left(1 - \frac{\epsilon^2\kappa_\vartheta\|H_\vartheta(\theta^*, \vartheta^*)\|_F^2}{B}\right) \leq \frac{B}{\kappa_\theta\eta^2}, \tag{11}$$

where B is the batch size, κ is the coercive coefficient, ϵ is the attack budget, and η is the step size.

Remark C.2. *$\mathcal{L}(\theta_0, \vartheta_0) > 0$ means that $V^{\pi_{\theta^*} \circ \nu_{\vartheta^*}}(\mu_0) > V^{\pi_{\theta_0} \circ \nu_{\vartheta_0}}(\mu_0)$, which holds in practical training from the scratch.*

Proof. Because $\mathcal{L}(\theta_0, \vartheta_0) > 0$, by recursion, we can prove that $\mathcal{L}(\theta_{k-1}, \vartheta_k) > 0$ and $\mathcal{L}(\theta_k, \vartheta_k) > 0, \forall k \geq 1$. Then, we have that

$$\begin{aligned}
&\mathcal{L}(\theta_{k+1}, \vartheta_{k+1}) \\
&= \frac{1}{2}\underbrace{(\theta_{k+1} - \theta^*)^\top H_\theta(\theta^*, \vartheta^*)(\theta_{k+1} - \theta^*)}_{I} + \frac{1}{2}\underbrace{(\vartheta_{k+1} - \vartheta^*)^\top H_\vartheta(\theta^*, \vartheta^*)(\vartheta_{k+1} - \vartheta^*)}_{II}
\end{aligned}$$

Without loss of generality, we can let $\theta^* = \vartheta^* = 0$. Denote $H_1 := H_\theta(\theta^*, \vartheta^*)$, $H_2 := H_\vartheta(\theta^*, \vartheta^*)$. According to the definition of the sampled full-batch gradient noise, we have that $\xi_\theta^B(\theta, \vartheta) = \nabla_\theta\hat{\mathcal{L}}_\xi(\theta, \vartheta) - \nabla_\theta\mathcal{L}(\theta, \vartheta)$, and $\xi_\vartheta^B(\theta, \vartheta) = \nabla_\vartheta\hat{\mathcal{L}}_\xi(\theta, \vartheta) - \nabla_\vartheta\mathcal{L}(\theta, \vartheta)$.

Then, on one hand, we have that

$$\begin{aligned}
&\mathbb{E}\left[I\right] \\
&= \mathbb{E}\left[(\theta_k - \eta\nabla_\theta\hat{\mathcal{L}}_\xi(\theta_k, \vartheta_{k+1}))^\top H_1(\theta_k - \eta\nabla_\theta\hat{\mathcal{L}}_\xi(\theta_k, \vartheta_{k+1}))\right] \\
&= \mathbb{E}\left[(\theta_k - \eta\nabla_\theta\mathcal{L}(\theta_k, \vartheta_{k+1}) - \eta\xi_\theta^B(\theta_k, \vartheta_{k+1}))^\top H_1(\theta_k - \eta\nabla_\theta\mathcal{L}(\theta_k, \vartheta_{k+1}) - \eta\xi_\theta^B(\theta_k, \vartheta_{k+1}))\right] \\
&= \mathbb{E}\left[(\theta_k - \eta\nabla_\theta\mathcal{L}(\theta_k, \vartheta_{k+1}))^\top H_1(\theta_k - \eta\nabla_\theta\mathcal{L}(\theta_k, \vartheta_{k+1}))\right] \\
&\quad + \eta^2\mathbb{E}\left[\xi_\theta^B(\theta_k, \vartheta_{k+1})^\top H_1\xi_\theta^B(\theta_k, \vartheta_{k+1})\right] \\
&= \mathbb{E}\left[(\theta_k - \eta\nabla_\theta\mathcal{L}(\theta_k, \vartheta_{k+1}))^\top H_1(\theta_k - \eta\nabla_\theta\mathcal{L}(\theta_k, \vartheta_{k+1}))\right] + \frac{\eta^2}{B}\mathbb{E}\left[\mathrm{Tr}\left(\Sigma_\theta(\theta_k, \vartheta_{k+1})H_1\right)\right] \\
&\geq \mathbb{E}\left[(\theta_k - \eta\nabla_\theta\mathcal{L}(\theta_k, \vartheta_{k+1}))^\top H_1(\theta_k - \eta\nabla_\theta\mathcal{L}(\theta_k, \vartheta_{k+1}))\right] + \frac{2\eta^2\kappa_\theta\|H_1\|_F^2}{B}\mathbb{E}\left[\mathcal{L}(\theta_k, \vartheta_{k+1})\right] \\
&= \mathbb{E}\left[\theta_k^\top(I - \eta H_1)H_1(I - \eta H_1)\theta_k\right] + \frac{2\eta^2\kappa_\theta\|H_1\|_F^2}{B}\mathbb{E}\left[\mathcal{L}(\theta_k, \vartheta_{k+1})\right] \\
&\geq \mathbb{E}\left[\theta_k^\top H_1\theta_k\right] + \frac{2\eta^2\kappa_\theta\|H_1\|_F^2}{B}\mathbb{E}\left[\mathcal{L}(\theta_k, \vartheta_{k+1})\right] \\
&= 2\mathbb{E}\left[\mathcal{L}_\theta(\theta_k, \vartheta_k)\right] + \frac{2\eta^2\kappa_\theta\|H_1\|_F^2}{B}\mathbb{E}\left[\mathcal{L}(\theta_k, \vartheta_{k+1})\right].
\end{aligned}$$

The third equation comes from $\mathbb{E}\left[\xi_\theta^B(\theta, \vartheta)\right] = 0$. The fourth equation comes from (9). The first inequality comes from Assumption C.6. Because of $\eta \geq \frac{2}{\lambda_{\min}(H_1)}$, we have that $H_1 \succeq \frac{2}{\eta}I$. This

comes that $H_1 - 2\eta H_1^2 + \eta^2 H_1^3 \succeq H_1$, which leads to the last inequality. Now, we need to estimate the lower bound of $\mathbb{E}\left[\mathcal{L}_\theta(\theta_k, \vartheta_{k+1})\right]$.

$$\begin{aligned}
&\mathbb{E}\left[\mathcal{L}(\theta_k, \vartheta_{k+1})\right] \\
=& \frac{1}{2}\mathbb{E}\left[\theta_k^\top H_1 \theta_k + \vartheta_{k+1}^\top H_2 \vartheta_{k+1}\right] \\
=& \mathbb{E}\left[\mathcal{L}_\theta(\theta_k, \vartheta_k)\right] + \frac{1}{2} II.
\end{aligned}$$

On the other hand, we have that

$$\begin{aligned}
&\mathbb{E}\left[II\right] \\
=& \mathbb{E}\left[(\vartheta_k + \epsilon\nabla_\vartheta \hat{\mathcal{L}}_\xi(\theta_k, \vartheta_k))^\top H_2 (\vartheta_k + \epsilon\nabla_\vartheta \hat{\mathcal{L}}_\xi(\theta_k, \vartheta_k))\right] \\
=& \mathbb{E}\left[(\vartheta_k + \epsilon\nabla_\vartheta \mathcal{L}(\theta_k, \vartheta_k) + \epsilon\xi_\vartheta^B(\theta_k, \vartheta_k))^\top H_2 (\vartheta_k + \epsilon\nabla_\vartheta \mathcal{L}(\theta_k, \vartheta_k) + \epsilon\xi_\vartheta^B(\theta_k, \vartheta_k))\right] \\
=& \mathbb{E}\left[(\vartheta_k + \epsilon\nabla_\vartheta \mathcal{L}(\theta_k, \vartheta_k))^\top H_2 (\vartheta_k + \epsilon\nabla_\vartheta \mathcal{L}(\theta_k, \vartheta_k))\right] + \epsilon^2 \mathbb{E}\left[\xi_\vartheta^B(\theta_k, \vartheta_k)^\top H_2 \xi_\vartheta^B(\theta_k, \vartheta_k)\right] \\
=& \mathbb{E}\left[(\vartheta_k + \epsilon\nabla_\vartheta \mathcal{L}(\theta_k, \vartheta_k))^\top H_2 (\vartheta_k + \epsilon\nabla_\vartheta \mathcal{L}(\theta_k, \vartheta_k))\right] + \frac{\epsilon^2}{B}\mathbb{E}\left[\mathrm{Tr}\left(\Sigma_\vartheta(\theta_k, \vartheta_k) H_2\right)\right] \\
\geq& \mathbb{E}\left[(\vartheta_k + \epsilon\nabla_\vartheta \mathcal{L}(\theta_k, \vartheta_k))^\top H_2 (\vartheta_k + \epsilon\nabla_\vartheta \mathcal{L}(\theta_k, \vartheta_k))\right] - \frac{2\epsilon^2 \kappa_\vartheta \|H_2\|_F^2}{B}\mathbb{E}\left[\mathcal{L}(\theta_k, \vartheta_k)\right] \\
=& \mathbb{E}\left[\vartheta_k^\top (I + \epsilon H_2) H_2 (I + \epsilon H_2)\vartheta_k\right] - \frac{2\epsilon^2 \kappa_\vartheta \|H_2\|_F^2}{B}\mathbb{E}\left[\mathcal{L}(\theta_k, \vartheta_k)\right] \\
\geq& \mathbb{E}\left[\vartheta_k^\top H_2 \vartheta_k\right] - \frac{2\epsilon^2 \kappa_\vartheta \|H_2\|_F^2}{B}\mathbb{E}\left[\mathcal{L}(\theta_k, \vartheta_k)\right] \\
=& 2\mathbb{E}\left[\mathcal{L}_\vartheta(\theta_k, \vartheta_k)\right] - \frac{2\epsilon^2 \kappa_\vartheta \|H_2\|_F^2}{B}\mathbb{E}\left[\mathcal{L}(\theta_k, \vartheta_k)\right].
\end{aligned}$$

The third equation comes from $\mathbb{E}\left[\xi_\vartheta^B(\theta, \vartheta)\right] = 0$. The fourth equation comes from (10). The first inequality comes from Assumption C.6. Because of $\epsilon \leq \frac{2}{\lambda_{\max}(-H_2)}$, we have that $H_2 \succeq -\frac{2}{\epsilon} I$. This comes that $(I + \epsilon H_2) H_2 (I + \epsilon H_2) = H_2 + 2\epsilon H_2^2 + \epsilon^2 H_2^3 \succeq H_2$, which leads to the last inequality. Therefore, we have that

$$\mathbb{E}\left[\mathcal{L}(\theta_k, \vartheta_{k+1})\right] \geq \left(1 - \frac{\epsilon^2 \kappa_\vartheta \|H_2\|_F^2}{B}\right)\mathbb{E}\left[\mathcal{L}(\theta_k, \vartheta_k)\right]. \tag{12}$$

Because of $B \geq d\epsilon^2 \kappa_\vartheta \lambda_{\max}(-H_2)^2$, we have that

$$\|H_2\|_F^2 \leq d\lambda_{\max}(-H_2)^2 \leq \frac{B}{\epsilon^2 \kappa_\vartheta},$$

which indicates that $1 - \frac{\epsilon^2 \kappa_\vartheta \|H_2\|_F^2}{B} > 0$.

Furthermore, we have that

$$\mathbb{E}\left[\mathcal{L}(\theta_{k+1}, \vartheta_{k+1})\right] \geq \left(1 + \frac{\eta^2 \kappa_\theta \|H_1\|_F^2}{B}\right)\left(1 - \frac{\epsilon^2 \kappa_\vartheta \|H_2\|_F^2}{B}\right)\mathbb{E}\left[\mathcal{L}(\theta_k, \vartheta_k)\right]. \tag{13}$$

Hence, (θ^*, ϑ^*) is locally stable for stochastic ARPO, so the following inequality must hold:

$$\left(1 + \frac{\eta^2 \kappa_\theta \|H_1\|_F^2}{B}\right)\left(1 - \frac{\epsilon^2 \kappa_\vartheta \|H_2\|_F^2}{B}\right) \leq 1. \tag{14}$$

In conclusion, we have that for a local optimizer (θ^*, ϑ^*) of $V^{\pi_\theta \circ \nu_\vartheta}(\mu_0)$, it holds that:

$$\left(\|H_1\|_F^2 + \frac{B}{\kappa_\theta \eta^2}\right)\left(1 - \frac{\epsilon^2 \kappa_\vartheta \|H_2\|_F^2}{B}\right) \leq \frac{B}{\kappa_\theta \eta^2}. \tag{15}$$

This completes the proof. □

From Theorem C.3, we observe that for FOSP in ARPO, if the adversary-side curvature is bounded as $\|\nabla^2_{\vartheta\vartheta} V^{\pi_{\theta^*} \circ \nu_{\vartheta^*}}(\mu_0)\|_F^2 \leq B/(2\kappa_\vartheta \epsilon^2)$, then the policy-side curvature in ARPO matches that of SPO (as later shown in Theorem C.4), i.e., $\|\nabla^2_{\theta\theta} V^{\pi_{\theta^*} \circ \nu_{\vartheta^*}}(\mu_0)\|_F^2 \leq B/(\kappa_\theta \eta^2)$. This implies that if ARPO achieves sufficiently strong robustness, i.e., flat adversarial curvature, it can preserve generalization comparable to SPO. Moreover, greater robustness may further enhance generalization. However, if robustness is insufficient, generalization may be significantly degraded.

C.3.2 Learning Dynamics Near FOSPs in SPO

Similarly, for an FOSP θ^* in SPO, we establish the learning dynamics analysis. Let θ^* be a first-order stationary policy-adversary of $V^{\pi_\theta}(\mu_0)$. To simplify analysis, we consider θ^* satisfies the following second-order optimality conditions:

$$\nabla_\theta V^{\pi_{\theta^*}}(\mu_0) = 0,\ \nabla^2_{\theta\theta} V^{\pi_{\theta^*}}(\mu_0) \prec 0. \tag{16}$$

Note that it makes no sense on the gradient when the objective adds a constant. Therefore, to explore the local properties around θ^*, denote $\mathcal{L}(\theta) := V^{\pi_{\theta^*}}(\mu_0) - V^{\pi_\theta}(\mu_0)$. In the neighborhoods of θ^*, we considering the local quadratic approximation of $\mathcal{L}(\theta)$ as:

$$\mathcal{L}(\theta) = \frac{1}{2}(\theta - \theta^*)^\top H_\theta(\theta^*)(\theta - \theta^*), \tag{17}$$

where $H_\theta(\theta^*) := \nabla^2_{\theta\theta}\mathcal{L}(\theta^*)$ is the Hessians with respect to θ respectively. Then, we have the following optimality conditions from (16).

$$\nabla_\theta \mathcal{L}(\theta^*) = 0,\ \nabla^2_{\theta\theta}\mathcal{L}(\theta^*) \succ 0. \tag{18}$$

For a sampling trajectory $\tau = (s_0, a_0, r_0, \dots) \sim \pi_\theta, \mathbb{P}$, denote the unbiased estimation of the action-value function Q^{π_θ} as

$$\widehat{Q^{\pi_\theta}}(s_t, a_t) := \sum_{t' \geq t} \gamma^{t'-t} r(s_{t'}, a_{t'}), \forall (s_t, a_t) \in \tau.$$

For simplicity of writing and reading of the latter, denote the sampled estimate as:

$$\hat{v}(s, a; \theta) := \frac{1}{1-\gamma} \operatorname{sg}\left(\widehat{Q^{\pi_\theta}}(s, a)\right) \cdot \log \pi_\theta(a|s), \tag{19}$$

whereas $\operatorname{sg}(\cdot)$ is the stop-gradient operator, meaning that $\widehat{Q^{\pi_\theta}}(s, a)$ is seen as a function according to (s, a) and is detached from the gradient operation for θ in the following context.

Let ξ denote the stochastic variable of sampling and let the sampled estimation $f(s; \theta) := -\hat{v}(s, a; \theta)$ as defined in (19). Denote the sampled policy gradient estimation as

$$\nabla_\theta \hat{\mathcal{L}}_\xi(\theta) = \frac{1}{B} \sum_{i \in \xi} \nabla_\theta f(s_i; \theta).$$

Consider the following SPO iteration:

$$\theta_{k+1} = \theta_k - \eta \nabla_\theta \hat{\mathcal{L}}_\xi(\theta_k). \tag{SPO Iterator}$$

Policy Gradient Noise in SPO. Denote the 1-batch gradient noise as $\xi_{\theta,i}(\theta) = \nabla_\theta f(s_i; \theta) - \nabla_\theta \mathcal{L}(\theta)$. Let $\Sigma_\theta(\theta) := \mathbb{E}\left[\xi_{\theta,i}(\theta)\xi_{\theta,i}(\theta)^\top\right]$ as the 1-batch gradient noise covariance. Then, we have that

$$\Sigma_\theta(\theta) = \mathbb{E}\left[\nabla_\theta f(s_i; \theta) \nabla_\theta f(s_i; \theta)^\top\right] - \nabla_\theta \mathcal{L}(\theta) \nabla_\theta \mathcal{L}(\theta)^\top, \tag{20}$$

Furthermore, denote the sampled full-batch gradient noise as $\xi^B_\theta(\theta) := \nabla_\theta \hat{\mathcal{L}}_\xi(\theta) - \nabla_\theta \mathcal{L}(\theta) = \frac{1}{B}\sum_{i \in \xi} \xi_{\theta,i}(\theta)$. Then, for the full-batch gradient noise, we have that

$$\mathbb{E}\left[\xi^B_\theta(\theta)\xi^B_\theta(\theta)^\top\right] = \frac{1}{B}\mathbb{E}\left[\xi_{\theta,i}(\theta)\xi_{\theta,i}(\theta)^\top\right] = \frac{1}{B}\Sigma_\theta(\theta). \tag{21}$$

Based on these notations, we make a coercive assumption about gradient noise based on Hessians. Similar insights have been theoretically and empirically validated in a variety of studies about stochastic gradient descent in supervised learning settings (Zhu et al., 2019; Feng & Tu, 2021; Wu et al., 2020; 2022b; Mori et al., 2022; Wang & Wu, 2023; Wojtowytsch, 2024; Zhou et al., 2025).

Assumption C.7 (Coercive Policy Gradient Noise in SPO). *There exists $\kappa > 0$, such that for all θ, the following coercive conditions hold:*

$$\mathrm{Tr}\left(\frac{\Sigma_\theta(\theta)}{|\mathcal{L}(\theta)|}H_\theta(\theta)\right) \geq 2\kappa_\theta \|H_\theta(\theta)\|_F^2.$$

Local Stability of SPO. Similar to the linear stability of stochastic gradient descent (Wu et al., 2022b) and sharpness-aware minimization (Zhou et al., 2025), we define the local stability of SPO. Note that in the practical optimization process, only local stable optima can be selected.

Definition C.3 (Local Stability of SPO). *The first-order stationary policy θ^* is said to be locally stable if there exists a constant $C > 0$ such that for the SPO Iterator, the local quadratic model (17) $\mathcal{L}(\theta)$ satisfies $\mathbb{E}[\mathcal{L}(\theta_k)] \leq C\mathbb{E}[\mathcal{L}(\theta_0)]$, $\forall k \geq 0$.*

Based on these, we characterize the Hessian properties of FOSPs in SPO.

Theorem C.4 (Flatness Bound of FOSPs in SPO). *Let θ^* be a first-order stationary policy in SPO that satisfies the second-order optimality condition. If θ^* is locally stable, $\mathcal{L}(\theta_0) > 0$, and Assumption C.7 holds, then for SPO, we have that*

$$\|H_\theta(\theta^*)\|_F^2 \leq \frac{B}{\kappa\eta^2}. \tag{22}$$

Proof. Because $\mathcal{L}(\theta_0) > 0$, by recursion, we can prove that $\mathcal{L}(\theta_k) > 0, \forall k \geq 1$. Then, we have that

$$\mathcal{L}(\theta_{k+1}) = \frac{1}{2}(\theta_{k+1} - \theta^*)^\top H_\theta(\theta^*)(\theta_{k+1} - \theta^*).$$

Without loss of generality, we can let $\theta^* = 0$. Denote $H_1 := H_\theta(\theta^*)$. According to the definition of the sampled full-batch gradient noise, we have that $\xi_\theta^B(\theta) = \nabla_\theta \hat{\mathcal{L}}_\xi(\theta) - \nabla_\theta \mathcal{L}(\theta)$.

Then, we have that

$$\begin{aligned}
&\mathbb{E}\left[\theta_{k+1}^\top H_\theta(\theta^*)\theta_{k+1}\right] \\
&= \mathbb{E}\left[(\theta_k - \eta\nabla_\theta\hat{\mathcal{L}}_\xi(\theta_k))^\top H_1(\theta_k - \eta\nabla_\theta\hat{\mathcal{L}}_\xi(\theta_k))\right] \\
&= \mathbb{E}\left[(\theta_k - \eta\nabla_\theta\mathcal{L}(\theta_k) - \eta\xi_\theta^B(\theta_k))^\top H_1(\theta_k - \eta\nabla_\theta\mathcal{L}(\theta_k) - \eta\xi_\theta^B(\theta_k))\right] \\
&= \mathbb{E}\left[(\theta_k - \eta\nabla_\theta\mathcal{L}(\theta_k))^\top H_1(\theta_k - \eta\nabla_\theta\mathcal{L}(\theta_k))\right] + \eta^2\mathbb{E}\left[\xi_\theta^B(\theta_k)^\top H_1 \xi_\theta^B(\theta_k)\right] \\
&= \mathbb{E}\left[(\theta_k - \eta\nabla_\theta\mathcal{L}(\theta_k))^\top H_1(\theta_k - \eta\nabla_\theta\mathcal{L}(\theta_k))\right] + \frac{\eta^2}{B}\mathbb{E}\left[\mathrm{Tr}\left(\Sigma_\theta(\theta_k)H_1\right)\right] \\
&\geq \mathbb{E}\left[(\theta_k - \eta\nabla_\theta\mathcal{L}(\theta_k))^\top H_1(\theta_k - \eta\nabla_\theta\mathcal{L}(\theta_k))\right] + \frac{2\eta^2\kappa_\theta\|H_1\|_F^2}{B}\mathbb{E}\left[\mathcal{L}(\theta_k)\right] \\
&= \mathbb{E}\left[\theta_k^\top(I - \eta H_1)H_1(I - \eta H_1)\theta_k\right] + \frac{2\eta^2\kappa_\theta\|H_1\|_F^2}{B}\mathbb{E}\left[\mathcal{L}(\theta_k)\right] \\
&\geq \frac{2\eta^2\kappa_\theta\|H_1\|_F^2}{B}\mathbb{E}\left[\mathcal{L}(\theta_k)\right].
\end{aligned}$$

The third equation comes from $\mathbb{E}\left[\xi_\theta^B(\theta, \vartheta)\right] = 0$. The fourth equation comes from (21). The first inequality comes from Assumption C.7. Because of $H_1 \succeq 0$, we have that $H_1 - 2\eta H_1^2 + \eta^2 H_1^3 \succeq 0$, which leads to the last inequality.

Furthermore, we have that

$$\mathbb{E}\left[\mathcal{L}(\theta_{k+1})\right] \geq \frac{\eta^2\kappa_\theta\|H_1\|_F^2}{B}\mathbb{E}\left[\mathcal{L}(\theta_k)\right]. \tag{23}$$

Hence, θ^* is locally stable for stochastic SPO, so the following inequality must hold:

$$\frac{\eta^2\kappa_\theta\|H_1\|_F^2}{B} \leq 1. \tag{24}$$

In conclusion, we have that for a local optimizer θ^* of $V^{\pi_\theta}(\mu_0)$, it holds that:

$$\|H_1\|_F^2 \leq \frac{B}{\kappa\eta^2}. \tag{25}$$

This completes the proof. □

D ANALYSIS ON INTUITIVE ISA-MDPS

In this section, we illustrate and analyze detailed two-state and two-action ISA-MDPs to provide intuitive explanations from the numerical properties and their value space geometry. These examples are drawn on Dadashi et al. (2019).

Lemma D.1 (Line Theorem (Dadashi et al., 2019))**.** *Let s be a state and π a policy. Then there exist two s-deterministic policies in $Y^{\pi}_{S\setminus\{s\}}$, denoted π_ℓ, π_u, such that for all $\pi' \in Y^{\pi}_{S\setminus\{s\}}$,*

$$f_v(\pi_\ell) \preceq f_v(\pi') \preceq f_v(\pi_u),$$

where $f_v(\pi) = V^\pi$, and $Y^{\pi}_{S\setminus\{s\}}$ describe the set of policies that agree with π on all states except s.

Furthermore, the image of f_v restricted to $Y^{\pi}_{S\setminus\{s\}}$ is a line segment, and the following three sets are equivalent:

(i) $f_v\left(Y^{\pi}_{S\setminus\{s\}}\right)$,

(ii) $\{f_v\left(\alpha\pi_\ell + (1-\alpha)\pi_u\right) \mid \alpha \in [0,1]\}$,

(iii) $\{\alpha f_v(\pi_\ell) + (1-\alpha) f_v(\pi_u) \mid \alpha \in [0,1]\}$.

Based on the above Lemma, we derive the following Proposition.

Proposition D.1. *There exists an ISA-MDP that satisfies the following properties:*

(1) Its robust policy space has a cut point, i.e., there exists a policy π such that $\Pi_{Robust}/\{\pi\}$ is disconnected, where $\Pi_{Robust} = \{\pi \in \Pi | V^\pi(s) = V^{\pi\circ\nu^*(\pi)}(s), \forall s\}$.

(2) The FOSPs in ARPO are more than those in SPO. Moreover, let π_S be a FOSP under SPO, and π_A be a FOSP under ARPO. Then, π_A is a robust policy with $V^{\pi_A}(\mu_0) - V^-(\mu_0) < \frac{1}{2}(V^{\pi_S}(\mu_0) - V^-(\mu_0))$, where $V^-(\mu_0) = \min_\pi V^\pi(\mu_0)$ is the worst value in ISA-MDP.

Proof. Consider a two-state, two-action ISA-MDP $\mathcal{M} = (\mathcal{S}, \mathcal{A}, r, P, \gamma, B)$, with $\mathcal{S} = \{s_1, s_2\}$, $\mathcal{A} = \{a_1, a_2\}$, and reward and transition structure specified as

$$r(s_i, a_j) = \hat{r}[(i-1)|\mathcal{A}| + j - 1], \quad P(s_k|s_i, a_j) = \hat{P}[(i-1)|\mathcal{A}| + j - 1][k],$$

where

$$\hat{r} = [-0.45, -0.1, 0.5, 0.5], \quad \hat{P} = [[0.7, 0.3], [0.99, 0.01], [0.2, 0.8], [0.99, 0.01]].$$

Set the discount factor $\gamma = 0.9$, and let $B(s_1) = B(s_2) = \{s_1, s_2\}$. Parametrize policies as $\Theta = \{(\alpha, \beta) : 0 \le \alpha \le 1, 0 \le \beta \le 1\}$, with $\pi_{\alpha,\beta}(a_1|s_1) = \alpha$, $\pi_{\alpha,\beta}(a_1|s_2) = \beta$.

The robust policy parameter space is defined as

$$\Theta_{Robust} = \{(\alpha, \beta) \in \Theta : V^{\pi_{\alpha,\beta}\circ\nu^*(\pi_{\alpha,\beta})} = V^{\pi_{\alpha,\beta}}\}.$$

We derive that:

$$V^{\pi_{\alpha,\beta}}(s_1) = \frac{A_{\alpha,\beta}}{P_{\alpha,\beta}}, \tag{26}$$

$$V^{\pi_{\alpha,\beta}}(s_2) = \frac{B_{\alpha,\beta}}{P_{\alpha,\beta}}, \tag{27}$$

$$\frac{\partial V^{\pi_{\alpha,\beta}}(s_1)}{\partial \alpha} = \frac{0.24885\beta - 0.21635}{P_{\alpha,\beta}} - \frac{0.0261 A_{\alpha,\beta}}{{P_{\alpha,\beta}}^2}, \tag{28}$$

$$\frac{\partial V^{\pi_{\alpha,\beta}}(s_1)}{\partial \beta} = \frac{0.24885\alpha + 0.0711}{P_{\alpha,\beta}} + \frac{0.0711 A_{\alpha,\beta}}{{P_{\alpha,\beta}}^2}, \tag{29}$$

$$\frac{\partial V^{\pi_{\alpha,\beta}}(s_2)}{\partial \alpha} = \frac{0.24885\beta - 0.18135}{P_{\alpha,\beta}} - \frac{0.0261 B_{\alpha,\beta}}{{P_{\alpha,\beta}}^2}, \tag{30}$$

$$\frac{\partial V^{\pi_{\alpha,\beta}}(s_2)}{\partial \beta} = \frac{0.24885\alpha + 0.0711}{P_{\alpha,\beta}} + \frac{0.0711 B_{\alpha,\beta}}{{P_{\alpha,\beta}}^2}, \tag{31}$$

where

$$\begin{aligned}
P_{\alpha,\beta} &= |I - \gamma P^{\pi_{\alpha,\beta}}| \\
&= (0.991 - 0.711\beta)(0.261\alpha + 0.109) + (0.261\alpha + 0.009)(0.711\beta - 0.891), \\
A_{\alpha,\beta} &= 0.1305\alpha + (0.35\alpha + 0.1)(0.711\beta - 0.991) + 0.0045, \\
B_{\alpha,\beta} &= 0.1305\alpha + (0.35\alpha + 0.1)(0.711\beta - 0.891) + 0.0545.
\end{aligned}$$

Direct calculation from (26) and (27) shows that the policy $\pi_{1,1}$ achieves the highest value, i.e., $\pi_{1,1}$ is globally optimal. Moreover, the following ordering holds:

$$\begin{aligned}
V^{\pi_{1,1}} \approx (0.16, 1.89)^\top \succeq V^{\pi_{0,1}} \approx (-0.81, 1.26)^\top \\
\succeq V^{\pi_{0,0}} \approx (-0.95, -0.35)^\top \succeq V^{\pi_{1,0}} \approx (-2.47, -1.71)^\top.
\end{aligned} \tag{32}$$

To further analyze value relations, define

$$f(\beta, s) := V^{\pi_{1,\beta}}(s) - V^{\pi_{0,\beta}}(s), \qquad s \in \{s_1, s_2\}.$$

Explicit calculation shows there exists a threshold $\tilde{\beta} \approx 0.777$ such that

$$\begin{cases}
f(\beta, s) > 0, & \text{if } \beta > \tilde{\beta}, \\
f(\beta, s) = 0, & \text{if } \beta = \tilde{\beta}, \\
f(\beta, s) < 0, & \text{if } \beta < \tilde{\beta},
\end{cases} \tag{33}$$

and this sign structure holds identically for both s_1 and s_2.

Applying the Line Theorem D.1, for any $0 \le \alpha_1 < \alpha_2 \le 1$ and for each fixed s,

$$\begin{cases}
V^{\pi_{\alpha_1,\beta}}(s) < V^{\pi_{\alpha_2,\beta}}(s), & \text{if } \beta > \tilde{\beta}, \\
V^{\pi_{\alpha_1,\beta}}(s) = V^{\pi_{\alpha_2,\beta}}(s), & \text{if } \beta = \tilde{\beta}, \\
V^{\pi_{\alpha_1,\beta}}(s) > V^{\pi_{\alpha_2,\beta}}(s), & \text{if } \beta < \tilde{\beta},
\end{cases} \tag{34}$$

again for both s_1 and s_2.

Now, for value improvement in the β direction, define

$$g(\alpha, s) := V^{\pi_{\alpha,1}}(s) - V^{\pi_{\alpha,0}}(s).$$

Explicit computation confirms that $g(\alpha, s) \ge 0$ for any $0 \le \alpha \le 1$ and both s_1, s_2. Thus, for any $0 \le \beta_1 < \beta_2 \le 1$ and fixed α,

$$V^{\pi_{\alpha,\beta_1}}(s) < V^{\pi_{\alpha,\beta_2}}(s). \tag{35}$$

Let us now determine the structure of the robust policy region. By definition, for any $(\alpha, \beta) \in \Theta$, $\pi_{\alpha,\beta} \circ \nu^*(\pi_{\alpha,\beta}) = \arg\min_{\pi \in \Pi_{\alpha,\beta}} V^\pi$, where $\Pi_{\alpha,\beta} = \{\pi_{\alpha,\alpha}, \pi_{\alpha,\beta}, \pi_{\beta,\alpha}, \pi_{\beta,\beta}\}$.

If $\alpha = \beta$, then $\Pi_{\alpha,\alpha} = \{\pi_{\alpha,\alpha}\}$, so (α, β) is always robust. If $\beta \le \min\{\alpha, \tilde{\beta}\}$: Using (34) for $\beta \le \alpha$ gives $V^{\pi_{\alpha,\beta}}(s) \le V^{\pi_{\alpha,\alpha}}(s)$, and $V^{\pi_{\beta,\alpha}}(s) \ge V^{\pi_{\beta,\beta}}(s)$. Together with (35) and $\beta \le \tilde{\beta}$, $V^{\pi_{\alpha,\beta}}(s) \le V^{\pi_{\beta,\beta}}(s)$. Therefore, $V^{\pi_{\alpha,\beta}}(s)$ is the minimal value in $\Pi_{\alpha,\beta}$ for both states, so robustness holds.

For other regions $(\alpha, \beta) \notin \{\alpha = \beta\} \cup \{\beta \le \min\{\alpha, \tilde{\beta}\}\}$, by similarly using (34) and (35), one can verify that the minimal value in $\Pi_{\alpha,\beta}$ is always attained at a different policy (specifically, at $\pi_{\beta,\alpha}$, $\pi_{\alpha,\alpha}$, or $\pi_{\beta,\beta}$ in the respective regions). Thus, the robust region is exactly the union

$$\Theta_{Robust} = \{(\alpha, \beta) : \alpha = \beta\} \cup \{(\alpha, \beta) : \beta \le \min\{\alpha, \tilde{\beta}\}\}.$$

Notably, the point $(\tilde{\beta}, \tilde{\beta})$ serves as a cut point: removing it disconnects Θ_{Robust}. This completes the proof of property (1).

For property (2), we show that, unlike SPO, the ARPO objective can admit more FOSP. Indeed, we focus on

$$\max_{\alpha,\beta} V^{\pi_{\alpha,\beta}}(s) \qquad \text{subject to: } \begin{cases}
\alpha - \beta \ge 0, \\
\beta \ge 0, \\
\tilde{\beta} - \beta \ge 0, \\
1 - \alpha \ge 0.
\end{cases}$$

We analyze the Karush-Kuhn-Tucker (KKT) conditions at $(\alpha, \beta) = (0, 0)$ to verify FOSP. The Lagrangian is defined as:

$$L(s, \alpha, \beta, \lambda) = V^{\pi_{\alpha,\beta}}(s) + \lambda_1(\alpha - \beta) + \lambda_2\beta + \lambda_3(\tilde{\beta} - \beta) + \lambda_4(1 - \alpha).$$

The KKT conditions at $(\alpha, \beta) = (0, 0)$ are:

Stationarity:

$$\frac{\partial V^{\pi_{\alpha,\beta}}(s)}{\partial \alpha}|_{(0,0)} + \lambda_1 - \lambda_4 = 0,$$
$$\frac{\partial V^{\pi_{\alpha,\beta}}(s)}{\partial \beta}|_{(0,0)} - \lambda_1 + \lambda_2 - \lambda_3 = 0.$$

Primal feasibility: $(0, 0)$ satisfies all inequality constraints.

Dual feasibility: $\lambda_j \geq 0, \quad j = 1, 2, 3, 4,$

Complementary slackness:

$$\lambda_1(\alpha - \beta) = 0,\ \lambda_2\beta = 0,\ \lambda_3(\tilde{\beta} - \beta) = \lambda_3\tilde{\beta} = 0,\ \lambda_4(1 - \alpha) = 0.$$

Since at $(\alpha, \beta) = (0, 0)$, the gradients $\frac{\partial V^{\pi_{\alpha,\beta}}(s)}{\partial \alpha}|_{(0,0)}$ and $\frac{\partial V^{\pi_{\alpha,\beta}}(s)}{\partial \beta}|_{(0,0)}$ both exist, and by the structure of the problem the corresponding dual variables can be chosen to satisfy the equations above, all KKT conditions are satisfied. Therefore, $(0, 0)$ is a FOSP for ARPO, even though it is not a FOSP for SPO.

Let $\pi_S = \pi_{1,1}, \pi_A = \pi_{0,0}$, μ_0 is the uniform distribution on $\mathcal{S}$. In this example, $\pi^- = \pi_{1,0}$. By (32), we know that

$$V^{\pi_S}(\mu_0) \approx 1.03,\ V^{\pi_A}(\mu_0) = -0.65,\ V^-(\mu_0) = -2.09.$$

Then, we have that

$$V^{\pi_S}(\mu_0) - V^-(\mu_0) = 3.12,\ V^{\pi_A}(\mu_0) - V^-(\mu_0) = 1.44 < \frac{1}{2}(V^{\pi_S}(\mu_0) - V^-(\mu_0)).$$

This completes the proof. □

E Analysis on Surrogate Adversary

In this section, we provide the analysis and proof about the surrogate adversary.

Theorem E.1 (Surrogate Adversary)**.** *For any policy π_θ, state $s \in \mathcal{S}$, and $K > 0$, let the adversary ϑ be computed via K-step gradient descent on the adversarial value function, i.e., $\vartheta_{s,k} = \vartheta_{s,k-1} - \eta_{s,k-1}\nabla_{\vartheta_s} V^{\pi_\theta \circ \nu_\vartheta}(s)|_{\vartheta_s = \vartheta_{s,k-1}}, 1 \leq k \leq K$. Assume step sizes $\eta_{s,k} \leq 1/(\lambda_s + \delta)$ for some $\delta > 0$, and if $G(s; \pi, \nu) := \mathcal{D}_{\mathrm{KL}}(\pi(\cdot|s)\|(\pi \circ \nu)(\cdot|s)) \ll 1$. Then, we have*

$$V^{\pi_\theta}(s) - V^{\pi_\theta \circ \nu_\vartheta}(s) \geq \frac{2\delta}{\lambda_{\max}(F_{s,\theta})K} G(s; \pi_\theta, \nu_\vartheta) + O\left(G(s; \pi_\theta, \nu_\vartheta)^{\frac{3}{2}}\right),$$

where $F_{s,\theta}$ is the Fisher information matrix of $\log(\pi_\theta \circ \nu_\vartheta)(a|s)$ with respect to $\vartheta_s = 0$, defined as $F_{s,\theta} := F(\theta, s) = \mathbb{E}_{a\sim\pi_\theta(\cdot|s)}\left[(\nabla_{\vartheta_s} \log \pi_\theta(a|s + \vartheta_s)|_{\vartheta_s=0})\,(\nabla_{\vartheta_s} \log \pi_\theta(a|s + \vartheta_s)|_{\vartheta_s=0})^T\right]$, $\lambda_s = \max_{s+\vartheta_s \in B(s)} \lambda_{\max}(\nabla^2_{\vartheta\vartheta} V^{\pi_\theta \tilde{\circ} \nu_\vartheta}(s)|_{\vartheta=\vartheta_s})$ and $\lambda_{\max}(\cdot)$ is the largest eigenvalue of matrix.

Proof. We begin by examining the local behavior of the KL-divergence between the policy at the original and perturbed state:

$$G(s; \pi_\theta, \nu_\vartheta) := D_{\mathrm{KL}}\left(\pi_\theta(\cdot|s)\|\pi_\theta(\cdot|s + \vartheta_s)\right).$$

Let us expand $G(s; \pi_\theta, \nu_\vartheta)$ for small ϑ_s:

$$\begin{aligned} G(s; \pi_\theta, \nu_\vartheta) &= \sum_a \pi_\theta(a|s) \log \frac{\pi_\theta(a|s)}{\pi_\theta(a|s + \vartheta_s)} \\ &= \mathbb{E}_{a\sim\pi_\theta(\cdot|s)}\left[\log \pi_\theta(a|s) - \log \pi_\theta(a|s + \vartheta_s)\right]. \end{aligned}$$

Now, expand $\log \pi_\theta(a|s+\vartheta_s)$ at $\vartheta_s = 0$ using a Taylor expansion:

$$\log \pi_\theta(a|s+\vartheta_s) = \log \pi_\theta(a|s) + \nabla_{\vartheta_s} \log \pi_\theta(a|s)|_{\vartheta_s=0}^\top \vartheta_s + \frac{1}{2}\vartheta_s^\top \nabla_{\vartheta_s}^2 \log \pi_\theta(a|s)|_{\vartheta_s=0}\vartheta_s + O(\|\vartheta_s\|_2^3).$$

Plugging this into the difference, $\log \pi_\theta(a|s) - \log \pi_\theta(a|s+\vartheta_s)$, and taking the expectation over $a \sim \pi_\theta(\cdot|s)$:

$$\mathbb{E}_{a\sim\pi_\theta(\cdot|s)}\left[-\nabla_{\vartheta_s} \log \pi_\theta(a|s)|_{\vartheta_s=0}^\top \vartheta_s - \frac{1}{2}\vartheta_s^\top \nabla_{\vartheta_s}^2 \log \pi_\theta(a|s)|_{\vartheta_s=0}\vartheta_s\right] + O(\|\vartheta_s\|_2^3).$$

The first term equals zero because

$$\mathbb{E}_{a\sim\pi_\theta(\cdot|s)}[\nabla_{\vartheta_s} \log \pi_\theta(a|s)|_{\vartheta_s=0}] = \nabla_{\vartheta_s} \sum_a \pi_\theta(a|s+\vartheta_s)|_{\vartheta_s=0} = 0,$$

since the sum of probabilities is always 1.

The second term can also be separated using Fisher information matrix properties:

$$F_{s,\theta} := \mathbb{E}_{a\sim\pi_\theta(\cdot|s)}\left[\nabla_{\vartheta_s} \log \pi_\theta(a|s) \nabla_{\vartheta_s} \log \pi_\theta(a|s)^\top\right],$$

and

$$\mathbb{E}_{a\sim\pi_\theta(\cdot|s)}[\nabla_{\vartheta_s}^2 \log \pi_\theta(a|s)] = -F_{s,\theta}.$$

Therefore, combining the above,

$$G(s;\pi_\theta,\nu_\vartheta) = \frac{1}{2}\vartheta_s^\top F_{s,\theta}\vartheta_s + O(\|\vartheta_s\|_2^3).$$

From the expansion above, since $F_{s,\theta}$ is positive definite (or at least positive semi-definite), we have:

$$\frac{1}{2}\lambda_{\min}(F_{s,\theta})\|\vartheta_s\|_2^2 \le \frac{1}{2}\vartheta_s^\top F_{s,\theta}\vartheta_s \le \frac{1}{2}\lambda_{\max}(F_{s,\theta})\|\vartheta_s\|_2^2.$$

Neglecting the lower bound (since we only need an upper bound for $\|\vartheta_s\|_2^2$), isolate $\|\vartheta_s\|_2^2$:

$$\|\vartheta_s\|_2^2 \le \frac{2}{\lambda_{\max}(F_{s,\theta})} G(s;\pi_\theta,\nu_\vartheta) + O(G(s;\pi_\theta,\nu_\vartheta)^{3/2}).$$

Here, the $O(G^{3/2})$ term comes from inverting the Taylor expansion when ϑ_s is small. We now analyze the decrease in the value function resulting from K steps of gradient descent:

For each step,

$$\vartheta_{s,k} = \vartheta_{s,k-1} - \eta_{s,k-1}\nabla_{\vartheta_s} V^{\pi_\theta \circ \nu_\vartheta}(s)|_{\vartheta_s=\vartheta_{s,k-1}}.$$

Let $V_k = V^{\pi_\theta \circ \nu_{\vartheta_{s,k}}}(s)$. Expanding V_k around $\vartheta_{s,k-1}$ using Taylor's theorem:

$$\begin{aligned} V_k = V_{k-1} &+ \nabla_{\vartheta_s} V^{\pi_\theta \circ \nu_\vartheta}(s)|_{\vartheta_s=\vartheta_{s,k-1}}^\top (\vartheta_{s,k} - \vartheta_{s,k-1}) \\ &+ \frac{1}{2}(\vartheta_{s,k} - \vartheta_{s,k-1})^\top \nabla_{\vartheta_s}^2 V^{\pi_\theta \circ \nu_\vartheta}(s)|_{\vartheta_s=\vartheta_{s,k-1}} (\vartheta_{s,k} - \vartheta_{s,k-1}) + O(\|\vartheta_{s,k} - \vartheta_{s,k-1}\|_2^3). \end{aligned}$$

Summing over $k = 1$ to K and noting telescoping sum of $V_{k-1} - V_k$:

$$\begin{aligned} V^{\pi_\theta}(s) - V^{\pi_\theta \circ \nu_{\vartheta_{s,K}}}(s) &= \sum_{k=1}^K (V^{\pi_\theta \circ \nu_{\vartheta_{s,k-1}}}(s) - V^{\pi_\theta \circ \nu_{\vartheta_{s,k}}}(s)) \\ &\quad + O\left(\sum_{k=1}^K \|\vartheta_{s,k} - \vartheta_{s,k-1}\|_2^3\right) \\ &= -\sum_{k=1}^K \nabla_{\vartheta_s} V^{\pi_\theta \circ \nu_\vartheta}(s)|_{\vartheta_s=\vartheta_{s,k-1}}^\top (\vartheta_{s,k} - \vartheta_{s,k-1}) \\ &\quad - \frac{1}{2}\sum_{k=1}^K (\vartheta_{s,k} - \vartheta_{s,k-1})^\top \nabla_{\vartheta_s}^2 V^{\pi_\theta \circ \nu_\vartheta}(s)|_{\vartheta_s=\vartheta_{s,k-1}} (\vartheta_{s,k} - \vartheta_{s,k-1}) \\ &\quad + O\left(\sum_{k=1}^K \|\vartheta_{s,k} - \vartheta_{s,k-1}\|_2^3\right). \end{aligned}$$

The gradient update yields:

$$\vartheta_{s,k} - \vartheta_{s,k-1} = -\eta_{s,k-1} \nabla_{\vartheta_s} V^{\pi_\theta \circ \nu_\vartheta}(s)|_{\vartheta_s = \vartheta_{s,k-1}}.$$

For small enough steps, and since the step size $\eta_{s,k-1} \leq 1/(\lambda_s + \delta)$ ensures sufficient decrease (similar to the classic descent lemma in optimization), we can bound the value difference as:

$$V^{\pi_\theta}(s) - V^{\pi_\theta \circ \nu_{\vartheta_{s,K}}}(s) \geq \delta \sum_{k=1}^{K} \|\vartheta_{s,k} - \vartheta_{s,k-1}\|_2^2 + O\left(\sum_{k=1}^{K} \|\vartheta_{s,k} - \vartheta_{s,k-1}\|_2^3\right).$$

By Jensen's inequality,

$$\sum_{k=1}^{K} \|\vartheta_{s,k} - \vartheta_{s,k-1}\|_2^2 \geq \frac{1}{K} \left\| \sum_{k=1}^{K} (\vartheta_{s,k} - \vartheta_{s,k-1}) \right\|_2^2 = \frac{1}{K} \|\vartheta_{s,K}\|_2^2.$$

Now substitute the earlier quadratic relationship between $\|\vartheta_{s,K}\|^2$ and $G(s; \pi_\theta, \nu_{\vartheta_{s,K}})$:

$$\begin{aligned} V^{\pi_\theta}(s) - V^{\pi_\theta \circ \nu_{\vartheta_{s,K}}}(s) &\geq \frac{\delta}{K} \|\vartheta_{s,K}\|_2^2 + O(\|\vartheta_{s,K}\|_2^3) \\ &\geq \frac{2\delta}{\lambda_{\max}(F_{s,\theta})K} G(s; \pi_\theta, \nu_{\vartheta_{s,K}}) + O(G(s; \pi_\theta, \nu_{\vartheta_{s,K}})^{3/2}). \end{aligned}$$

This completes the proof. □

F Additional Algorithm Details

F.1 Adversarially Robust Proximal Policy Optimization (AR-PPO)

We apply the ARPO paradigm on top of the PPO algorithm and further incorporate the SPO-based guidance, yielding Adversarily Robust Proximal Policy Optimization (AR-PPO). The overall algorithm is presented in Algorithm 2.

F.2 Bilevel Adversarially Robust Proximal Policy Optimization (BAR-PPO)

We apply the BARPO paradigm on top of the PPO algorithm and further incorporate the SPO-based guidance, yielding the Bilevel Adversarially Robust Proximal Policy Optimization (BAR-PPO). The overall algorithm is presented in Algorithm 3.

F.3 Additional Implementation Details

We run 2048 simulation steps per iteration and use a simple MLP network for all agents. SA-PPO, WocaR-PPO, and BAR-PPO are trained for 2 million steps (976 iterations) on Hopper, Walker2d, and Halfcheetah, and 10 million steps (4882 iterations) on Ant for convergence. RADIAL-PPO is trained for 4 million steps (2000 iterations) on Hopper, Walker2d, and Halfcheetah following the official implementation and 10 million steps (4882 iterations) on Ant. The attack budget ϵ is linearly increased from 0 to the target value during the first 732 iterations on Hopper, Walker2d, and Halfcheetah, and 3662 iterations on Ant, before continuing with the target value for the remaining iterations. This scheduler is aligned with Zhang et al. (2020c); Liang et al. (2022) without extra tuning. The regularization weight κ is chosen from $\{0.1, 0.3, 1.0\}$ for BAR-PPO. We run 10 iterations with step size $\epsilon/10$ for both methods and set the temperature parameter $\beta = 1 \times 10^{-5}$ for SGLD.

We implement all PPO agents with the same fully connected (MLP) structure as Zhang et al. (2020c); Oikarinen et al. (2021). In the Ant environment, we choose the best regularization parameter κ in $\{0.01, 0.03, 0.1, 0.3, 1.0\}$ for SA-PPO, RADIAL-PPO, and WocaR-PPO to achieve better robustness. For fair and comparable agent selection, we conduct multiple experiments for each setup, repeating each 17 times to account for the inherent performance variability in RL. After training, we attack all agents using random, critic, MAD, and RS attacks. Then, we select the median agent by considering the natural and robust returns as our final agent. This chosen agent is then attacked using the SA-RL and PA-AD attacks to further robustness evaluation, because these attacks involve quite high computational costs.

F.4 EXPERIMENTS COMPUTE RESOURCES

All MuJoCo experiments were conducted on a machine with an AMD EPYC 7742 CPU and no GPU acceleration.

BARPO's training takes approximately 2 hours for Hopper, Walker2d, and HalfCheetah, and 9 hours for the more complex Ant environment. This represents roughly a 2x increase in wall-clock time compared to standard, non-robust PPO training. Crucially, this overhead is on par with other leading robust baselines (Zhang et al., 2020c; Oikarinen et al., 2021; Liang et al., 2022), which require similar inner-loop computations to find the adversary. The choice of a CPU-only setup follows baselines, as the wall-clock time in these MuJoCo tasks is overwhelmingly dominated by the environment simulation overhead, ensuring a fair comparison of the algorithmic sample complexity.

Furthermore, we confirm that BARPO introduces no significant additional memory overhead compared to standard PPO training.

Algorithm 2 Adversarially Robust Proximal Policy Optimization (AR-PPO).

Input: Number of iterations T, a schedule ϵ_t for the perturbation radius ϵ, robustness weighting κ.

1: Initialize policy network $\pi_\theta(a|s)$ and value network $V_{\theta_V}(s)$.
2: **for** $t = 1$ **to** T **do**
3: Run π_{θ_t} in the environment to collect a set of trajectories $\mathcal{D} = \{\tau_k\}$ containing $|\mathcal{D}|$ episodes, each τ_k is a trajectory containing $|\tau_k|$ samples, $\tau_k := \{(s_{k,i}, a_{k,i}, r_{k,i}, s_{k,i+1})\}, i \in [|\tau_k|]$.
4: Compute reward-to-go $\hat{R}_{k,i}$ for each step i in every episode k using the trajectories and discount factor γ.
5: Update value network $V_{\theta_V}(s)$ by regression on the mean-square error:

$$\theta_V \leftarrow \arg\min_{\theta_V} \frac{1}{\sum_k |\tau_k|} \sum_{\tau_k \in D} \sum_{i=0}^{|\tau_k|} \left(V(s_{k,i}) - \hat{R}_{k,i} \right)^2.$$

6: Estimate advantage $\hat{A}_{k,i}$ for each step i in every episode k using generalized advantage estimation (GAE) and the current value function $V_{\theta_V}(s)$.
7: Solve the inner optimization using gradient descent (PGD):
8: For all k, i, run PGD to solve (the objective can be solved in a batch):

$$s_{i,\nu} = \arg\min_{s_\nu \in B_{\epsilon_t}(s_{k,i})} g\left(\frac{\pi_\theta(a_{k,i}|s_\nu)}{\pi_{\theta_t}(a_{k,i}|s_{k,i})}, \hat{A}_{k,i} \right),$$

where $g(x, y) = \min\{x \cdot y, \text{clip}(x, 1-\eta, 1+\eta) \cdot y\}$.
9: Compute the approximation of the outer optimization:

$$\mathcal{L}_{ar}(\theta) = \frac{1}{\sum_k |\tau_k|} \sum_{\tau_k \in D} \sum_{i=0}^{|\tau_k|} \left(-\frac{1}{\beta} \mathcal{H}(\pi_\theta(\cdot|s_{k,i})) - g\left(\frac{\pi_\theta(a_{k,i}|s_{i,\nu})}{\pi_{\theta_t}(a_{k,i}|s_{k,i})}, \hat{A}_{k,i} \right) \right).$$

10: Update the policy network by minimizing the vanilla PPO objective and the AR objective (the minimization is solved using ADAM):

$$\theta_{t+1} \leftarrow \arg\min_{\theta} \frac{1}{\sum_k |\tau_k|} \sum_{\tau_k \in D} \sum_{i=0}^{|\tau_k|} -g\left(\frac{\pi_\theta(a_{k,i}|s_{k,i})}{\pi_{\theta_t}(a_{k,i}|s_{k,i})}, \hat{A}_{k,i} \right) + \kappa \cdot \mathcal{L}_{ar}(\theta).$$

11: **end for**

Algorithm 3 Bilevel Adversarially Robust Proximal Policy Optimization (BAR-PPO).

Input: Number of iterations T, a schedule ϵ_t for the perturbation radius ϵ, robustness weighting κ.

1: Initialize policy network $\pi_\theta(a|s)$ and value network $V_{\theta_V}(s)$.
2: **for** $t = 1$ **to** T **do**
3: Run π_{θ_t} in the environment to collect a set of trajectories $\mathcal{D} = \{\tau_k\}$ containing $|\mathcal{D}|$ episodes, each τ_k is a trajectory containing $|\tau_k|$ samples, $\tau_k := \{(s_{k,i}, a_{k,i}, r_{k,i}, s_{k,i+1})\}, i \in [|\tau_k|]$.
4: Compute reward-to-go $\hat{R}_{k,i}$ for each step i in every episode k using the trajectories and discount factor γ.
5: Update value network $V_{\theta_V}(s)$ by regression on the mean-square error:

$$\theta_V \leftarrow \arg\min_{\theta_V} \frac{1}{\sum_k |\tau_k|} \sum_{\tau_k \in D} \sum_{i=0}^{|\tau_k|} \left(V(s_{k,i}) - \hat{R}_{k,i} \right)^2 .$$

6: Estimate advantage $\hat{A}_{k,i}$ for each step i in every episode k using generalized advantage estimation (GAE) and the current value function $V_{\theta_V}(s)$.
7: Solve the inner optimization using stochastic gradient Langevin dynamics (SGLD):
8: For all k, i, run SGLD to solve (the objective can be solved in a batch):

$$s_{i,\nu} = \arg\max_{s_\nu \in B_{\epsilon_t}(s_{k,i})} \mathrm{KL}\left(\pi_\theta(\cdot|s_{k,i}) \| \pi_\theta(\cdot|s_\nu)\right).$$

9: Compute the approximation of the outer optimization:

$$\mathcal{L}_{bar}(\theta) = \frac{1}{\sum_k |\tau_k|} \sum_{\tau_k \in D} \sum_{i=0}^{|\tau_k|} \left(-\frac{1}{\beta} \mathcal{H}\left(\pi_\theta(\cdot|s_{k,i})\right) - g\left(\frac{\pi_\theta(a_{k,i}|s_{i,\nu})}{\pi_{\theta_t}(a_{k,i}|s_{k,i})}, \hat{A}_{k,i} \right) \right),$$

where $g(x, y) = \min\{x \cdot y, \mathrm{clip}(x, 1-\eta, 1+\eta) \cdot y\}$.
10: Update the policy network by minimizing the vanilla PPO objective and the BAR objective (the minimization is solved using ADAM):

$$\theta_{t+1} \leftarrow \arg\min_{\theta} \frac{1}{\sum_k |\tau_k|} \sum_{\tau_k \in D} \sum_{i=0}^{|\tau_k|} -g\left(\frac{\pi_\theta(a_{k,i}|s_{k,i})}{\pi_{\theta_t}(a_{k,i}|s_{k,i})}, \hat{A}_{k,i} \right) + \kappa \cdot \mathcal{L}_{bar}(\theta).$$

11: **end for**

G Additional Experiment Results

G.1 Comparison of SPO, ARPO, BARPO Without Guidance, and BARPO

In Table 4, we compare the natural and robust performance of SPO, ARPO, BARPO without guidance, and BARPO for continuous control tasks in MuJoCo. We also plot Figure 7, the version of Figure 5 without the standard deviation. We can see that BARPO, without guidance, consistently and significantly outperforms ARPO in natural and robust returns with respect to the mean performance. Moreover, BARPO further improves the overall performance by utilizing the SPO guidance.

G.2 Statistical Significance of Comparison Results

We discuss the statistical significance of comparison results between BARPO and baselines from two key considerations: (1) the comparison of mean performance, and (2) a comprehensive analysis incorporating both the mean and the standard deviation.

Superiority in Mean Performance. From the perspective of mean returns, BARPO demonstrates a clear and significant advantage. To quantify this, we have calculated the average improvement of BARPO's mean returns over each baseline across all four environments, both with and with-

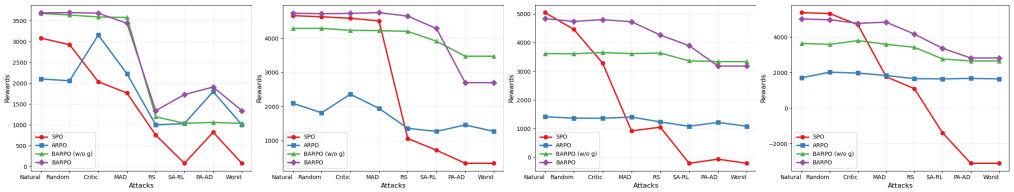

(a) Hopper (b) Walker2d (c) Halfcheetah (d) Ant

Figure 7: Natural and robust performance of SPO, ARPO, BARPO without guidance, and BARPO for four continuous control tasks. BARPO (w/o g) consistently outperforms ARPO.

Table 4: Natural and robust performance of SPO, ARPO, BARPO without SPO-guidance, and BARPO for continuous control tasks in MuJoCo. Bold and underlined values indicate the top and second-best performances, respectively.

Environment	Paradigms	Natural Return	Return under Attack							Worst-case Robustness
			Random	Critic	MAD	RS	SA-RL	PA-AD	Worst	
Hopper ($\epsilon = 0.075$)	SPO	3081 ± 638	2923 ± 767	2035 ± 1035	1763 ± 619	756 ± 36	79 ± 2	823 ± 182	79 ± 2	-0.974
	ARPO	2101 ± 588	2058 ± 559	3155 ± 528	2225 ± 641	1001 ± 30	1032 ± 47	1799 ± 547	1001 ± 30	**-0.524**
	BARPO (w/o g)	3675 ± 15	3634 ± 170	3588 ± 263	**3575** ± 295	1195 ± 79	1037 ± 24	1060 ± 125	1037 ± 24	-0.718
	BARPO	**3684** ± 20	**3692** ± 24	**3678** ± 19	3437 ± 555	**1340** ± 42	**1728** ± 62	**1908** ± 410	**1340** ± 42	-0.636
Walker2d ($\epsilon = 0.05$)	SPO	4662 ± 22	4628 ± 21	4584 ± 15	4507 ± 675	1062 ± 150	719 ± 1079	336 ± 252	336 ± 252	-0.928
	ARPO	2095 ± 983	1815 ± 930	2360 ± 1021	1944 ± 976	1360 ± 835	1270 ± 502	1460 ± 739	1270 ± 502	-0.394
	BARPO (w/o g)	4287 ± 15	4289 ± 17	4231 ± 10	4223 ± 406	4201 ± 44	3913 ± 694	**3473** ± 495	**3473** ± 495	**-0.190**
	BARPO	**4732** ± 86	**4718** ± 59	**4727** ± 36	**4750** ± 65	**4646** ± 53	**4285** ± 1282	2699 ± 1192	2699 ± 1192	-0.436
Halfcheetah ($\epsilon = 0.15$)	SPO	**5048** ± 526	4463 ± 650	3281 ± 1101	918 ± 541	1049 ± 50	-213 ± 103	-69 ± 22	-213 ± 103	-1.042
	ARPO	1412 ± 99	1363 ± 285	1359 ± 59	1402 ± 64	1230 ± 75	1079 ± 48	1216 ± 458	1079 ± 48	-0.236
	BARPO (w/o g)	3619 ± 44	3612 ± 28	3654 ± 28	3616 ± 37	3636 ± 523	3365 ± 40	**3337** ± 45	**3337** ± 45	**-0.078**
	BARPO	4837 ± 99	**4741** ± 501	**4803** ± 54	**4729** ± 105	**4265** ± 1077	**3894** ± 1322	3181 ± 1593	3181 ± 1593	-0.342
Ant ($\epsilon = 0.15$)	SPO	**5381** ± 1308	**5329** ± 976	4696 ± 1015	1768 ± 929	1097 ± 633	-1398 ± 318	-3107 ± 1071	-3107 ± 1071	-1.577
	ARPO	1709 ± 564	2026 ± 38	1976 ± 131	1839 ± 350	1661 ± 593	1648 ± 666	1675 ± 573	1648 ± 666	**-0.034**
	BARPO (w/o g)	3647 ± 128	3590 ± 431	3802 ± 84	3597 ± 357	3429 ± 679	2769 ± 608	2659 ± 541	2659 ± 541	-0.270
	BARPO	5024 ± 117	4979 ± 114	**4777** ± 122	**4843** ± 120	**4171** ± 826	**3367** ± 902	**2825** ± 757	**2825** ± 757	-0.438

out attacks. The results, summarized in Table 5, show that BARPO consistently and substantially outperforms the baselines on average.

Table 5: The average improvement of BARPO's mean of returns over baselines.

Compared Method	Natural Return	Random	Critic	MAD	RS	SA-RL	PA-AD	Worst
SA	-0.85%	+4.17%	-2.19%	+8.20%	+28.29%	+48.31%	+85.93%	+74.96%
RADIAL	+29.40%	+37.89%	+34.20%	+48.35%	+77.60%	+294.27%	+24.88%	+156.68%
WocaR	+10.59%	+8.94%	+7.21%	+13.28%	+28.34%	+92.61%	+31.30%	+65.65%
SPO	+2.56%	+6.94%	+82.99%	+197.59%	+350.34%	+1238.33%	+1708.38%	+1000.94%
ARPO	+159.37%	+158.24%	+128.23%	+149.80%	+168.34%	+167.73%	+80.29%	+103.16%

Advantage Considering Standard Deviation. Beyond the mean, a robust comparison must account for performance variance. Our results show that BARPO's advantage holds even when considering the standard deviation. (1) In the majority of cases, the upper performance bound of the baselines (i.e., mean + standard deviation) is still lower than the mean performance of BARPO alone. (2) More strikingly, in several scenarios, the upper bound of a baseline's performance (mean + standard deviation) is lower than the lower performance bound of BARPO (mean - standard deviation).

These points strongly indicate that the performance distributions are well-separated, and BARPO's superiority is not an artifact of sampling variance. This demonstrates a statistically significant edge over existing methods.

G.3 Extended Experiments on Humanoid Task

Humanoid task in the MuJoCo environment is a 3D bipedal robot designed to simulate a human and is widely considered the most difficult MuJoCo locomotion task, featuring:

- A 348-dimensional observation space (31.6x Hopper, 20.5x Walker2d/HalfCheetah, 3.3x Ant).

- A 17-dimensional action space (5.7x Hopper, 2.8x Walker2d/HalfCheetah, 2.1x Ant).

For this challenging environment, we implemented a comprehensive comparison of methods: SPO, ARPO, BARPO (w/o g), ARPO (w/ g), BARPO, and the robust baseline SA-PPO. Each method's training was repeated 17 times. We evaluated both the natural performance and the robust performance under four different attack types, and we report the results of the median-performing agent. For the training of ARPO (w/ g), BARPO, and SA-PPO, the hyperparameter κ was selected via a grid search over the set $\{0.1, 0.3, 1.0\}$.

Our results, shown in Tables 6 and 7, demonstrate that BARPO continues to achieve a strong natural and robust performance even in this significantly more complex environment. This further validates the effectiveness of our approach.

Table 6: Performance of SPO, ARPO, and BARPO without guidance in the Humanoid task.

Paradigm	Natural Return	Random	Critic	MAD	RS
SPO	5227 ± 963	5320 ± 730	4232 ± 1545	1059 ± 563	910 ± 595
ARPO	551 ± 44	544 ± 47	553 ± 51	554 ± 52	522 ± 60
BARPO (w/o g)	**6177** ± 21	**6177** ± 18	**6204** ± 13	**6180** ± 18	**5871** ± 1066

Table 7: Performance of SA-PPO, ARPO with guidance, and BARPO in the Humanoid task.

Paradigm	Natural Return	Random	Critic	MAD	RS
SA-PPO	6315 ± 12	6313 ± 16	6385 ± 10	6321 ± 15	5889 ± 92
ARPO (w/ g)	6035 ± 38	6041 ± 41	5978 ± 559	5940 ± 93	5637 ± 622
BARPO	**6615** ± 39	**6612** ± 32	**6698** ± 33	**6623** ± 40	**6031** ± 827

G.4 Ablations on Regularization Coefficient

The regularization coefficient κ plays a key role in robust training. Following baselines (Zhang et al., 2020c; Oikarinen et al., 2021; Liang et al., 2022), we performed a limited grid search for BARPO in $\{0.1, 0.3, 1.0\}$. We emphasize that adversarial RL typically requires moderate tuning, and our method introduces no additional burdens than standard methods in the field. We also add ablations to reflect the performance of BARPO across different κ choices in Table 8.

Table 8: Natural and worst-case robust performance of BARPO across various κ.

Env	κ	Natural Return	Worst Robust Return
Hopper	1.0	3636	1083
	0.3	**3684**	**1340**
	0.1	2151	959
Walker2d	1.0	4401	**3254**
	0.3	**4732**	2669
	0.1	4672	1615
Halfcheetah	1.0	3843	**3436**
	0.3	4837	3181
	0.1	**5133**	749
Ant	1.0	5024	**2825**
	0.3	5557	1413
	0.1	**5596**	439

G.5 Ablations on Inner Steps and Step Sizes

We further compare the BARPO's performance with different inner steps (10, 15, 20) and varying step sizes (scaling from $1\times$ to $3\times$ the base ratio of ϵ/steps) in Tables 9 and 10. Across these variations, BARPO consistently maintained its performance, indicating it is not sensitive to specific parameter tuning.

Table 9: Natural and worst-case robust performance of BARPO across various inner steps.

Env	Return	10-steps	15-steps	20-steps
Hopper	Natural	3677	**3742**	3652
	Worst	**1240**	1049	1194
Walker2d	Natural	4401	**4733**	4519
	Worst	**4140**	3536	3913
Halfcheetah	Natural	**4623**	4408	4455
	Worst	3453	3845	**3972**
Ant	Natural	**5024**	4917	4852
	Worst	4171	**4333**	4303

Table 10: Natural and worst-case robust performance of BARPO across various inner step sizes.

Env	Return	ϵ/steps	2ϵ/steps	3ϵ/steps
Hopper	Natural	**3677**	3573	3673
	Worst	1240	1242	**1250**
Walker2d	Natural	4401	**4424**	4219
	Worst	4140	**4284**	3159
Halfcheetah	Natural	**4623**	4307	4549
	Worst	3453	3754	**3988**
Ant	Natural	**5024**	4772	4853
	Worst	4171	4124	**4226**

G.6 Further Ablations on Effects of the Bilevel Structure and SPO

As shown in "Effect of SPO Guidance" of Section 5.3 (Figures 5 and 6), we perform ablations comparing BARPO with and without SPO guidance, showing that SPO improves natural return but reduces robustness. Additionally, as detailed in the second part of this section, Table 3 shows that introducing bilevel optimization on top of SPO substantially improves robust return with only minor degradation in natural return.

To further disentangle the effects of the bilevel structure and SPO, we now include additional comparisons (ARPO, ARPO w/ g, BARPO w/o g) and report the relative improvements of ARPO w/ g and BARPO w/o g compared to ARPO in Table 11.

Table 11: Relative improvements of ARPO w/ g and BARPO w/o g compared to ARPO

Env	Paradigm	Natural Return	Random	Critic	MAD	RS	SA-RL	PA-AD	Worst
Hopper	ARPO (w g)	**+76.0%**	**+77.5%**	**+17.1%**	+40.8%	+12.9%	**+23.8%**	**-2.4%**	**+12.9%**
	BARPO (w/o g)	+74.9%	+76.6%	+13.7%	**+60.7%**	**+19.4%**	+0.5%	-41.1%	+3.6%
Walker2d	ARPO (w g)	+100.8%	+133.1%	**+81.5%**	**+117.4%**	+130.8%	+180.7%	+70.9%	+96.5%
	BARPO (w/o g)	**+104.6%**	**+136.3%**	+79.3%	+117.2%	**+208.9%**	**+208.1%**	**+137.9%**	**+173.5%**
Halfcheetah	ARPO (w g)	**+253.9%**	**+261.9%**	**+270.9%**	+83.3%	+193.1%	+25.7%	-10.7%	+0.6%
	BARPO (w/o g)	+156.3%	+165.0%	+168.8%	**+157.9%**	**+195.6%**	**+211.9%**	**+174.4%**	**+209.3%**
Ant	ARPO (w g)	**+215.3%**	**+158.0%**	**+141.3%**	**+120.7%**	+60.7%	-28.1%	+4.9%	-28.1%
	BARPO (w/o g)	+113.4%	+77.2%	+92.3%	+95.6%	**+106.4%**	**+68.0%**	**+58.7%**	**+61.3%**

G.7 Combination Effect of Bilevel Framework and KL Surrogate

We have found that BARPO improves the optimization landscape. We further analyze whether the improvement primarily arises from the bilevel optimization structure itself or from the KL surrogate objective. We clarify that the improved optimization landscape in BARPO arises from the combination effect of both the bilevel optimization structure and the KL surrogate objective. This means that neither component alone is sufficient to achieve the observed improvements.

First, a bilevel structure by itself does not guarantee a smooth or well-behaved landscape. As noted in Section 4.1, both SPO and ARPO can be interpreted as special cases of bilevel optimization. However, they suffer from undesirable first-order stationary policies. The empirical improvements of BARPO over SPO and ARPO thus highlight the importance of a well-chosen surrogate objective. Our Theorem 4.1 provides theoretical support for using the KL divergence as a meaningful and tractable surrogate. In contrast, poorly chosen surrogates without such properties may result in

worse behavior. In particular, the reformulation (36) offers a promising direction for identifying optimal surrogates theoretically.

Second, the KL surrogate alone is insufficient without the bilevel structure. To disentangle the contributions of each component, we conducted an ablation study comparing BARPO to an augmented version of SPO that uses the KL surrogate directly within a minimax formulation. The results (see Table 12) show that BARPO consistently achieves a better trade-off between natural and robust returns. Specifically, in Hopper and HalfCheetah environments, BARPO outperforms the Minimax baseline on both metrics. In Walker2d and Ant, BARPO achieves slightly lower natural returns but significantly higher robust performance, suggesting a better robustness-optimality balance overall.

Table 12: Comparison of KL surrogate with minimax and bilevel structure.

Env	Structure	Natural Return	Worst Robust Return
Hopper	Minimax	3518	1286
	Bilevel	**3684**	**1340**
Walker2d	Minimax	**4875**	997
	Bilevel	4732	**2669**
Halfcheetah	Minimax	4780	1443
	Bilevel	**4837**	**3181**
Ant	Minimax	**5367**	2355
	Bilevel	5024	**2825**

H Additional Discussions and Clarifications

H.1 Discussion on Assumptions in Theoretical Analysis of Convergence

We offer the following clarifications and discussions on the assumptions in the theoretical analysis of convergence for ARPO.

Clarification for core contributions. Our main contribution is not the convergence proof itself, but the identification of a fundamental tension between optimality and robustness in policy gradient methods, and further developing a principled solution to mitigate this tradeoff. Our theoretical analysis reveals the root cause of this tradeoff, the landscape distortion induced by the strongest adversaries, and motivates the design of a bilevel framework to alleviate it. The convergence proof merely supports the conclusion that ARPO converges to FOSPs.

Justification of assumptions. We acknowledge that assumptions like Lipschitz smoothness and strong convexity may not strictly hold for deep neural networks. However, they are widely adopted in prior works on adversarial robustness (Sinha et al., 2018; Wang et al., 2019). Lipschitz continuity of sampled policy gradients has been explored and supported in various works (Allen-Zhu et al., 2019; Du et al., 2019; Zou et al., 2020) that study smoothness properties of deep neural networks. The assumption of locally strongly convex adversaries is also common in robust optimization literature (Sinha et al., 2018; Lee & Raginsky, 2018) and can be justified through its connection with distributionally robust optimization.

Potential relaxations. These conditions can be further relaxed. Specifically, the Lipschitz gradient assumption can be relaxed to (L_0, L_1)-smoothness (Zhang et al., 2020d;a), generalized smoothness (Li et al., 2023), or smooth adaptivity (Bauschke et al., 2017; Bolte et al., 2018; Ding et al., 2025). Strong convexity can be weakened to weak strong convexity (Necoara et al., 2019), restricted secant inequality (Agarwal et al., 2012), PL condition (Karimi et al., 2016), KL condition (Bolte et al., 2014), error bounds, and quadratic growth conditions (Drusvyatskiy & Lewis, 2018).

H.2 Clarification on Novelty of the Bilevel Framework

We clarify that our core contributions extend significantly beyond the proposal of using a bilevel framework. We view the bilevel framework not as the end goal, but as a significant tool to address fundamental challenges in adversarial robust policy optimization that we, to our knowledge, are the first to identify and analyze. Our key contributions are cohesively threefold:

New Insight into Inherent Vulnerability. We reveal that even under theoretically aligned models, standard policy optimization is inherently vulnerable. We pinpoint the underlying cause: its tendency to converge to fragile first-order stationary policies. This vulnerability is not due to model mismatch but a fundamental issue in the optimization process, which is a perspective overlooked in the prior literature.

Revealing and Analyzing a New Optimality-Robustness Tension. We uncover and analyze a fundamental tension between optimality and adversarial robustness in practical policy gradient methods. We further attribute this trade-off to an intrinsic *reshaping effect* induced by the strongest adversary on the optimization landscape, an insight not explicitly identified in prior works. This analysis explains why naively optimizing for robustness can degrade performance.

A Principled Solution to Mitigate the Trade-off. Motivated by the above findings, we propose the bilevel optimization framework. More importantly, we propose a practical, theoretically grounded instantiation of this framework designed specifically to mitigate this trade-off and find policies that are both high-performing and robust.

While bilevel optimization as a concept is not new, **its application to analyze and solve this specific, newly identified problem in policy-based RL is, to the best of our knowledge, entirely novel**. We believe the main novelty lies in the complete narrative: identifying the problem, analyzing its root cause, and providing a theoretically-principled solution.

To the best of our knowledge, we are the first to use a bilevel framework to analyze the adversarial robustness of policy-based reinforcement learning.

H.3 Quantify the Gap Between BARPO and ARPO

We quantify the connection between our KL-based bilevel formulation (BARPO) and the original minimax formulation (ARPO) from two perspectives.

Theoretical alignment. We emphasize that under ISA-MDP, BARPO and ARPO share the same global optima in theory. Theorem 4.1 further shows that BARPO's inner optimization is approximately equivalent to that of ARPO.

Optimization proximity. Following Kwon et al. (2023); Lu & Mei (2024), for sufficiently large α, BARPO can be reformulated:

$$\max_{\theta,\nu^\diamond} \min_{\vartheta} L^\alpha(\theta,\nu^\diamond,\vartheta) = \mathbb{E}_{s\sim\mu_0}\left[V^{\pi_\theta\circ\nu^\diamond}(s)\right] + \alpha\mathbb{E}_{s\sim\mu_0}\left[\mathrm{KL}\left(\pi_\theta(s)\|\pi_\theta\circ\nu^\diamond(s)\right) - \mathrm{KL}\left(\pi_\theta(s)\|\pi_\theta\circ\nu_\vartheta(s)\right)\right].$$

We quantify the deviation from the original objective using the bound:

$$|L^\alpha(s;\theta,\nu^\diamond,\vartheta) - V^{\pi_\theta\circ\nu_\vartheta}(s)| \le |V^{\pi_\theta\circ\nu^\diamond}(s) - V^{\pi_\theta\circ\nu_\vartheta}(s)| + \alpha|\,\mathrm{KL}\left(\pi_\theta(s)\|\pi_\theta\circ\nu^\diamond(s)\right) - \mathrm{KL}\left(\pi_\theta(s)\|\pi_\theta\circ\nu_\vartheta(s)\right)|.$$

The first term is bounded by $C\sqrt{\mathrm{KL}(\pi_\theta\circ\nu^\diamond\|\pi_\theta\circ\nu_\vartheta)}$ through Theorem 5 in Zhang et al. (2020c). The second term can be bounded by $C\left\|\frac{\pi_\theta}{\pi_\theta\circ\nu^\diamond}\right\|_\infty\left\|\frac{\pi_\theta\circ\nu^\diamond}{\pi_\theta\circ\nu_\vartheta}\right\|_\infty\sqrt{\mathrm{KL}(\pi_\theta\circ\nu^\diamond\|\pi_\theta\circ\nu_\vartheta)}$ by reverse Pinsker's and Pinsker's inequalities. Specifically, when $\pi_\theta\circ\nu^\diamond$ and $\pi_\theta\circ\nu_\vartheta$ are not too far apart, the second term is also $O\left(\sqrt{\mathrm{KL}(\pi_\theta\circ\nu^\diamond\|\pi_\theta\circ\nu_\vartheta)}\right)$ by Taylor expansion. Thus, the deviation between BARPO and ARPO can be controlled by the square root of the maximum KL divergence between $\pi_\theta\circ\nu^\diamond$ and $\pi_\theta\circ\nu_\vartheta$.

These connections indicate that BARPO, while structurally different, retains a strong theoretical connection to the ARPO.

H.4 Further Theoretical Understanding of BARPO

We further delve into a deeper theoretical understanding of how BARPO reshapes the optimization landscape from three complementary perspectives:

Adversarial Value Improvement through Landscape Lifting. Let $\nu^\diamond$ denote the solution to BARPO's inner problem and ν^* denote the strongest adversary defined in ARPO. By definition, $V^{\pi\circ\nu^\diamond(\pi)} \geq V^{\pi\circ\nu^*(\pi)}$, indicating that BARPO tends to elevate low-value regions in ARPO's landscape. Furthermore, Theorem 4.1 shows that maximizing the KL surrogate aligns with minimizing adversarial value: when the KL surrogate is high, the adversarial value is correspondingly low. This provides a theoretical link between BARPO's surrogate objective and ARPO's robustness.

Smoothing via Regularized Maximin Reformulation. Following prior work (Kwon et al., 2023; Lu & Mei, 2024), when α is sufficiently large, BARPO can be reformulated as an equivalent maximin problem:

$$\max_{\theta,\nu^\diamond} \min_{\vartheta} L^\alpha(\theta,\nu^\diamond,\vartheta) = \mathbb{E}_{s\sim\mu_0}[V^{\pi_\theta\circ\nu^\diamond}(s)+\alpha(\mathrm{KL}\left(\pi_\theta(s)\|\pi_\theta\circ\nu^\diamond(s)\right)-\mathrm{KL}\left(\pi_\theta(s)\|\pi_\theta\circ\nu_\vartheta(s)\right))]. \tag{36}$$

Compared to ARPO's objective, this formulation introduces a regularization term that has a smoothing effect on the outer landscape. Structurally, this resembles the use of Bregman divergences in defining the Moreau envelope (Bauschke et al., 2018), which is known to smooth the nonsmooth optimization problems.

Robustness under Date-driven Value Approximation. In practice, ARPO optimizes a lower bound $L(\pi,\nu) \leq V^{\pi\circ\nu}$ due to practical data-driven estimation for $V^{\pi\circ\nu}$, i.e., the practical objective becomes $\max_\pi \min_\nu L(\pi,\nu)$, which is no longer equivalent to the ideal adversarial objective. In contrast, BARPO's inner optimization minimizes an upper bound on the adversarial value, while the outer loop maximizes a lower bound. This formulation is more faithful to the original robust motivation and offers better resilience under value function approximation, helping to improve performance in practice.

We believe these perspectives offer promising foundations toward a more complete theoretical understanding of BARPO and plan to explore them in greater depth in future work.

I Limitations and Future Work

Despite the advancements introduced in this work, several challenges remain open for future research. First, we solve BARPO using a straightforward approach that ignores the second-order term. This solution process can be further improved via an advanced optimization method on a bilevel problem, such as transforming the bilevel optimization into a penalty-based minimax formulation and then solving it via fully first-order gradient methods. Additionally, we derive a surrogate for the strongest adversaries under specific conditions, which approximates but does not coincide with the strongest adversary. Nonetheless, BARPO, based on this surrogate, achieves strong robustness, even significantly outperforming ARPO, which relies on the strongest adversary, in tasks like Walker2d and HalfCheetah. While these empirical results are somewhat aligned with theoretical consistency between optimality and robustness, there remains a larger theoretical space to further explore. Finally, our analysis and results can be naturally extended to more general settings where strict theoretical consistency may not hold, offering valuable insights for related fields.

J Use of Large Language Models

The core method development in this research does not involve large language models (LLMs) as any important, original, or non-standard components. We utilized the LLM to assist only in the writing process of this manuscript. All content, ideas, and arguments were conceived and written by the human authors. The LLM was then used to provide suggestions for improving grammar, phrasing, and readability. The authors reviewed these suggestions and retained full editorial control, taking sole responsibility for the final version of the text.